A novel multi-target modular probe for multiple Large-Volume Metrology systems

Title: A novel multi-target modular probe for multiple Large-Volume Metrology systems

Author: Domenico Maisano Luca Mastrogiacomo

PII: S0141-6359(17)30214-3
DOI: http://dx.doi.org/doi:10.1016/j.precisioneng.2017.08.017
Reference: PRE 6646

To appear in: *Precision Engineering*

Received date: 14-4-2017
Revised date: 25-7-2017
Accepted date: 18-8-2017

Please cite this article as: Maisano D, Mastrogiacomo L, A novel multi-target modular probe for multiple Large-Volume Metrology systems, *Precision Engineering* (2017), http://dx.doi.org/10.1016/j.precisioneng.2017.08.017

A novel multi-target modular probe for multiple Large-Volume Metrology systems

Domenico Maisano[1] and Luca Mastrogiacomo[2]

[1] *domenico.maisano@polito.it* [2] *luca.mastrogiacomo@polito.it*

Politecnico di Torino, DIGEP (Department of Management and Production Engineering), Corso Duca degli Abruzzi 24, 10129, Torino (Italy)

Abstract

Recent studies show that the combined use of Large-Volume Metrology (LVM) systems (e.g., laser trackers, rotary-laser automatic theodolites (R-LATs), photogrammetric cameras, etc.) can lead to a systematic reduction in measurement uncertainty and a better exploitation of the available equipment. Unfortunately, the sensors of a specific LVM system are usually able to localize only specific targets (i.e., active/passive elements positioned in the measurement volume) and not necessarily those related to other systems (e.g., the reflective markers for photogrammetric cameras cannot be used for R-LATs or laser trackers); this represents an obstacle when using combinations of different LVM systems.

This paper describes the design of a new modular probe, with different typologies of targets and integrated sensors, which allows to simplify the measurement process. The probe is versatile as the number of targets, their typology and spatial position can be customized depending on the combination of LVM systems in use.

A detailed analysis of the technical and functional characteristics of the probe is followed by the presentation of a mathematical/statistical model for the real-time probe localization. Description is supported by realistic application examples.

Keywords: Large-volume metrology, Distributed sensors, Multi-target probe, Modularity, 6DOF probing, Probe-localization model.

1. Introduction

The field of *Large-Volume Metrology* (LVM) deals with objects with linear dimensions ranging from several meters to tens of meters (Estler et al., 2002; Peggs et al., 2009; Franceschini et al., 2011). Typical industrial applications concern

dimensional verification and assembly of large-sized mechanical components, in which levels of uncertainty of several tenths of millimetre are tolerated (Maropoulos et al., 2014). These applications are generally performed using technologically advanced LVM systems, which are very expensive and may require time consuming set-up and measurement operations (Franceschini and Maisano, 2014).

LVM systems are usually equipped with *sensors*, which are able to perform local measurements of distances and/or angles. Depending on the sensor layout, LVM systems can be classified into: (i) *centralized*, if sensors are grouped into a unique stand-alone unit (e.g., a laser tracker), or (ii) *distributed*, if sensors are spread around the measurement volume (e.g., a set of rotary-laser automatic theodolites (R-LATs)). Even though the existing measuring systems may differ in technology and metrological characteristics, two common features are: (i) the use of some *targets* to be localized, generally mounted on a hand-held probe for localizing the points of interest or in direct contact with the measured object's surface, and (ii) the fact that target localization is performed using local measurements by sensors.

For distributed LVM systems, sensors are arranged around the measured object and there are three possible approaches for target localization (Franceschini et al., 2011):

- *Multilateration*, which uses the *distances* between targets and sensors;
- *Multiangulation*, which uses the *angles* subtended by targets with respect to sensors;
- *Hybrid techniques*, based on the combined use of angles and distances between targets and sensors.

Although several types of LVM systems are (not rarely) available in the same industrial workshop or metrology laboratory, they are often used independently of each other (e.g., a laser tracker is used for certain tasks, a photogrammetric system for others, and so on). This is a rather myopic view because it ignores the benefits that may result from the combination of multiple systems, including but not limited to: (i) overcoming the limitations of the individual systems, (ii) improving measurement accuracy and coverage, and (iii) reducing the risk of measurement errors, due to measurement redundancy.

Franceschini et al. (2016) recently proposed a novel cooperative approach, in which a combination of LVM systems equipped with sensors of different nature – i.e., sensors based on different technologies and metrological characteristics, which are able to perform distance and/or angular measurements – share their measurement data and cooperate for determining a unique localization of the target. In other words, data provided by a number of sensors from different LVM systems are joined together and processed in order to localize the target. According to this philosophy, the set of multiple LVM systems (centralized and/or distributed) that are used in conjunction can be seen as a single *distributed* LVM "macro-system", consisting of sensors of different nature, which are distributed around the measurement volume.

The combined use of multiple LVM systems is allowed by an innovative mathematical model for target localization that can be adapted to a variety of practical contexts (Galetto et al., 2015; Franceschini et al., 2016; Maisano and Mastrogiacomo, 2016). A significant limitation of the above model is the assumption that the same target is simultaneously visible from sensors of different nature; in other words, it was assumed the existence of a "universal" target, compatible with any sensor, e.g., a target simultaneously visible from R-LATs, photogrammetric cameras, laser-trackers, etc..

Unfortunately, universal targets do not exist yet. Nevertheless, the above target-localization model can be applied adopting the following method: (i) targets of different nature are in turn repositioned in the same point and (ii) (distance or angular) local measurements by the sensor(s) compatible with them are gradually collected. See the example in Fig. 1(a).

This method has several weaknesses:

1. Repositioning different targets in the same position can be difficult. E.g., a solution is to use spherical targets with identical diameter, positioned in turn on a sphere mount with fixed position (e.g., attached to the surface of the object to be measured). Unfortunately, constructing spherical targets is not feasible for some sensor typologies (e.g., specific targets for US transducers or R-LATs); additionally, attaching a sphere mount to the surface of the object to be measured is not very practical.

2. The collection of the sensor local measurements is made slower, as it is fragmented into multiple turns.
3. The procedure is impracticable for dynamic measurements, in which targets are constantly moving and should be localized in real time.

The goal of this paper is to describe a new *modular* probe equipped with targets of different nature and a tip in contact with the point of interest (*P* in Fig. 1), which allows the localization in a single turn (see Fig. 1(b)). In other words, this probe allows to implement the cooperative-fusion paradigm – according to which data from sensors with different technical and metrological characteristics are fused (Franceschini et al., 2016) – in a practical and efficient way.

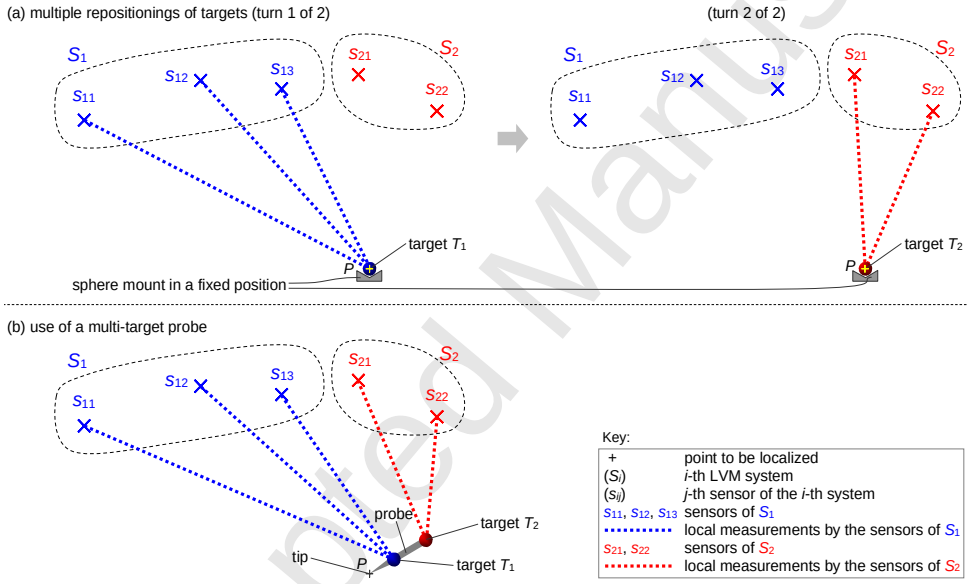

Fig. 1. Cooperative localization of the point *P* when using two targets (T_1 and T_2), which are visible from different sensors: (a) the two targets are in turn repositioned in the same point and the acquisition of the local measurements is broken into two turns; (b) a probe equipped with the two targets and a tip in contact with *P* allows to gather the sensor local measurements and to localize *P* in a single turn.

The scientific literature – regarding both scientific articles and patents – includes probes that are able to achieve the above requirements only partially. For example, the probe equipping the Leica T-Probe incorporates an array of infrared light-emitting diodes (LEDs), clustered around a conventional retro-reflecting laser-tracker target

along with an extended stylus (Kyle, 2006; Peggs et al., 2009). The resulting six degrees of freedom (6DOF) probe is capable of measuring features that would otherwise be out of sight. A camera mounted on the tracker head and associated image-processing hardware and software can determine the three angular DOF of the probe by analysing the positions of the LED targets in the camera image. Unfortunately, this probe is *rigid*, since it has fixed geometry and number of targets, and is closely related to a specific LVM system, thus it is not adaptable to combinations of other LVM systems.

The proposed modular probe overcomes the above limitations, thanks to several innovative features:

- The number and typology of targets mounted on the probe can be varied depending on the specific application;
- The geometry of the probe, i.e., the relative position between any target and the tip, can be varied depending on the specific application;
- The (dis)assembly of several targets is quick and practical, thanks to the use of modules with quick coupling systems;
- The probe can integrate other sensors that are able to provide additional data – e.g., inclinometer and compass. To avoid ambiguity, the LVM-systems' sensors positioned around the measurement volume will be hereafter denominated as *distributed*, while those embedded in the probe as *integrated*.

Modularity is a feature that characterizes the probes of some commercial LVM systems, e.g., the GOM's 3D ATOS Digitizer or NDI's ProCMM (GOM, 2016; NDI, 2016), for which it is possible to vary the number and position of the probe targets, depending on the application. However, these probes are exclusively equipped with sensors of the same typology (e.g., reflective markers for photogrammetric cameras). An important innovation of the new probe is to extend the modularity feature to targets of different nature.

After having described the probe in detail, this paper will also present a new mathematical/statistical model for the probe localization and estimate of the relevant uncertainty, which takes into account the following factors:

- Relative position between distributed sensors and probe targets.
- Uncertainty in the position/orientation of any distributed sensor, which is generally determined through initial calibration process(es) (Bar-Shalom, et al., 2001).
- Uncertainty in the local (distance and/or angular) measurements by distributed sensors, with respect to probe targets.
- Number, typology and relative position of the probe targets (and corresponding uncertainty) with respect to the probe tip.
- Angular measurements (and relevant uncertainty) provided by integrated sensors embedded in the probe.

The remainder of this paper is organized into five sections. Sect. 2 describes in detail the technical and functional characteristics of the probe. Sect. 3 summarizes the mathematical/statistical model for the probe localization and estimate of the relevant uncertainty; detailed information on this model is contained in the appendix. Sect. 4 exemplifies two of the possible probe configurations, applying the above probe-localization model. Sect. 5 summarizes the original contributions of this paper, focusing on its practical implications, limitations and future developments.

2.Technical and functional characteristics of the probe

The probe has a modular structure. The main module, or *primary* module consists of a bar with a handle for the operator, two ends with several calibrated holes (in predefined positions), in which different types of *secondary* modules can be plugged in, and a power-supply and data-transmission system (see Fig. 2(1)). In the following list, we describe the different types of secondary modules:

1. *Sphere mount* (e.g., with conical surface), where to put spherical targets (e.g., the reflective markers for photogrammetric cameras or the spherically mounted retroreflectors (SMRs) for laser trackers). Target locking can be performed using some magnets embedded in the mounts, assuming that targets are made of ferromagnetic metal. Mounts have a calibrated shaft, which can be plugged into the holes of the primary module or those of other secondary modules described at point (3).

2. *Targets* of different nature – such as those for R-LAT systems or ultrasonic (US) sensors – with a calibrated shaft, which can be plugged into the holes of the primary module or those of other secondary modules described at point (3).
3. Variable-length *extensions*, to be interposed between the primary module and the elements described at points (1) and (2), so as to vary the distance/position between targets and primary module.
4. *Stylus with a tip* in contact with the points of interest, which also includes a calibrated shaft that can be plugged into the holes of the primary module or those of other secondary modules described at point (3).

An important requirement is that these secondary modules are coupled on the primary module or other modules, quickly, precisely and with a certain repeatability (e.g., consider a target plugged into an extension, which is in turn plugged into the primary module, in Fig. 2(3)). This requirement can be achieved by adopting different technical solutions, such as providing the calibrated holes and shafts with threads or adopting quick coupling systems with magnetic lock. The geometric characteristics of the parts coupled, calibrated shafts/holes especially, should be precise enough, so that (1) coaxiality is obtained and (2) the modules are in the correct relative positions when coupled. To facilitate the achievement of these requirements, secondary modules have cylindrical symmetry (Fig. 2(2)).

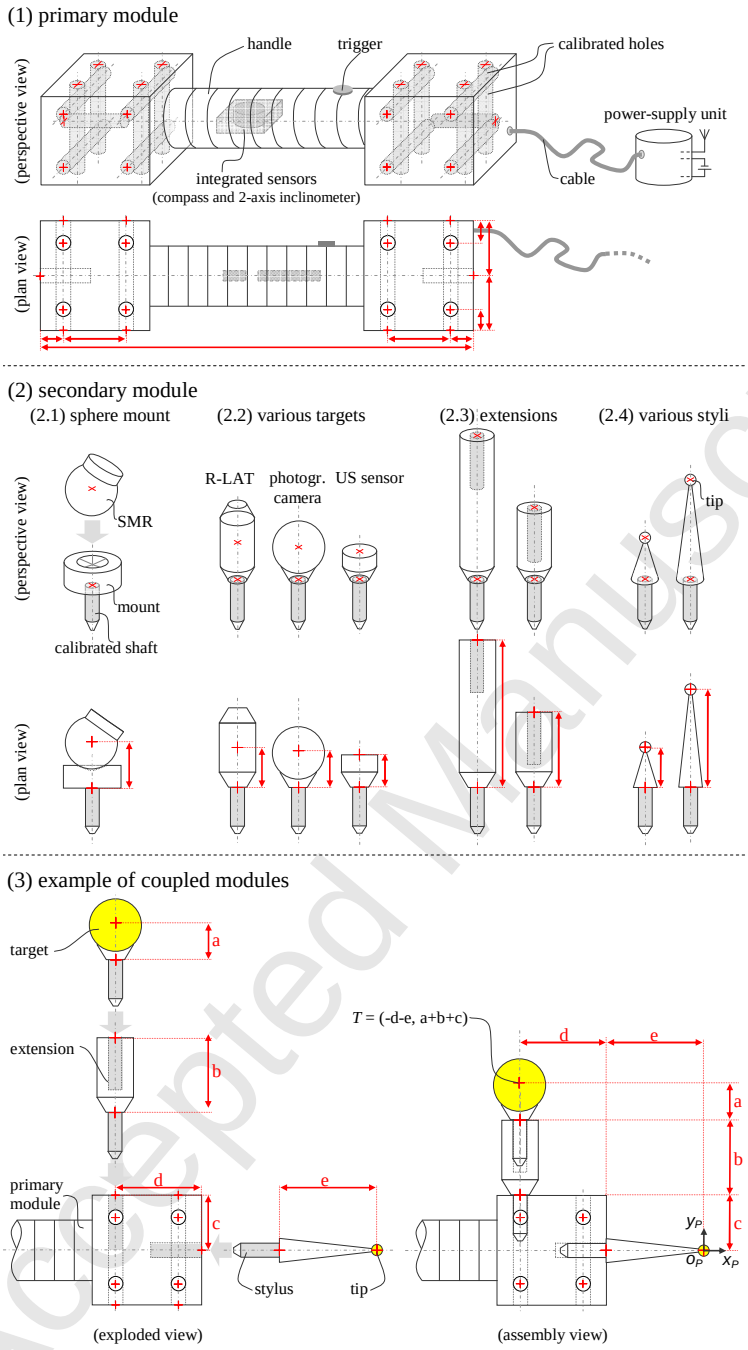

Fig. 2. Schematic representation of (1) the primary and (2) secondary module of the probe, and (3) example of coupling between them. Highlighted in grey the calibrated shafts/holes (i.e., the coupled elements) of the modules. The distances between the points indicated by the symbol "+" (in red) are supposed to be known, with some uncertainty.

In the representation in Fig. 2, specific reference points of the modules (e.g., points on the axis of calibrated holes/shafts and/or mating plane with other modules, centre of targets, etc.) are denoted by the symbol "+". When two or more modules are coupled together, these points should be in the expected positions, with relatively small uncertainties, in the order of a few hundredths of a millimetre (i.e., about one to two orders of magnitude lower than the typical uncertainties on the spatial localization of the individual targets, for most of the LVM systems). Using relatively accurate instruments, such as Coordinate Measuring Machines (CMMs), the (primary and secondary) modules can be calibrated through a preliminary *ad hoc* calibration process. This also allow to estimate the repeatability of the coupling systems (e.g., in terms of uncertainty in the relative positions of the modules) and – for a specific probe configuration – to determine the relative positions (and relevant uncertainties) of targets with respect to the tip.

In the example in Fig. 2(3), some modules (one primary module and three secondary ones: spherical target, extension and tip) are coupled together. Considering a 2D local Cartesian coordinate system ($o_P x_P y_P$) centred in the probe tip and assuming that the geometry of the modules is known, the relative position of the centre of the spherical target with respect to the centre of the probe tip can be determined as x_P = -d-e, y_P = a+b+c.

Focusing the attention on targets, some ones are *passive* (such as reflective markers and SMRs), while other ones *active* (such as arrays of LEDs, US transducers, and R-LATs targets), because they require a suitable system for power-supply, data-transmission and control. A practical solution is to connect the active targets to a *power-supply/data-transmission/control unit*[1] on the primary module (see Fig. 2), using electrical contacts between the shafts/holes of the coupled modules. This unit should be in turn able to transmit/receive data from other external units (e.g., a central processing unit or some of the distributed sensors), in a wireless or wired manner.

[1] For simplicity, it will be hereafter referred to as "*power-supply unit*".

The primary module has appropriate housings to lodge some integrated inertial sensors – such as inclinometer and/or compass – which should be also connected to the power-supply unit; since these integrated sensors exclusively estimate the probe orientation angles, it is not necessary that they have a precise position.

The primary module is also equipped with a trigger for the acquisition of the point of interest: when the trigger is pressed, the probe tip is localized on the basis of the data collected by the probe targets/sensors at that time.

For the purpose of example, Fig. 3 shows some pictures of a prototype that we are currently developing at the Politecnico di Torino – DIGEP. Structural elements (i.e., the "endoskeleton" of the primary module and shafts of secondary modules) are made of carbon fibre, since this material is relatively rigid, lightweight, and with a small thermal-expansion coefficient. The jack-based coupling system guarantees a relatively quick, precise and repeatable insertion of secondary modules into the primary one.

Once the primary and secondary modules are assembled, the relative positions between the probe targets and tip can be measured using a standard CMM with a relevant uncertainty lower than of few hundredths of a millimetre. At this stage, a local Cartesian coordinate system ($o_P x_P y_P z_P$) – with origin (o_P) in the probe tip, and y_P and z_P axes perpendicular to two reference planes on the surface of the primary module) – can also be defined (see Fig. 3(a)).

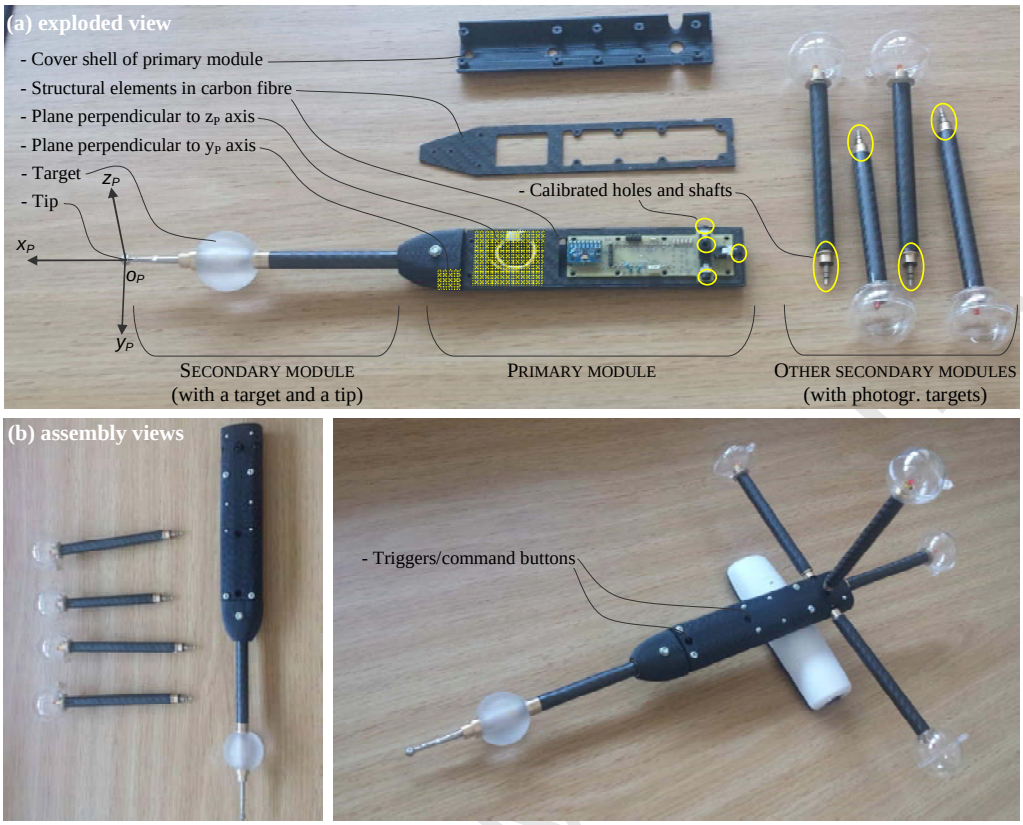

Fig. 3. Pictures of a prototype probe, which is still under development at Politecnico di Torino - DIGEP. In these pictures, the prototype is equipped with active photogrammetric targets only.

3. Mathematical/statistical model for probe localization

3.1 Main features of the model

In general, each *i*-th LVM system (S_i) includes a number of sensors; we conventionally indicate the generic *j*-th sensor of S_i – or, for simplicity, the *ij*-th sensor – as s_{ij} (e.g., s_{i1}, s_{i2}, …, s_{ij}, …). The probe includes a number of targets of different nature and a tip, in contact with the points of interest on the surface of the measured object. T_k conventionally denotes a generic *k*-th target mounted on the probe[2].

Sensors can be classified in two typologies:

1. *distance* sensors, which are able to measure their distance (d_{ijk}) from the *k*-th target;

[2] For simplicity, targets and sensors are considered as punctiform elements; this assumption is commonly adopted when dealing with LVM systems (Franceschini et al., 2011).

2. *angular* sensors, which are able to measure the azimuth (θ_{ijk}) and elevation (φ_{ijk}) angle subtended by the *k*-th target.

The subscript "*ijk*" refers to the local measurements (of distances or angles) by the *ij*-th sensor with respect to the *k*-th probe target. It is worth remarking that each *ij*-th sensor is not necessarily able to perform local measurements with respect to each *k*-th probe target, for two basic reasons:

- The communication range of the *ij*-th sensor should include the *k*-th target and there should be no interposed obstacle. For example, the communication range of a high-quality photogrammetric camera is approximately 6-8 m (Maisano and Mastrogiacomo, 2016).
- Even if a *k*-th target is included in the communication range of the *ij*-th sensor, local measurements can be performed only if they are compatible; e.g., the R-LAT target is not compatible with a photogrammetric camera or a laser tracker. Also, some sensors (such as photogrammetric cameras, US or R-LAT sensors) can perform local measurements with respect to multiple targets, while other sensors (such as laser trackers/tracers) with respect to a single target at a time.

In the case of compatibility between the *ij*-th sensor and the *k*-th target, we can define some (linearized) equations related to the local measurements:

$$\begin{matrix} \boldsymbol{A}_{ijk}^{dist} \cdot \boldsymbol{X} - \boldsymbol{B}_{ijk}^{dist} = \boldsymbol{0} & \text{one equation related to an } ij\text{th distance sensor and } k\text{th target} \\ \boldsymbol{A}_{ijk}^{ang} \cdot \boldsymbol{X} - \boldsymbol{B}_{ijk}^{ang} = \boldsymbol{0} & \text{two equations related to an } ij\text{th angular sensor and } k\text{th target} \end{matrix}, \quad (1)$$

where $\boldsymbol{X} = [X_P,\ Y_P,\ Z_P,\ \omega_P,\ \phi_P,\ \kappa_P]^T$ is the (unknown) vector containing the spatial coordinates (X_P, Y_P, Z_P) of the centre of the probe tip (*P*) and the angles (ω_P, ϕ_P, κ_P) of spatial orientation of the probe, referring to a global Cartesian coordinate system *OXYZ*. Matrices related to distance sensors are labelled with superscript "*dist*", while those related to angular sensors with superscript "*ang*". The matrices $\boldsymbol{A}_{ijk}^{dist}$, $\boldsymbol{B}_{ijk}^{dist}$, $\boldsymbol{A}_{ijk}^{ang}$ and $\boldsymbol{B}_{ijk}^{ang}$ contain:

- the position/orientation parameters ($X_{0_{ij}}$, $Y_{0_{ij}}$, $Z_{0_{ij}}$, ω_{ij}, ϕ_{ij} and κ_{ij}) related to the *ij*-th sensor;

- the distance (d_{ijk}) and/or angles (θ_{ijk}, φ_{ijk}) subtended by the k-th target, with respect to a local Cartesian coordinate system $o_{ij}x_{ij}y_{ij}z_{ij}$ of the ij-th sensor.

Since the "true" values of the above parameters are never known exactly, they can be replaced with appropriate estimates, i.e., $\hat{X}_{0_{ij}}, \hat{Y}_{0_{ij}}, \hat{Z}_{0_{ij}}$, $\hat{\omega}_{ij}$, $\hat{\phi}_{ij}$, $\hat{\kappa}_{ij}$, resulting from initial calibration process(es), $\hat{d}_{ijk}$ resulting from distance measurements, and $\hat{\theta}_{ijk}$ and $\hat{\varphi}_{ijk}$, resulting from angular measurements. For details on the construction of the above matrices, see the appendix.

As already said, the probe can also be equipped with some *integrated sensors* – such as two-axis inclinometer and compass – which are able to perform angular measurements for estimating the spatial orientation of the probe, through the following linearized equations:

$$\boldsymbol{A}^{int} \cdot \boldsymbol{X} - \boldsymbol{B}^{int} = \boldsymbol{0} \quad \text{three equations related to three angular measurements.} \tag{2}$$

Matrices $\boldsymbol{A}^{int}$ and $\boldsymbol{B}^{int}$ contain local measurements of three angles (ω_I, ϕ_I, κ_I) depicting the orientation of the integrated sensors with respect to a ground-referenced coordinate system ($x_I y_I z_I$). For details, see the appendix.

The probe localization problem can therefore be formulated through the following linear model, which encapsulates the relationships in Eqs. 1 and 2:

$$\boldsymbol{A} \cdot \boldsymbol{X} - \boldsymbol{B} = \begin{bmatrix} \boldsymbol{A}^{dist} \\ \boldsymbol{A}^{ang} \\ \boldsymbol{A}^{int} \end{bmatrix} \cdot \boldsymbol{X} - \begin{bmatrix} \boldsymbol{B}^{dist} \\ \boldsymbol{B}^{ang} \\ \boldsymbol{B}^{int} \end{bmatrix} = \boldsymbol{0}\,, \tag{3}$$

where blocks $\boldsymbol{A}^{dist}$, $\boldsymbol{A}^{ang}$, $\boldsymbol{B}^{dist}$ and $\boldsymbol{B}^{ang}$ are defined as:

$$\boldsymbol{A}^{dist} = \begin{bmatrix} \vdots \\ \boldsymbol{A}^{dist}_{ijk} \\ \vdots \end{bmatrix}_{ijk \in I^{dist}}, \quad \boldsymbol{A}^{ang} = \begin{bmatrix} \vdots \\ \boldsymbol{A}^{ang}_{ijk} \\ \vdots \end{bmatrix}_{ijk \in I^{ang}}, \quad \boldsymbol{B}^{dist} = \begin{bmatrix} \vdots \\ \boldsymbol{B}^{dist}_{ijk} \\ \vdots \end{bmatrix}_{ijk \in I^{dist}}, \quad \boldsymbol{B}^{ang} = \begin{bmatrix} \vdots \\ \boldsymbol{B}^{ang}_{ijk} \\ \vdots \end{bmatrix}_{ijk \in I^{ang}},$$

I^{dist} and I^{ang} being the sets of index-pair values (ijk) relating to the ij-th distance/angular sensors seeing the k-th target.

We remark that all the equations of the system in Eq. 3 are referenced to a unique global Cartesian coordinate system, *OXYZ*. These equations therefore include the roto-translation transformations to switch from other reference systems (e.g., the local reference system related to each distributed sensor, that one related to the probe, or the ground-referenced system of the integrated probe sensors) to *OXYZ*. For more information, see the appendix.

The six unknown parameters in $\boldsymbol{X}$ can be determined solving the system in Eq. 3, which is generally *overdefined*, i.e., there are more equations than unknown parameters: one for each combination of *ij*-th distance sensor and *k*-th target, two for each combination of *ij*-th angular sensor and *k*-th target, and three for the integrated sensors (i.e., two for the two-axis inclinometer and one for the compass).

The equations of the system may differently contribute to the uncertainty in the probe localization. Five important factors affecting this uncertainty are:

1. *Uncertainty in the position/orientation of distributed sensors* ($\hat{X}_{0_{ij}}, \hat{Y}_{0_{ij}}, \hat{Z}_{0_{ij}}$, $\hat{\omega}_{ij}$, $\hat{\phi}_{ij}$ and $\hat{\kappa}_{ij}$), resulting from initial calibration process(es);
2. *Uncertainty in the local measurements* ($\hat{d}_{ijk}$, $\hat{\theta}_{ijk}$ and $\hat{\varphi}_{ijk}$) *by the distributed sensors* with respect to probe targets, which depends on their metrological characteristics;
3. *Relative position between each probe target (T_k) and each ij-th distributed sensor*; e.g., for angular sensors, the uncertainty in target localization tends to increase proportionally to the distance between target and sensors (Maisano and Mastrogiacomo, 2016);
4. *Uncertainty in the relative position between the probe targets and the tip (P)*, which may depend on the accuracy of the manufacturing processes of the probe modules.
5. *Uncertainty in the angular measurements* ($\hat{\omega}_I$, $\hat{\phi}_I$ and $\hat{\kappa}_I$) *by the probe's integrated sensors*, which depends on their metrological characteristics.

Consequently, it would be appropriate to solve the system in Eq. 3, giving greater weight to the equations producing less uncertainty and *vice versa*. To this purpose, a practical method is that of *Generalized Least Squares* (GLS) (Franceschini et al., 2011; Kariya and Kurata, 2004), in which a weight matrix (***W***), which takes into account the uncertainty produced by the equations, is defined as:

$$\boldsymbol{W} = \left[\boldsymbol{J}^T \cdot \sum_{\xi} \cdot \boldsymbol{J}\right]^{-1}, \tag{4}$$

where ***J*** is the Jacobian matrix containing the partial derivatives of the elements in the first member of Eq. 3 (i.e., $\boldsymbol{A}\cdot\boldsymbol{X} - \boldsymbol{B}$) with respect to the parameters contained in the vector $\boldsymbol{\xi}$, i.e., the position/orientation of distributed sensors, the local measurements by the distributed sensors available, the angular measurements by the integrated sensors, and the relative position of the probe targets with respect to the tip. For details, see the appendix. $\sum_{\xi}$ is the covariance matrix of $\boldsymbol{\xi}$, which represents the variability of the parameters in $\boldsymbol{\xi}$.

The parameters in $\sum_{\xi}$ can be determined in several ways: (i) from manuals or technical documents relating to the distributed/integrated sensors in use, or (ii) estimated through *ad hoc* experimental tests. We remark that these parameters should reflect the measurement uncertainty of the elements of $\boldsymbol{\xi}$, in realistic working conditions – e.g., in the presence of vibrations, light/temperature variations and other typical disturbance factors.

By applying the GLS method to the system in Eq. 3, we obtain the final estimate of ***X*** as:

$$\hat{\boldsymbol{X}} = \left(\boldsymbol{A}^T \cdot \boldsymbol{W} \cdot \boldsymbol{A}\right)^{-1} \cdot \boldsymbol{A}^T \cdot \boldsymbol{W} \cdot \boldsymbol{B}\,. \tag{5}$$

For further details on the GLS method, see (Kariya and Kurata, 2004).

We remark that this probe-localization approach can be classified as *cooperative fusion* as it may fuse data from sensors with different technical and metrological characteristics (Franceschini et al., 2016).

The metrological traceability of the probe localization, i.e., "*the property of a measurement result* (i.e., probe localization) *whereby the result can be related to a*

reference (i.e., a measurement unit of length) *through a documented unbroken chain of calibrations, each contributing to the measurement uncertainty*" (ISO/IEC Guide 99:2007, 2007)), is ensured by the initial calibration process(es) to determine the spatial position/orientation of the distributed sensors and that to determine the relative position of the probe targets. In fact, these processes are generally based on the use of physical artefacts (such as calibrated bars with multiple reference positions) or measuring instruments (such as CMMs), which are traceable to the measurement unit of length (Peggs et al., 2009).

3.2 Estimation of the measurement uncertainty

The mathematical/statistical model shown in the previous section can also be used to estimate the uncertainty in the probe localization. For each localization, we can determine the covariance matrix $\sum_{\xi}$, applying the *Multivariate Law of Propagation of Uncertainty* (MLPU) to the system of (linearized) equations in Eq. 3, referring to the parameters affected by uncertainty and contained in the vector $\boldsymbol{\xi}$ (Hall, 2004):

$$\sum_{\boldsymbol{X}} = \left(\boldsymbol{A}^{T} \cdot \boldsymbol{W} \cdot \boldsymbol{A}\right)^{-1}. \tag{6}$$

The resulting 6x6 matrix, containing the variances (in the diagonal) and covariances (off-diagonal) related to the six elements in $\boldsymbol{X}$, is:

$$\sum_{\boldsymbol{X}} = \begin{bmatrix} \hat{\sigma}^2_{X_P} & \hat{\sigma}_{X_P Y_P} & \hat{\sigma}_{X_P Z_P} & \hat{\sigma}_{X_P \omega_P} & \hat{\sigma}_{X_P \phi_P} & \hat{\sigma}_{X_P \kappa_P} \\ \hat{\sigma}_{Y_P X_P} & \hat{\sigma}^2_{Y_P} & \hat{\sigma}_{Y_P Z_P} & \hat{\sigma}_{Y_P \omega_P} & \hat{\sigma}_{Y_P \phi_P} & \hat{\sigma}_{Y_P \kappa_P} \\ \hat{\sigma}_{Z_P X_P} & \hat{\sigma}_{Z_P Y_P} & \hat{\sigma}^2_{Z_P} & \hat{\sigma}_{Z_P \omega_P} & \hat{\sigma}_{Z_P \phi_P} & \hat{\sigma}_{Z_P \kappa_P} \\ \hat{\sigma}_{\omega_P X_P} & \hat{\sigma}_{\omega_P Y_P} & \hat{\sigma}_{\omega_P Z_P} & \hat{\sigma}^2_{\omega_P} & \hat{\sigma}_{\omega_P \phi_P} & \hat{\sigma}_{\omega_P \kappa_P} \\ \hat{\sigma}_{\phi_P X_P} & \hat{\sigma}_{\phi_P Y_P} & \hat{\sigma}_{\phi_P Z_P} & \hat{\sigma}_{\phi_P \omega_P} & \hat{\sigma}^2_{\phi_P} & \hat{\sigma}_{\phi_P \kappa_P} \\ \hat{\sigma}_{\kappa_P X_P} & \hat{\sigma}_{\kappa_P Y_P} & \hat{\sigma}_{\kappa_P Z_P} & \hat{\sigma}_{\kappa_P \omega_P} & \hat{\sigma}_{\kappa_P \phi_P} & \hat{\sigma}^2_{\kappa_P} \end{bmatrix}. \tag{7}$$

The $\boldsymbol{\Sigma}_{\boldsymbol{X}}$ matrix will vary from point to point, depending on the position and orientation of the probe, the number and metrological characteristics of the distributed/integrated sensors, and the probe targets in use. It is worth remarking that the quality of estimates of the parameters contained in $\boldsymbol{\Sigma}_{\boldsymbol{X}}$ is closely related to the quality of estimates of the

parameters contained in $\boldsymbol{\Sigma}_{\boldsymbol{\xi}}$; therefore, we reiterate that the latter parameters should reflect the measurement uncertainty the elements of $\boldsymbol{\xi}$ in realistic working conditions.

From the practical point of view, the most interesting part of the $\boldsymbol{\Sigma}_{\boldsymbol{X}}$ matrix is the top-left 3x3 block, which depicts the variability in the $\hat{X}_P$, $\hat{Y}_P$, $\hat{Z}_P$ estimates. On the other hand, the remainder of the matrix contains information on the variability related to the estimate of the probe orientation (ω_P, ϕ_P and κ_P) and correlations between spatial coordinates and orientation angles.

Returning to the top-left 3x3 block, the diagonal elements – i.e., $\hat{\sigma}_{X_P}$, $\hat{\sigma}_{Y_P}$ and $\hat{\sigma}_{Z_P}$ – are respectively the combined standard uncertainties related to the estimates of X_P, Y_P and Z_P. The relevant expanded uncertainties – i.e., U_{X_P}, U_{Y_P} and U_{Z_P} – can be calculated as:

$$\begin{aligned} U_{X_P} &= k \cdot \sqrt{\sum_{\boldsymbol{X},11}} = k \cdot \hat{\sigma}_{X_P} \\ U_{Y_P} &= k \cdot \sqrt{\sum_{\boldsymbol{X},22}} = k \cdot \hat{\sigma}_{Y_P} \\ U_{Z_P} &= k \cdot \sqrt{\sum_{\boldsymbol{X},33}} = k \cdot \hat{\sigma}_{Z_P} \end{aligned} , \tag{8}$$

where k is the coverage factor, generally fixed at $k = 2$, which means that, assuming a normal distribution of the estimates of X_P, Y_P, Z_P, the corresponding coverage probability is 95% (JCGM 100:2008, 2008).

A synthetic estimate of the expanded measurement uncertainty related to the position of the probe tip, with a coverage factor k, can be obtained through the sum of squared uncertainties in Eq. 8:

$$U_P = \sqrt{U_{X_P}^2 + U_{Y_P}^2 + U_{Z_P}^2} = k \cdot \sqrt{\hat{\sigma}_{X_P}^2 + \hat{\sigma}_{Y_P}^2 + \hat{\sigma}_{Z_P}^2} , \tag{9}$$

The uncertainties related to the positions of individual points can be used to determine those related to more complex datums, which are constructed using multiple points, e.g., distance between two points, centre and radius of a sphere, axis and radius of a cylinder, etc.. To this purpose, the typical least-square fitting techniques of *Surface Metrology* can be used (Whitehouse , 1994; Bosch, 1995).

An intuitive representation of the probe-tip localization uncertainty can be obtained through the so-called *uncertainty ellipsoids*, whose construction is based on the following steps: (i) diagonalization of the top-left 3x3 block of $\mathbf{\Sigma}_X$, (ii) determination of the principal axes (X', Y', Z'), and (iii) construction of a 3D ellipsoid with centroid in the point X_P, Y_P, Z_P, semi-axes oriented along X', Y', Z', and proportional to the diagonal elements of the diagonalized matrix.

For the purpose of example, Fig. 4 illustrates three ellipsoids related to three different localizations (*A*, *B* and *C*) of the probe in the measurement volume. These results are produced through simulated experiments, which consider a specific network of distributed sensors and a specific probe configuration. Since the distributed sensors and probe targets that are involved in each probe localization may change from case to case (e.g., depending on the relative position/orientation of the probe), the resulting uncertainty in the probe-localization may change from case to case too: e.g., it can be noticed that the uncertainty concerning the localization (*A*) is lower than that concerning (*B*) or (*C*). It is also clear that the uncertainty contribution related to three localizations are not necessarily isotropic with respect to the three spatial coordinates X_P, Y_P, Z_P (if so, each ellipsoid would degenerate into a sphere); in addition, the three resulting ellipsoids have different principal orientations (see Fig. 4), corresponding to the directions of their axes. This effect may be due to the non-uniform spatial distribution of the sensors positioned around the measurement volume (Maisano and Matrogiacomo, 2016).

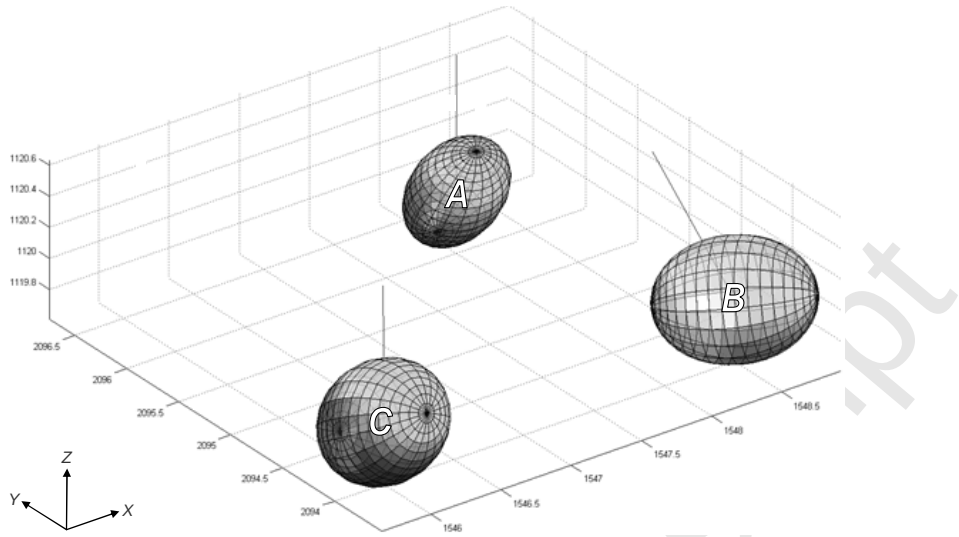

Fig. 4. Representation of three uncertainty ellipsoids related to three different probe localizations (*A*, *B* and *C*) into the measurement volume. The segments culminating into the ellipsoids represent the probe orientations.

4. Application examples

The following subsections describe two probe configurations, based on different combinations of LVM systems, and exemplify the application of the probe-localization model and relevant uncertainty estimation.

4.1 First application example

We consider a combination of two LVM systems (see Fig. 5):

(S_1) A distributed photogrammetric system consisting of two Hitachi Gigabit Ethernet photogrammetric infrared cameras (s_{11} and s_{12}) – pixel resolution: 1360x1024, frame rate: 30 fps (Hitachi Kokusai Electric Inc., 2016) – using 38.1 mm reflective spherical targets. Each camera is able to provide the azimuth (θ_{11k} and θ_{12k}) and elevation (φ_{11k} and φ_{12k}) angular measurements with respect to the *k*-th target;

(S_2) A laser tracker API Radian™ (API, 2016) with a 38.1 mm SMR. S_2 is equipped with an ADM (s_{21}), providing distance measurements and an angular sensor (s_{22}),

providing angular measurements of the *k*-th target. The local Cartesian coordinate systems of the two sensors are coincident.

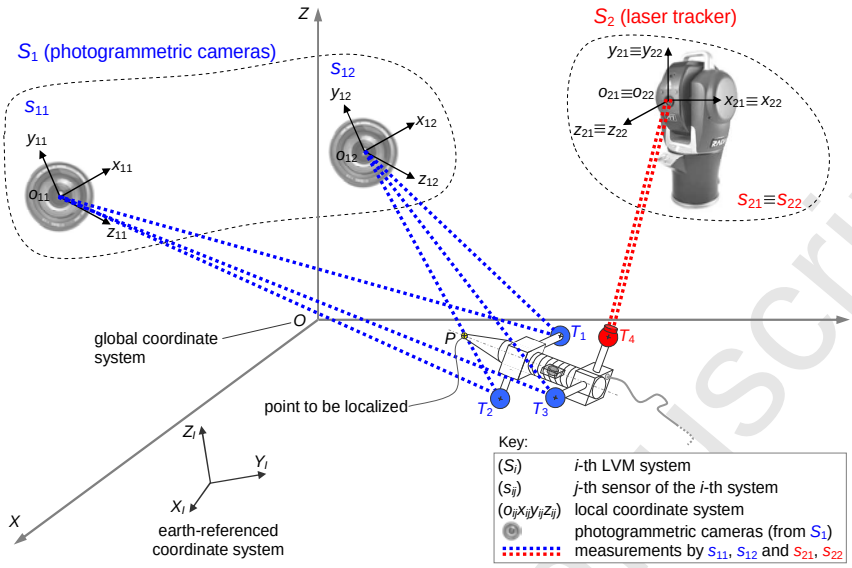

Fig. 5. Qualitative representation of the combination of two LVM systems used in the first application example.

This combination of LVM systems can be interpreted as a single "macro-system" consisting of total four sensors, distributed around the measurement volume. The distributed-sensor positions/orientations and the respective uncertainties were determined through suitable calibration/alignment processes (see Tab. 1), referring to the global reference system *OXYZ*.

Distributed sensor		Description	(a) Position [mm]				(b) Orientation [degrees]			
			$\hat{x}_{0_{ij}}$	$\hat{y}_{0_{ij}}$	$\hat{z}_{0_{ij}}$	st.dev.	ω_{ij}	ϕ_{ij}	κ_{ij}	st.dev.
From S_1:	s_{11}	Photogrammetric camera	324	-156	2340	≈0.01	5.23	3.11	28.53	≈0.003
	s_{12}	Photogrammetric camera	2214	-50	2126	≈0.01	11.51	358.48	345.31	≈0.003
From S_2:	s_{21}	ADM	1548	4568	1540	≈0.01	356.78	6.28	195.54	≈0.003
	s_{22}	Angular encoder	idem	idem	idem	idem	idem	idem	idem	idem

Tab. 1. Data concerning position/orientation and relevant uncertainty of the distributed sensors used in the first application example.

The probe in use is equipped with: three reflective spherical markers (T_1, T_2 and T_3), visible from the photogrammetric cameras, a SMR (T_4) visible from the two laser-tracker sensors, a tip (P), in contact with the objects to be measured, and two integrated sensors (compass and two-axis inclinometer). Fig. 6 contains a qualitative

representation of the probe, while Tab. 2 contains detailed information on its geometric and functional characteristics.

In practice, an operator places the tip in contact with the point of interest (on the surface of the object to be measured) and pulls a trigger to command the acquisition of local measurements. Contact stability is certainly an important factor for localization accuracy: if the probe slightly moves during acquisition, the accuracy in its localization may deteriorate. However, this problem can be mitigated, adopting some practical solutions:

- Synchronizing distributed sensors and targets, so that their local measurements are acquired at the same time or – at least – in a very small time window;
- Ensuring that the sampling rate of local measurements is relatively high;
- Training operators to hold the probe as stable as possible during local-measurement acquisition;
- Implementing appropriate control systems to monitor the stability of the probe, e.g., real-time monitoring of the angular data from the probe's integrated sensors.

Regarding uncertainty modelling, it is important that the experimental measurements to estimate the uncertainty in the local (angular or distance) measurements are carried out under the usual measuring conditions – i.e. with an operator placing the probe in contact with points of interest and commanding the local-measurement acquisition.

The relative position of each k-th target with respect to a reference system ($o_P x_P y_P z_P$) fixed in the probe tip is known (see Tab. 2). Assuming that the probe modules were constructed through relatively accurate manufacturing processes, the corresponding uncertainty is assumed to be in the order of magnitude of a few hundredths of mm. For simplicity, we consider the same uncertainty along the three spatial directions x_P, y_P and z_P.

Secondary module	Description	Relative position with respect to P [mm]			
		$\hat{x}_k$	$\hat{y}_k$	$\hat{z}_k$	st. dev.
T_1	Reflective marker visible from s_{11} and s_{12}	-100	-150	0	≈0.001
T_2	Reflective marker visible from s_{11} and s_{12}	-100	0	-150	≈0.001
T_3	Reflective marker visible from s_{11} and s_{12}	-300	150	0	≈0.001
T_4	SMR visible from s_{21} and s_{22}	-300	0	150	≈0.001

Tab. 2. Details on the geometric and functional characteristics of the probe, in the first application example.

For obvious reasons of compatibility, the reflective markers (T_1, T_2 and T_3) are visible from the photogrammetric cameras (s_{11} and s_{12}) only, while the SMR is visible from the laser tracker sensors (s_{21} and s_{22}) only. The only sensor that is able to perform distance measurements is s_{21}, while the other ones perform angular measurements.

The dispersions related to the measurements of the four distributed sensors and two integrated sensors are supposed to be known and are related to their metrological characteristics. For simplicity, the standard deviations of homologous sensors are supposed to be equal (e.g., those related to the angular sensor of S_1 are coincident: $\hat{\sigma}_{\theta_{1jk}} = \hat{\sigma}_{\varphi_{1jk}} \approx 0.01\,\text{deg}, \forall j \in \{1,2\} \wedge \forall k \in \{1,3\}$).

Sensor	Target(s)	Distributed sensors					Integrated sensors			
		$\hat{d}_{ijk}$ [mm]	st.dev. [mm]	$\hat{\theta}_{ijk}$ [deg]	$\hat{\varphi}_{ijk}$ [deg]	st.dev. [deg]	$\hat{\omega}_I$ [deg]	$\hat{\phi}_I$ [deg]	$\hat{\kappa}_I$ [deg]	st.dev. [deg]
s_{11}	T_1	-	-	129.56	-28.88	≈0.003	-	-	-	-
idem	T_2	-	-	124.92	-27.67	≈0.003	-	-	-	-
idem	T_3	-	-	124.94	-27.03	≈0.003	-	-	-	-
s_{12}	T_1	-	-	143.587	-27.376	≈0.02	-	-	-	-
idem	T_2	-	-	139.663	-27.5978	≈0.02	-	-	-	-
idem	T_3	-	-	134.663	-27.66	≈0.02	-	-	-	-
s_{21}	T_4	2371.98	≈0.012	-	-	-	-	-	-	-
s_{22}	T_4	-	-	225.707	-16.681	≈0.001	-	-	-	-
s_{int}	N/A	-	-	-	-	-	272.8	336.3	244.3	≈0.1

Tab. 3. Local measurements related to the (integrated and distributed) sensors used in the first application example.

Fig. 6 contains a qualitative representation of the probe and its modules. As a curiosity, we notice that the two typologies of targets are both passive, therefore – differently from the integrated sensors (compass and inclinometer) – they should not be connected to the power-supply unit.

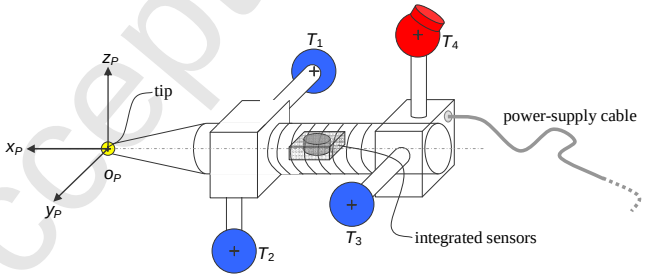

Fig. 6. Qualitative representation of the probe used in the first application example. Although the two typologies of targets (i.e., reflective spherical markers and SMR) are both passive, the integrated sensors need to be power-supplied.

Considering the spatial position/orientation of the distributed sensors (in Tab. 2), their local measurements with respect to the probe targets and those by the integrated sensors (in Tab. 3), we can apply the probe-localization model, obtaining the following results:

$$\boldsymbol{X} = [1545.95\ \text{mm} \quad 2093.89\ \text{mm} \quad 1119.93\ \text{mm} \quad 305.89\ \text{deg} \quad 102.02\ \text{deg} \quad 353.41\ \text{deg}]^T$$

$$\Sigma_{\boldsymbol{X}} = \begin{bmatrix} 7.3\cdot10^{-3}\,\text{mm}^2 & 1.2\cdot10^{-3}\,\text{mm}^2 & 2.4\cdot10^{-3}\,\text{mm}^2 & \cdots \\ 1.2\cdot10^{-3}\,\text{mm}^2 & 1.4\cdot10^{-2}\,\text{mm}^2 & -8.9\cdot10^{-4}\,\text{mm}^2 & \cdots \\ 2.4\cdot10^{-3}\,\text{mm}^2 & -8.9\cdot10^{-4}\,\text{mm}^2 & 4.8\cdot10^{-3}\,\text{mm}^2 & \cdots \\ \vdots & \vdots & \vdots & \ddots \end{bmatrix} \Rightarrow U_P = 0.32\,\text{mm} \quad , \quad (10)$$

U_P being the expanded measurement uncertainty related to the position of the probe tip, with a coverage probability of 95% (k = 2).

Fig. 7 represents the resulting probe-tip localization and the relevant uncertainty ellipsoid.

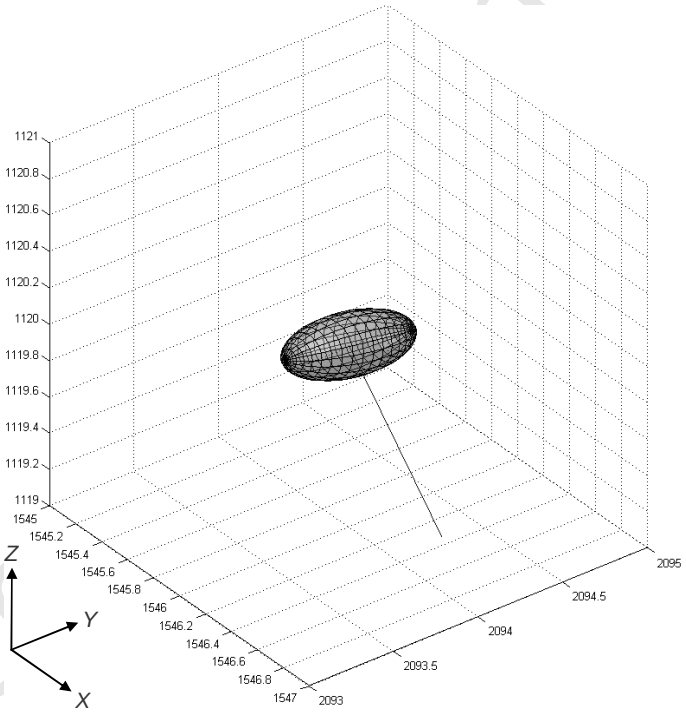

Fig. 7. Uncertainty ellipsoid (with 95% confidence interval) related to the localization of the probe tip in the first application example. The segment culminating into the ellipsoid represents the probe orientation.

4.1 Second application example

We consider a combination of the following two LVM systems (see Fig. 8):

(S_1) System consisting of three US sensors (s_{11}, s_{12}, s_{13}) with Murata MA40S4R piezoelectric US transceivers. These distributed sensors are able to measure their distance from targets with homologous US transceivers. For details on these transceivers, see (Priyantha et al., 2005; Franceschini et al ., 2010).

(S_2) System consisting of two R-LAT sensors (s_{11} and s_{12}) of an iGPS^{TM} (Maisano et al., 2008). These distributed sensors use rotating laser beams and infrared strobe lights to determine angle information to any *k*-th target simultaneously. Targets have photodiodes inside their modules that can sense the transmitted laser and infrared-light signals.

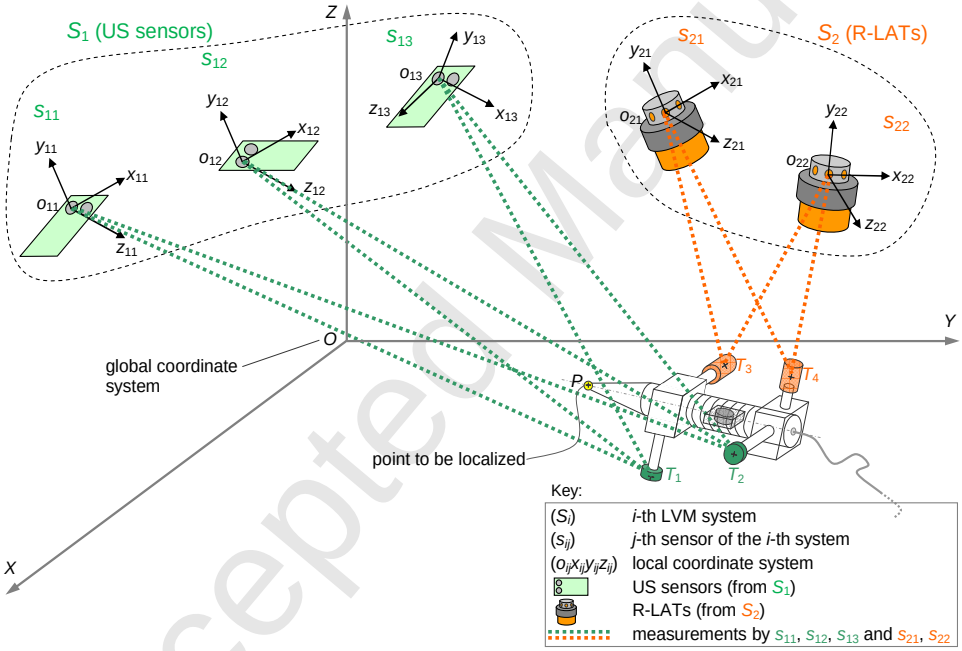

Fig. 8. Qualitative representation of the combination of two LVM systems used in the second application example.

Thanks to suitable calibration/alignment process, we determined the position/orientation and relevant uncertainties of the five sensors, referring to the global reference system *OXYZ* (see Tab. 4).

Distributed sensor	Description	(a) Position [mm]	(b) Orientation [degrees]

			$\hat{x}_{0_{ij}}$	$\hat{y}_{0_{ij}}$	$\hat{z}_{0_{ij}}$	st.dev.	ω_{ij}	ϕ_{ij}	κ_{ij}	st.dev.
From S_1:	s_{11}	US transceiver	352	-178	4040	≈0.4	-0.1	0.00	182.43	≈0.1
	s_{12}	US transceiver	2218	-50	4052	≈0.4	0.2	-0.1	179.11	≈0.1
	s_{13}	US transceiver	35	2252	4036	≈0.4	0.3	0.2	185.86	≈0.1
From S_2:	s_{21}	R-LAT	1228	-68	2126	≈0.02	0.01	-0.08	177.73	≈0.01
	s_{22}	R-LAT	97	1147	2165	≈0.02	-0.02	0.02	181.19	≈0.01

Tab. 4. Data concerning the position/orientation and relevant uncertainty of the distributed sensors used in the second application example.

The probe in use is equipped with two US transceiver (T_1 and T_2) visible from the three US sensors, two targets (T_3 and T_4) visible from the two R-LATs, a tip in contact with the points to be localized, and two integrated sensors (compass and two-axis inclinometer), which are able to estimate the orientation of the probe with respect to an earth-referenced coordinate system $X_I Y_I Z_I$ (see Fig. 9). Tab. 5 contains detailed data related to geometric and functional characteristics of the probe.

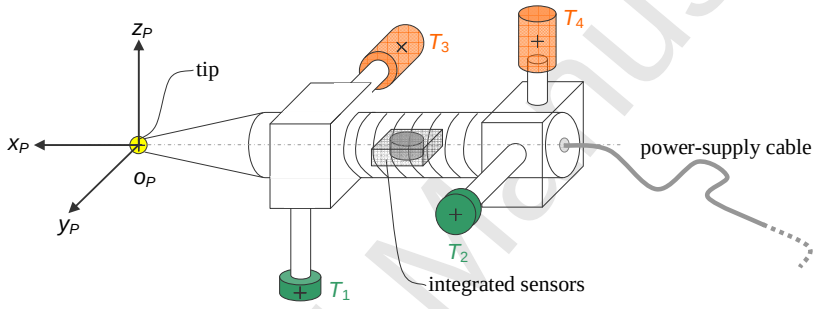

Fig. 9. Qualitative representation of the probe used in the second application example. T_1 and T_2 are two targets that are able to communicate with the three US sensors (s_{11}, s_{12} and s_{13}), while T_3 and T_4 are two targets that are able to communicate with the two R-LAT sensors (s_{21} and s_{22}).

Secondary module	Description	Relative position with respect to P [mm]			
		$\hat{x}_k$	$\hat{y}_k$	$\hat{z}_k$	st. dev.
T_1	US transceiver visible from s_{11}, s_{12} and s_{13}	-100.0	-150.0	0.0	≈0.01
T_2	US transceiver visible from s_{11}, s_{12} and s_{13}	-300.0	0.0	150.0	≈0.01
T_3	Targets visible from the R-LATs s_{21} and s_{22}	-100.0	0.0	-150.0	≈0.01
T_4	Targets visible from the R-LATs s_{21} and s_{22}	-300.0	150.0	0.0	≈0.01

Tab. 5. Details on the geometric and functional characteristics of the probe, in the second application example.

For reasons of compatibility, targets T_1 and T_2 can be seen by the US distributed sensors (s_{11}, s_{12} and s_{13}) only, while targets T_3 and T_4 are visible from the R-LAT sensors (s_{21} and s_{22}) only.

The uncertainties related to the local measurements of the distributed/integrated sensors are supposed to be known. The corresponding standard deviations, which are

related to the metrological characteristics of the sensors, can be estimated using data collected in the calibration process. For simplicity, the standard deviations of homologous sensors are supposed coincident (see Tab. 6).

The two types of targets in use, as well as the integrated sensors are active, therefore they have to be connected to the power-supply unit.

Sensor	Target(s)	Distributed sensors					Integrated sensors			
		$\hat{d}_{ijk}$ [mm]	st.dev. [mm]	$\hat{\theta}_{ijk}$ [deg]	$\hat{\varphi}_{ijk}$ [deg]	st.dev. [deg]	$\hat{\omega}_I$ [deg]	$\hat{\phi}_I$ [deg]	$\hat{\kappa}_I$ [deg]	st.dev. [deg]
s_{11}	T_1	3986.9	≈0.4	N/A	N/A	N/A	N/A	N/A	N/A	N/A
idem	T_2	3847.6	≈0.4	N/A	N/A	N/A	N/A	N/A	N/A	N/A
s_{12}	T_1	3808.7	≈0.4	N/A	N/A	N/A	N/A	N/A	N/A	N/A
Idem	T_2	3598.9	≈0.4	N/A	N/A	N/A	N/A	N/A	N/A	N/A
s_{13}	T_1	3437.1	≈0.4	N/A	N/A	N/A	N/A	N/A	N/A	N/A
Idem	T_2	3465.5	≈0.4	N/A	N/A	N/A	N/A	N/A	N/A	N/A
s_{21}	T_3	N/A	N/A	73.23	-26.11	≈0.01	N/A	N/A	N/A	N/A
Idem	T_4	N/A	N/A	78.16	-27.23	≈0.01	N/A	N/A	N/A	N/A
s_{22}	T_3	N/A	N/A	49.45	-34.27	≈0.01	N/A	N/A	N/A	N/A
Idem	T_4	N/A	N/A	39.01	-32.48	≈0.01	N/A	N/A	N/A	N/A
s_{int}	N/A	N/A	N/A	N/A	N/A	N/A	325.0	97.0	143.0	≈0.1

Tab. 6. Local measurements related to the (integrated and distributed) sensors used in the second application example.

Considering the spatial position/orientation of distributed sensors (in Tab. 5), their local measurements with respect to probe targets and those by the integrated sensors, we can apply the probe-localization model, obtaining the following results:

$$\boldsymbol{X} = [1550.6\ \text{mm} \quad 2094.2\ \text{mm} \quad 1120.0\ \text{mm} \quad 324.98\ \text{deg} \quad 97.05\ \text{deg} \quad 143.01\ \text{deg}]^T$$

$$\Sigma_{\boldsymbol{X}} = \begin{bmatrix} 0.058\,\text{mm}^2 & -0.002\,\text{mm}^2 & -0.022\,\text{mm}^2 & \cdots \\ -0.002\,\text{mm}^2 & 0.05\,\text{mm}^2 & 0.015\,\text{mm}^2 & \cdots \\ -0.022\,\text{mm}^2 & 0.015\,\text{mm}^2 & 0.108\,\text{mm}^2 & \cdots \\ \vdots & \vdots & \vdots & \ddots \end{bmatrix} \Rightarrow U_P = 0.93\,\text{mm} \quad , \quad (11)$$

U_P being the expanded measurement uncertainty related to the position of the probe tip, with a coverage probability of 95% (k = 2).

Fig. 10 depicts the resulting localization of the probe tip and the relevant uncertainty ellipsoid. The volume of this ellipsoid is considerably greater than that in the first example (in Fig. 7); the reason is that the measurement uncertainty is "inflated" by the presence of distributed US sensors, notoriously much less accurate than those related to other LVM systems.

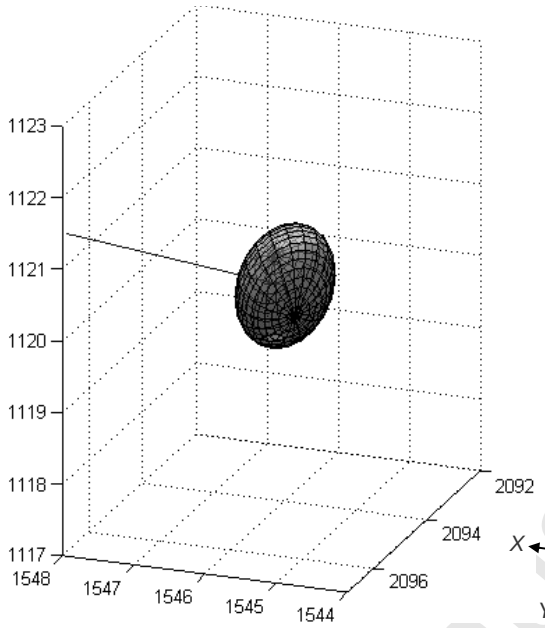

Fig. 10. Uncertainty ellipsoid (with 95% confidence interval) related to the localization of the probe tip in the first application example. The segment culminating into the ellipsoid represents the probe orientation.

6. Conclusions

This document has described a new modular and multi-target probe for determining the spatial coordinates of the points in contact with the tip, when using combinations of different LVM systems.

An important feature of the probe is that – depending on the LVM systems in use – it can be equipped with targets of different nature and additional sensors (such as two-axis inclinometer and compass), which contribute to the probe localization. Also it can be easily customized through the use of calibrated extensions and quick coupling systems.

Apart from the description of the technical and functional characteristics of the probe, a novel mathematical/statistical model for the real-time probe localization was presented. The model is *efficient*, as it is based on a system of linearized equations, and *effective*, as the equations are weighed with respect to their uncertainty contribution.

To improve the quality of the localization, it is important that all the parts of the probe, especially calibrated holes/shafts, have rather low uncertainties in the relative positions between targets and the tip (e.g., in the order of a few hundredths of millimetre).

The use of the probe can be extended from the measurement process to the distributed-sensor calibration process, which is generally based on repeated measurements of artefacts within the measurement volume (Peggs et al., 2009): thanks to its technical-functional characteristics, the probe can be seen as a special artefact. The calibration process may also include multiple repositionings of the probe in reference positions on other calibrated artefacts; see for example, the reference positions on the calibrated bar in Fig. 11. Since probe targets are placed at known distances, it is possible to determine the unknown position/orientation of the distributed sensors and estimate the relative uncertainty. This type of procedure (that we plan to develop in the future) is known in the scientific literature as *bundle adjustment* (Peggs et al., 2009).

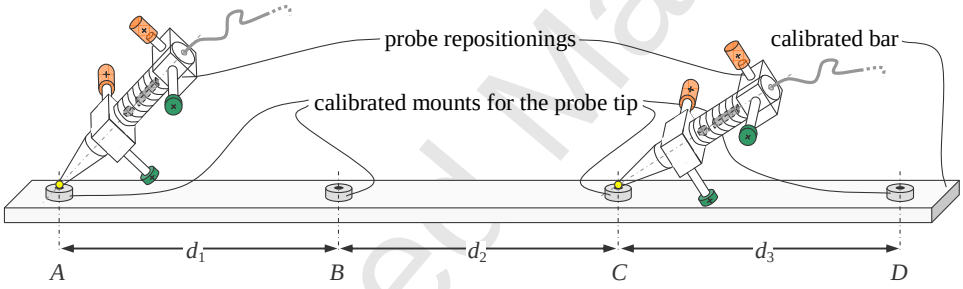

Fig. 11. Example of simultaneous use of two calibrated artefacts in the calibration process: (1) probe equipped with tip/targets and integrated sensors and (2) calibrated bar with several mounts (*A*, *B*, *C* and *D*) at known distances (d_1, d_2 and d_3).

Acknowledgements

This research was supported by the project Co-LVM “Cooperative multi-sensor data fusion for enhancing Large-Volume Metrology applications” (E19J14000950003), financed by *Fondazione CRT* under the initiative “La Ricerca dei Talenti”.

References

API (Automated Precision Inc.) (2016). RadianTM [accessed: 24-03-2016], http://www.apisensor.com.

Bar-Shalom, Y., Li, X.R., Kirubarajan, T. (2001) Estimation with applications to tracking and navigation. Wiley, New York.

Bosch J.A. (1995) Coordinate measuring machines and systems. Edited by Marcel Dekker, New York.

Estler, W.T., Edmundson, K.L., Peggs, G.N., Parker, D.H. (2002) Large-scale metrology—an update. CIRP Ann. Manuf. Technol., 51: 587-609.

Franceschini, F., Maisano, D., Mastrogiacomo, L., Pralio, B. (2010) Ultrasound transducers for large-scale metrology: a performance analysis for their use by the MScMS. Instrumentation and Measurement, IEEE Transactions on, 59(1): 110-121.

Franceschini, F., Galetto, M., Maisano, D., Mastrogiacomo, L., Pralio, B. (2011) Distributed Large-Scale Dimensional Metrology, Springer, London.

Franceschini, F., Maisano, D., Mastrogiacomo, L. (2014). Cooperative diagnostics for distributed large-scale dimensional metrology systems based on triangulation. Proceedings of the Institution of Mechanical Engineers, Part B: Journal of Engineering Manufacture, 228(4): 479-492.

Franceschini, F., Maisano, D. (2014). The evolution of large-scale dimensional metrology from the perspective of scientific articles and patents. The International Journal of Advanced Manufacturing Technology, 70(5-8), 887-909.

Franceschini, F., Galetto, M., Maisano, D., Mastrogiacomo, L. (2016). Combining multiple Large Volume Metrology systems: Competitive versus cooperative data fusion. Precision Engineering, 43: 514-524.

Galetto, M., Mastrogiacomo, L., Maisano, D., Franceschini, F. (2015). Cooperative fusion of distributed multi-sensor LVM (Large Volume Metrology) systems, CIRP Annals - Manufacturing Technology, 64(1): 483-486.

GOM (2016). GOM Touch Probe [accessed: 03-05-2016], http://www.gom.com/metrology-systems/system-overview/gom-touch-probe.html.

Hall, B.D. (2004). On the propagation of uncertainty in complex-valued quantities. Metrologia, 41(3): 173.

Hartley, R., Zisserman, A. (2003) Multiple view geometry in computer vision. Cambridge University, 2nd edition, Cambridge (UK).

Hitachi Kokusai Electric Inc. (2016). GigE(Gigabit Ethernet) 3CCD Cameras [accessed: 24-03-2016], http://www.hitachi-kokusai.co.jp.

JCGM 100:2008 (2008) Evaluation of measurement data - Guide to the expression of uncertainty in measurement, BIPM, Paris.

Kariya, T., Kurata, H. (2004) Generalized least squares, John Wiley & Sons, New York.

Kyle, S.A. (2006). Optically jointed probing systems for large volume coordinate metrology. Coordinate Measurement Systems Conference (CMSC), 17-21 July 2006, Orlando, US.

Maisano, D.A., Jamshidi, J., Franceschini, F., Maropoulos, P.G., Mastrogiacomo, L., Mileham, A., Owen, G. (2008). Indoor GPS: system functionality and initial performance evaluation. International Journal of Manufacturing Research, 3(3), 335-349.

Maisano, D., Mastrogiacomo, L. (2016). A new methodology to design multi-sensor networks for distributed large-volume metrology systems based on triangulation. Precision Engineering, 43, 105-118.

Maropoulos, P.G., Muelaner, J.E., Summers, M.D., Martin, O.C. (2014). A new paradigm in large-scale assembly—research priorities in measurement assisted assembly. The International Journal of Advanced Manufacturing Technology, 70(1-4):621-633.

NDI (2016). PRO CMM Overview [accessed: 03-05-2016], http://www.ndigital.com/msci/products/procmm/.

Peggs, G.N., Maropoulos, P.G., Hughes, E.B., Forbes, A.B., Robson, S., Ziebart, M., Muralikrishnan, B. (2009) Recent developments in large-scale dimensional metrology. Proceedings of the Institution of Mechanical Engineers, Part B: Journal of Engineering Manufacture, 223(6), 571-595.

Priyantha, N.B., Balakrishnan, H., Demaine, H.D., Teller, S. (2005) Mobile-assisted localization in wireless sensor networks, in Proc. 24th Annual Joint Conf. IEEE Commun. Soc. Comput. Commun. (INFOCOM), Miami, FL, Mar. 13-17, 2005, vol. 1, pp. 172-183.

ISO/IEC Guide 99:2007 (2007) International vocabulary of metrology – Basic and general concepts and associated terms (VIM), International Organization for Standardization, Geneva (2007), freely available at: http://www.bipm.org/en/publications/guides/vim.html.

Whitehouse, D. J. (1994). Handbook of surface metrology. CRC Press.

Wolberg, J. (2005) Data Analysis Using the Method of Least Squares: Extracting the Most Information from Experiments. Springer. ISBN 3-540-25674-1.

Appendix

Details on the mathematical/statistical model for probe localization

This section presents a detailed description of the new model for the localization of the multi-target probe, when adopting combinations of LVM systems.

We consider a set of LVM systems (S_i, being i = 1, 2, …), each of which is equipped with a number of sensors (s_{ij}, being j = 1, 2, …) positioned around the object to be measured, with a local Cartesian coordinate system ($o_{ij}x_{ij}y_{ij}z_{ij}$) roto-translated with respect to a global one ($OXYZ$, see Fig. A.1). The single LVM systems can be *centralized* or *distributed*: in the former case, sensors are rigidly connected to each other, while in the latter, they are not.

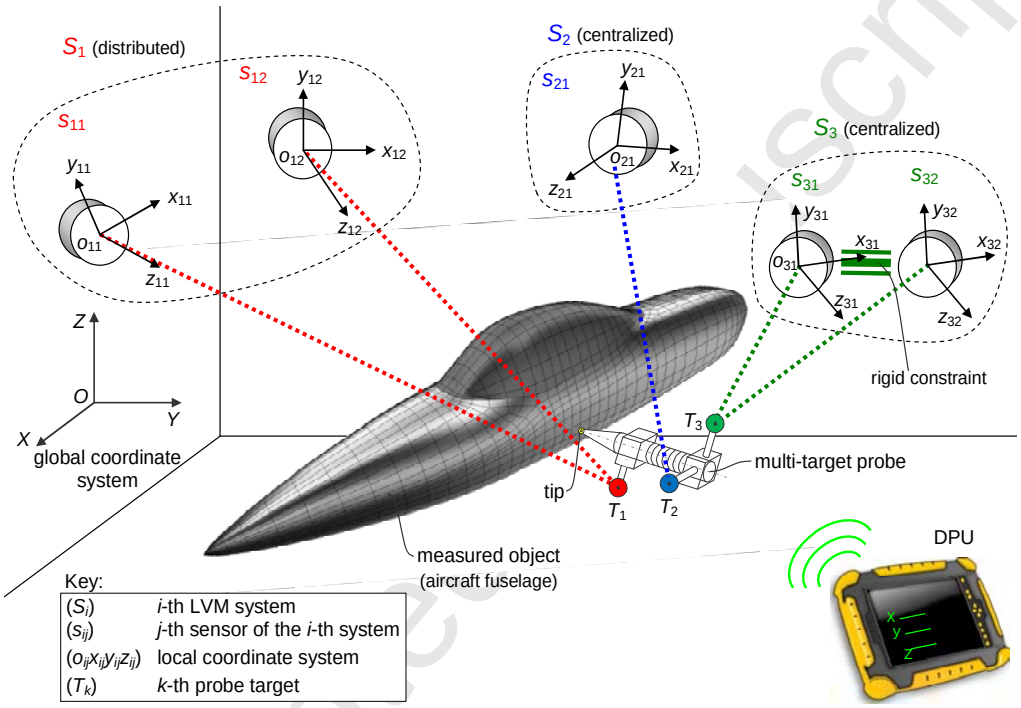

Fig. A.1. Schematic representation of the combination of three LVM systems: S_1 is a distributed system with two sensors (s_{11} and s_{12}), while S_2 and S_3 are two centralized systems with one sensor (s_{21}) and two sensors (s_{31} and s_{32}) respectively. A multi-target probe is equipped with three targets (T_1, T_2 and T_3), which can be seen only by those sensors compatible with them (e.g., T_1 can be seen by s_{11} and s_{12}, not by s_{21}, s_{31} and s_{32}).

A general transformation between a local and the global coordinate system is:

$$\begin{bmatrix} X \\ Y \\ Z \end{bmatrix} = \boldsymbol{R_{ij}} \cdot \begin{bmatrix} x_{ij} \\ y_{ij} \\ z_{ij} \end{bmatrix} + \begin{bmatrix} X_{0_{ij}} \\ Y_{0_{ij}} \\ Z_{0_{ij}} \end{bmatrix}. \qquad \text{(A1)}$$

$\boldsymbol{R_{ij}}$ is a 3x3 rotation matrix, which elements are functions of three rotation parameters ω_{ij}, ϕ_{ij}, κ_{ij}:

$$\boldsymbol{R_{ij}} = \begin{bmatrix} \cos\phi_{ij}\cos\kappa_{ij} & -\cos\phi_{ij}\sin\kappa_{ij} & \sin\phi_{ij} \\ \cos\omega_{ij}\sin\kappa_{ij} + \sin\omega_{ij}\sin\phi_{ij}\cos\kappa_{ij} & \cos\omega_{ij}\cos\kappa_{ij} - \sin\omega_{ij}\sin\phi_{ij}\sin\kappa_{ij} & -\sin\omega_{ij}\cos\phi_{ij} \\ \sin\omega_{ij}\sin\kappa_{ij} - \cos\omega_{ij}\sin\phi_{ij}\cos\kappa_{ij} & \sin\omega_{ij}\cos\kappa_{ij} + \cos\omega_{ij}\sin\phi_{ij}\sin\kappa_{ij} & \cos\omega_{ij}\cos\phi_{ij} \end{bmatrix}, \quad \text{(A2)}$$

where ω_{ij} represents a counterclockwise rotation around the x_{ij} axis; ϕ_{ij} represents a counterclockwise rotation around the new y_{ij} axis, which was rotated by ω_{ij}; κ_{ij} represents a counterclockwise rotation around the new z_{ij} axis, which was rotated by ω_{ij} and then ϕ_{ij}; for details, see (Franceschini et al., 2014).

$\left[X_{0_{ij}}, Y_{0_{ij}}, Z_{0_{ij}}\right]^T$ are the coordinates of the origin of $o_{ij}x_{ij}y_{ij}z_{ij}$, in the global coordinate system *OXYZ*.

The (six) location/orientation parameters related to each *ij*-th sensor (i.e., $X_{0_{ij}}, Y_{0_{ij}}, Z_{0_{ij}}$, ω_{ij}, ϕ_{ij}, κ_{ij}) are treated as known parameters, since they are measured in an initial calibration process. This process, which may vary depending on the specific technology of the individual measuring systems, generally includes multiple measurements of calibrated artefacts, within the measurement volume (Bai et al, 2014).

The above considerations apply to both *distributed* and *centralized* LVM systems. For the latter systems, sensors are rigidly connected (e.g., consider a photogrammetric tracking bar with three cameras, such as the OptiTrack V120-TRIO™), so there is an additional link (i.e., the so-called *rigid-body constraint*) between the sensors' position vectors ($\boldsymbol{X_{0_{ij}}}$) and the relevant $\boldsymbol{R_{ij}}$ matrices.

Focusing the attention on the probe, the point to be localized is $P = [X_P, Y_P, Z_P]^T$, which coincides with the centre of the spherical tip of a probe with a number of targets (T_1, T_2, … , T_k, …), e.g., three in the representation in Fig. A.1. The general position of the *k*-th target is $T_k = [X_k, Y_k, Z_k]^T$. In addition, the probe has a local Cartesian coordinate system $o_Px_Py_Pz_P$, for convenience centred with respect to the probe tip ($o_P = P$, see Fig. A.2). A general transformation between the coordinates of a generic point referred to $o_Px_Py_Pz_P$ (i.e., $[x, y, z]^T$) and those referred to the global coordinate system (i.e., $[X, Y, Z]^T$) is:

$$\begin{bmatrix} X \\ Y \\ Z \end{bmatrix} = \boldsymbol{R_P} \cdot \begin{bmatrix} x \\ y \\ z \end{bmatrix} + \begin{bmatrix} X_P \\ Y_P \\ Z_P \end{bmatrix}, \quad \text{(A3)}$$

where

$$\boldsymbol{R_P} = \begin{bmatrix} \cos\phi_P \cdot \cos\kappa_P & -\cos\phi_P \cdot \sin\kappa_P & \sin\phi_P \\ \cos\omega_P \cdot \sin\kappa_P + \sin\omega_P \cdot \sin\phi_P \cdot \cos\kappa_P & \cos\omega_P \cdot \cos\kappa_P - \sin\omega_P \cdot \sin\phi_P \cdot \sin\kappa_P & -\sin\omega_P \cdot \cos\phi_P \\ \sin\omega_P \cdot \sin\kappa_P - \cos\omega_P \cdot \sin\phi_P \cdot \cos\kappa_P & \sin\omega_P \cdot \cos\kappa_P + \cos\omega_P \cdot \sin\phi_P \cdot \sin\kappa_P & \cos\omega_P \cdot \cos\phi_P \end{bmatrix}$$

is a rotation matrix, whose elements are functions of three rotation parameters ω_P, ϕ_P and κ_P, which are analogous to the parameters ω_{ij}, ϕ_{ij} and κ_{ij} included in Eq. A2, but related to the axes x_P, y_P, z_P instead of x_{ij}, y_{ij}, z_{ij}. $[X_P, Y_P, Z_P]^T$ are the coordinates of *P*, i.e., the origin of $o_Px_Py_Pz_P$, in the global coordinate system *OXYZ*.

Assuming that the probe geometry is known (albeit with some uncertainty), for each k-th target we can define a position vector (x_k, y_k, z_k) related to the tip P, referring to the local reference system $o_P x_P y_P z_P$. The coordinates x_k, y_k, z_k should be interpreted as random variables related to the precision with which the various components of the probe (i.e., primary module, secondary ones and coupling systems) are manufactured and assembled together. Applying the rototranslation in Eq. A3, we can switch from the coordinates of the k-th target in the local coordinate system (i.e., x_k, y_k, z_k) to those in the global system (i.e., X_k, Y_k, Z_k), obtaining:

$$\begin{bmatrix} X_k \\ Y_k \\ Z_k \end{bmatrix} = \boldsymbol{R}_P \cdot \begin{bmatrix} x_k \\ y_k \\ z_k \end{bmatrix} + \begin{bmatrix} X_P \\ Y_P \\ Z_P \end{bmatrix}. \tag{A4}$$

We notice that the relationship in Eq. A4 includes six parameters related to the position of the probe tip and those related to the orientation of the probe itself, which are the unknown parameters of the problem: X_P, Y_P, Z_P, ω_P, ϕ_P, κ_P.

The probe-localization problem can be decomposed by considering (i) distance sensors, (ii) angular sensors, and (iii) integrated sensors separately, as discussed in Sects. A.1, A.2 and A.3 respectively.

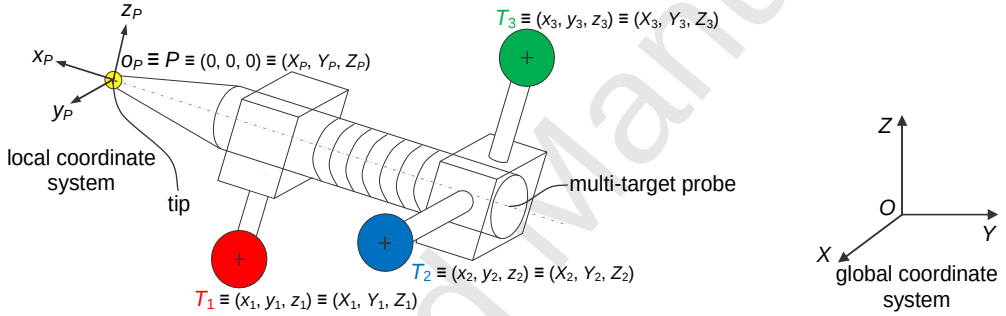

Fig. A.2. Schematic representation of the local coordinate system of the multi-target probe ($o_P x_P y_P z_P$) and the global one ($OXYZ$). The coordinates of the points representing the probe tip and targets can be referred to the local coordinate system, $o_P x_P y_P z_P$, and the global one, $OXYZ$.

A.1 Distance sensors

From the local perspective of a generic ij-th distance sensor, the distance between the k-th target $T_k = [X_k, Y_k, Z_k]^T$ and a local observation point – which we assume as coincident with the origin $o_{ij} = [\, X_{0_{ij}}, \, Y_{0_{ij}}, \, Z_{0_{ij}} \,]^T$ of the local coordinate system $o_{ij} x_{ij} y_{ij} z_{ij}$ – can be calculated as (see Fig. A.3):

$$d_{ijk} = \sqrt{\left(X_k - X_{0_{ij}}\right)^2 + \left(Y_k - Y_{0_{ij}}\right)^2 + \left(Z_k - Z_{0_{ij}}\right)^2}. \tag{A5}$$

Eq. A5 can be reformulated as a function of the probe-tip coordinates (X_P, Y_P, Z_P) and its orientation angles (ω_P, ϕ_P, κ_P), instead of X_k, Y_k, Z_k, applying the transformation in Eq. A4. Of course, the resulting equation – $d_{ijk}(\boldsymbol{X})$ – is not linear with respect to the unknown parameters of the problem, grouped in the vector $\boldsymbol{X} = [X_P, Y_P, Z_P, \omega_P, \phi_P, \kappa_P]^T$. However, a linearization can be obtained through a first order Taylor expansion with respect to the parameters contained in

$\boldsymbol{X}$, considering some $\hat{\hat{\boldsymbol{X}}} = \left[\hat{\hat{X}}_P, \hat{\hat{Y}}_P, \hat{\hat{Z}}_P, \hat{\hat{\omega}}_P, \hat{\hat{\phi}}_P, \hat{\hat{\kappa}}_P\right]^T$ values[1] reasonably close to them. This operation can be (at least partly) automated, using the Matlab's symbolic-calculation function "functionalDerivative".

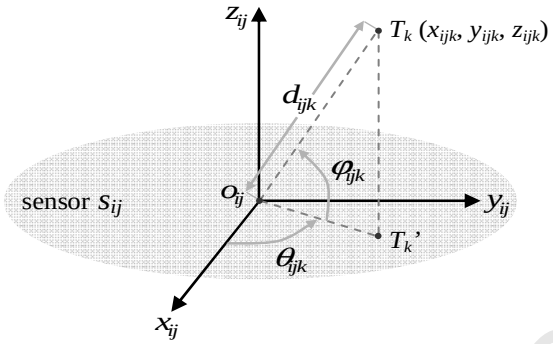

Fig. A.3. For a generic sensor (s_{ij}), a distance (d_{ijk}) and two angles – i.e., θ_{ijk} (azimuth) and φ_{ijk} (elevation) – are subtended by a line joining the k-th target (T_k) and the origin (o_{ij}) of the local coordinate system $o_{ij}x_{ij}y_{ij}z_{ij}$.

The resulting equation can be linearized and expressed in matrix form as:

$$\boldsymbol{A}_{ij}^{dist} \cdot \boldsymbol{X} - \boldsymbol{B}_{ij}^{dist} = 0\,, \tag{A6}$$

where $\boldsymbol{A}_{ij}^{dist} = \left[a_1^{dist}, a_2^{dist}, a_3^{dist}, a_4^{dist}, a_5^{dist}, a_6^{dist}\right]$, being

$$a_1^{dist} = \begin{bmatrix} 2\left(x_k\left(\cos\hat{\hat{\omega}}_P \sin\hat{\hat{\kappa}}_P + \cos\hat{\hat{\kappa}}_P \sin\hat{\hat{\omega}}_P \sin\hat{\hat{\phi}}_P\right) + y_k\left(\cos\hat{\hat{\omega}}_P \cos\hat{\hat{\kappa}}_P - \sin\hat{\hat{\kappa}}_P \sin\hat{\hat{\omega}}_P \sin\hat{\hat{\phi}}_P\right) - z_k\left(\sin\hat{\hat{\omega}}_P \cos\hat{\hat{\phi}}_P\right)\right) * \\ \left(\hat{\hat{Z}}_P - Z_{0_{ij}} + x_k\left(\sin\hat{\hat{\omega}}_P \sin\hat{\hat{\kappa}}_P - \cos\hat{\hat{\kappa}}_P \cos\hat{\hat{\omega}}_P \sin\hat{\hat{\phi}}_P\right) + y_k\left(\sin\hat{\hat{\omega}}_P \cos\hat{\hat{\kappa}}_P + \sin\hat{\hat{\kappa}}_P \cos\hat{\hat{\omega}}_P \sin\hat{\hat{\phi}}_P\right) + z_k\left(\cos\hat{\hat{\omega}}_P \cos\hat{\hat{\phi}}_P\right)\right) + \\ -2\left(x_k\left(\sin\hat{\hat{\omega}}_P \sin\hat{\hat{\kappa}}_P - \cos\hat{\hat{\kappa}}_P \cos\hat{\hat{\omega}}_P \sin\hat{\hat{\phi}}_P\right) + y_k\left(\sin\hat{\hat{\omega}}_P \cos\hat{\hat{\kappa}}_P + \sin\hat{\hat{\kappa}}_P \cos\hat{\hat{\omega}}_P \sin\hat{\hat{\phi}}_P\right) + z_k\left(\cos\hat{\hat{\omega}}_P \cos\hat{\hat{\phi}}_P\right)\right) * \\ \left(\hat{\hat{Y}}_P - Y_{0_{ij}} + x_k\left(\cos\hat{\hat{\omega}}_P \sin\hat{\hat{\kappa}}_P - \cos\hat{\hat{\kappa}}_P \sin\hat{\hat{\omega}}_P \sin\hat{\hat{\phi}}_P\right) + y_k\left(\cos\hat{\hat{\omega}}_P \cos\hat{\hat{\kappa}}_P - \sin\hat{\hat{\kappa}}_P \sin\hat{\hat{\omega}}_P \sin\hat{\hat{\phi}}_P\right) - z_k\left(\sin\hat{\hat{\omega}}_P \cos\hat{\hat{\phi}}_P\right)\right) \end{bmatrix},$$

$$a_2^{dist} = \begin{bmatrix} 2\left(x_k\left(\sin\hat{\hat{\omega}}_P \cos\hat{\hat{\kappa}}_P + \sin\hat{\hat{\kappa}}_P \cos\hat{\hat{\omega}}_P \sin\hat{\hat{\phi}}_P\right) - y_k\left(\sin\hat{\hat{\omega}}_P \sin\hat{\hat{\kappa}}_P - \cos\hat{\hat{\kappa}}_P \cos\hat{\hat{\omega}}_P \sin\hat{\hat{\phi}}_P\right)\right) * \\ \left(\hat{\hat{Z}}_P - Z_{0_{ij}} + x_k\left(\sin\hat{\hat{\omega}}_P \sin\hat{\hat{\kappa}}_P - \cos\hat{\hat{\kappa}}_P \cos\hat{\hat{\omega}}_P \sin\hat{\hat{\phi}}_P\right) + y_k\left(\sin\hat{\hat{\omega}}_P \cos\hat{\hat{\kappa}}_P + \sin\hat{\hat{\kappa}}_P \cos\hat{\hat{\omega}}_P \sin\hat{\hat{\phi}}_P\right) + z_k\left(\cos\hat{\hat{\omega}}_P \cos\hat{\hat{\phi}}_P\right)\right) + \\ +2\left(x_k\left(\cos\hat{\hat{\omega}}_P \cos\hat{\hat{\kappa}}_P - \sin\hat{\hat{\kappa}}_P \sin\hat{\hat{\omega}}_P \sin\hat{\hat{\phi}}_P\right) - y_k\left(\cos\hat{\hat{\omega}}_P \sin\hat{\hat{\kappa}}_P + \cos\hat{\hat{\kappa}}_P \sin\hat{\hat{\omega}}_P \sin\hat{\hat{\phi}}_P\right)\right) * \\ \left(\hat{\hat{Y}}_P - Y_{0_{ij}} + x_k\left(\cos\hat{\hat{\omega}}_P \sin\hat{\hat{\kappa}}_P + \cos\hat{\hat{\kappa}}_P \sin\hat{\hat{\omega}}_P \sin\hat{\hat{\phi}}_P\right) + y_k\left(\cos\hat{\hat{\omega}}_P \cos\hat{\hat{\kappa}}_P - \sin\hat{\hat{\kappa}}_P \sin\hat{\hat{\omega}}_P \sin\hat{\hat{\phi}}_P\right) - z_k\left(\sin\hat{\hat{\omega}}_P \cos\hat{\hat{\phi}}_P\right)\right) + \\ -2\left(y_k\left(\cos\hat{\hat{\kappa}}_P \cos\hat{\hat{\phi}}_P\right) + x_k\left(\cos\hat{\hat{\omega}}_P \sin\hat{\hat{\kappa}}_P\right)\right) * \left(\hat{\hat{X}}_P - X_{0_{ij}} + x_k\left(\cos\hat{\hat{\kappa}}_P \cos\hat{\hat{\phi}}_P\right) + y_k\left(\sin\hat{\hat{\kappa}}_P \cos\hat{\hat{\phi}}_P\right) - z_k\left(\sin\hat{\hat{\phi}}_P\right)\right) \end{bmatrix},$$

[1] The "double-hat" symbol "$\hat{\hat{\ }}$" indicates that a vector "close" to $\boldsymbol{X}$ can be obtained through a rough estimate of $\hat{\boldsymbol{X}}$, i.e., the (final) estimate of $\boldsymbol{X}$ itself. We will illustrate how to determine $\hat{\hat{\boldsymbol{X}}}$ later.

$$a_3^{dist}=\begin{bmatrix} 2\left(x_k\cos\hat{\hat{\kappa}}_P\sin\hat{\hat{\omega}}_P\cos\hat{\hat{\phi}}_P-y_k\sin\hat{\hat{\kappa}}_P\sin\hat{\hat{\omega}}_P\cos\hat{\hat{\phi}}_P+z_k\sin\hat{\hat{\omega}}_P\sin\hat{\hat{\phi}}_P\right)* \\ \left(\hat{\hat{Y}}_P-Y_{0_{ij}}+x_k\left(\cos\hat{\hat{\omega}}_P\sin\hat{\hat{\kappa}}_P+\cos\hat{\hat{\kappa}}_P\sin\hat{\hat{\omega}}_P\sin\hat{\hat{\phi}}_P\right)+y_k\left(\cos\hat{\hat{\omega}}_P\cos\hat{\hat{\kappa}}_P-\sin\hat{\hat{\kappa}}_P\sin\hat{\hat{\omega}}_P\sin\hat{\hat{\phi}}_P\right)-z_k\left(\sin\hat{\hat{\omega}}_P\cos\hat{\hat{\phi}}_P\right)\right) \\ -2\left(x_k\cos\hat{\hat{\kappa}}_P\cos\hat{\hat{\omega}}_P\cos\hat{\hat{\phi}}_P-y_k\sin\hat{\hat{\kappa}}_P\cos\hat{\hat{\omega}}_P\cos\hat{\hat{\phi}}_P+z_k\cos\hat{\hat{\omega}}_P\sin\hat{\hat{\phi}}_P\right)* \\ \left(\hat{\hat{Z}}_P-Z_{0_{ij}}+x_k\left(\sin\hat{\hat{\omega}}_P\sin\hat{\hat{\kappa}}_P-\cos\hat{\hat{\kappa}}_P\cos\hat{\hat{\omega}}_P\sin\hat{\hat{\phi}}_P\right)+y_k\left(\sin\hat{\hat{\omega}}_P\cos\hat{\hat{\kappa}}_P+\sin\hat{\hat{\kappa}}_P\cos\hat{\hat{\omega}}_P\sin\hat{\hat{\phi}}_P\right)+z_k\left(\cos\hat{\hat{\omega}}_P\cos\hat{\hat{\phi}}_P\right)\right)+ \\ 2\left(-x_k\cos\hat{\hat{\kappa}}_P\sin\hat{\hat{\phi}}_P+y_k\sin\hat{\hat{\kappa}}_P\sin\hat{\hat{\phi}}_P+z_k\cos\hat{\hat{\phi}}_P\right)*\left(\hat{\hat{X}}_P-X_{0_{ij}}+x_k\cos\hat{\hat{\kappa}}_P\cos\hat{\hat{\phi}}_P-y_k\sin\hat{\hat{\kappa}}_P\cos\hat{\hat{\phi}}_P-z_k\sin\hat{\hat{\phi}}_P\right) \end{bmatrix},$$

$$a_4^{dist}=\left[2\left(\hat{\hat{X}}_P-X_{0_{ij}}+x_k\cos\hat{\hat{\kappa}}_P\cos\hat{\hat{\phi}}_P-y_k\sin\hat{\hat{\kappa}}_P\cos\hat{\hat{\phi}}_P+z_k\sin\hat{\hat{\phi}}_P\right)\right],$$

$$a_5^{dist}=\left[2\left(\hat{\hat{Y}}_P-Y_{0_{ij}}+x_k\left(\cos\hat{\hat{\omega}}_P\sin\hat{\hat{\kappa}}_P+\cos\hat{\hat{\kappa}}_P\sin\hat{\hat{\omega}}_P\sin\hat{\hat{\phi}}_P\right)+y_k\left(\cos\hat{\hat{\omega}}_P\cos\hat{\hat{\kappa}}_P-\sin\hat{\hat{\kappa}}_P\sin\hat{\hat{\omega}}_P\sin\hat{\hat{\phi}}_P\right)-z_k\left(\sin\hat{\hat{\omega}}_P\cos\hat{\hat{\phi}}_P\right)\right)\right],$$

$$a_6^{dist}=\left[2\left(\hat{\hat{Z}}_P-Z_{0_{ij}}+x_k\left(\sin\hat{\hat{\omega}}_P\sin\hat{\hat{\kappa}}_P-\cos\hat{\hat{\kappa}}_P\cos\hat{\hat{\omega}}_P\sin\hat{\hat{\phi}}_P\right)+y_k\left(\sin\hat{\hat{\omega}}_P\cos\hat{\hat{\kappa}}_P+\sin\hat{\hat{\kappa}}_P\cos\hat{\hat{\omega}}_P\sin\hat{\hat{\phi}}_P\right)+z_k\left(\cos\hat{\hat{\omega}}_P\cos\hat{\hat{\phi}}_P\right)\right)\right],$$

and $\boldsymbol{B}_{ij}^{dist}=\boldsymbol{A}_{ij}^{dist}*\hat{\hat{\boldsymbol{X}}}-d_{ijk}\left(\hat{\hat{\boldsymbol{X}}}\right)$, being

$$d_{ijk}\left(\hat{\hat{\boldsymbol{X}}}\right)=\left(\hat{\hat{X}}_P-X_{0_{ij}}+x_k\cos\hat{\hat{\kappa}}_P\cos\hat{\hat{\phi}}_P-y_k\sin\hat{\hat{\kappa}}_P\cos\hat{\hat{\phi}}_P+z_k\sin\hat{\hat{\phi}}_P\right)^2+$$

$$+\left(\hat{\hat{Z}}_P-Z_{0_{ij}}+x_k\left(\sin\hat{\hat{\omega}}_P\sin\hat{\hat{\kappa}}_P-\cos\hat{\hat{\kappa}}_P\cos\hat{\hat{\omega}}_P\sin\hat{\hat{\phi}}_P\right)+y_k\left(\sin\hat{\hat{\omega}}_P\cos\hat{\hat{\kappa}}_P+\sin\hat{\hat{\kappa}}_P\cos\hat{\hat{\omega}}_P\sin\hat{\hat{\phi}}_P\right)+z_k\left(\cos\hat{\hat{\omega}}_P\cos\hat{\hat{\phi}}_P\right)\right)^2+$$

$$+\left(\hat{\hat{Y}}_P-Y_{0_{ij}}+x_k\left(\cos\hat{\hat{\omega}}_P\sin\hat{\hat{\kappa}}_P+\cos\hat{\hat{\kappa}}_P\sin\hat{\hat{\omega}}_P\sin\hat{\hat{\phi}}_P\right)+y_k\left(\cos\hat{\hat{\omega}}_P\cos\hat{\hat{\kappa}}_P-\sin\hat{\hat{\kappa}}_P\sin\hat{\hat{\omega}}_P\sin\hat{\hat{\phi}}_P\right)-z_k\left(\sin\hat{\hat{\omega}}_P\cos\hat{\hat{\phi}}_P\right)\right)^2+$$

$$-\hat{d}_{ijk}^{\,2}.$$

A.2 Angular sensors

From the local perspective of a generic *ij*-th angular sensor, two angles – i.e., θ_{ijk} (azimuth) and φ_{ijk} (elevation) – are subtended by the line passing through the *k*-th target T_k and o_{ij} (see Fig. A.3). Precisely, θ_{ijk} describes the inclination of segment $o_{ij}T_k$ with respect to the plane $x_{ij}y_{ij}$ (with a positive sign when $z_{ijk} > 0$), while φ_{ijk} describes the counterclockwise rotation of the projection ($o_{ij}T_k$') of $o_{ij}T_k$ on the $x_{ij}y_{ij}$ plane, with respect to the x_{ij} axis. Referring to the local coordinate system of the *ij*-th sensor, the following relationships hold:

$$\theta_{ijk}=\tan^{-1}\frac{y_{ijk}}{x_{ijk}} \qquad \begin{cases} \text{if } x_{ijk}\geq 0 \text{ then } -\dfrac{\pi}{2}\leq\theta_{ijk}\leq\dfrac{\pi}{2} \\ \text{if } x_{ijk}<0 \text{ then } \dfrac{\pi}{2}<\theta_{ijk}<\dfrac{3\pi}{2}. \end{cases} \tag{A7}$$

$$\varphi_{ijk}=\sin^{-1}\frac{z_{ijk}}{o_{ij}T_k} \qquad \left\{-\frac{\pi}{2}\leq\varphi_{ijk}\leq\frac{\pi}{2}\right.$$

Given that:

$$\tan\theta_{ijk}=\frac{\sin\theta_{ijk}}{\cos\theta_{ijk}} \tag{A8}$$

and

$$o_{ij}T_k = \frac{o_{ij}T_k'}{\cos\varphi_{ijk}} = \frac{x_{ijk}/\cos\theta_{ijk}}{\cos\varphi_{ijk}} = \frac{x_{ijk}}{\cos\theta_{ijk}\cdot\cos\varphi_{ijk}}, \tag{A9}$$

Eq. A7 can be reformulated as:

$$\begin{cases} x_{ijk}\cdot\sin\theta_{ijk} - y_{ijk}\cdot\cos\theta_{ijk} = 0 \\ x_{ijk}\cdot\sin\varphi_{ijk} - z_{ijk}\cdot\cos\theta_{ijk}\cdot\cos\varphi_{ijk} = 0 \end{cases}. \tag{A10}$$

We remark that the above two equations are coupled with respect to the two angles φ_{ijk} and θ_{ijk}, which means that they can be used only if the angular sensor is able to measure both angles simultaneously. In theory, these two equations could be decoupled, but this would unnecessarily complicate their formulation without any practical reason: in fact, it is very unlikely that the same angular sensor are able to measure just one angle and not the other one (e.g., consider a photogrammetric camera or a R-LAT).

The system in Eq. A10 can be expressed as a function of the global coordinates of point $T_k \equiv (X_k,\ Y_k,\ Z_k)$. Reversing Eq. A1, for switching from the sensor's local coordinates to the global ones, and considering that $\boldsymbol{R_{ij}}$ is orthonormal – therefore $\boldsymbol{R_{ij}^{-1}} = \boldsymbol{R_{ij}^{T}}$ (Hartley and Zisserman, 2003) – we obtain:

$$\begin{bmatrix} x_k \\ y_k \\ z_k \end{bmatrix} = \boldsymbol{R_{ij}^{-1}}\left\{\begin{bmatrix} X_k \\ Y_k \\ Z_k \end{bmatrix} - \begin{bmatrix} X_{0_{ij}} \\ Y_{0_{ij}} \\ Z_{0_{ij}} \end{bmatrix}\right\} = \boldsymbol{R_{ij}^{T}}\left\{\begin{bmatrix} X_k \\ Y_k \\ Z_k \end{bmatrix} - \begin{bmatrix} X_{0_{ij}} \\ Y_{0_{ij}} \\ Z_{0_{ij}} \end{bmatrix}\right\}. \tag{A11}$$

Combining Eq. A11 and Eq. A10, the above system can be expressed as a function of the global coordinates of the *k*-th target (demonstration omitted). Next, by applying the transformation in Eq. A4, the system can be expressed as a function of the six unknown parameters contained in vector $\boldsymbol{X} = [X_P,\ Y_P,\ Z_P,\ \omega_P,\ \phi_P,\ \kappa_P]^T$.

Obviously, the two resulting equations will not be linear with respect to the six (unknown) elements of $\boldsymbol{X}$. A linearization can be obtained through a first order Taylor expansion of the two equations, with respect to the parameters contained in $\boldsymbol{X}$, considering some $\hat{\boldsymbol{X}} = \left[\hat{X}_P, \hat{Y}_P, \hat{Z}_P, \hat{\omega}_P, \hat{\phi}_P, \hat{\kappa}_P\right]^T$ values reasonably close to them. The resulting linearized system can be expressed in matrix form as:

$$\boldsymbol{A_{ij}^{ang}}\cdot\boldsymbol{X} - \boldsymbol{B_{ij}^{ang}} = \boldsymbol{0}, \tag{A12}$$

where

$$\boldsymbol{A_{ij}^{ang}} = \begin{bmatrix} a_{11}^{ang} & a_{12}^{ang} & a_{13}^{ang} & a_{14}^{ang} & a_{15}^{ang} & a_{16}^{ang} \\ a_{21}^{ang} & a_{22}^{ang} & a_{23}^{ang} & a_{24}^{ang} & a_{25}^{ang} & a_{26}^{ang} \end{bmatrix}, \text{ being}$$

$$a_{11}^{ang} = \cos\hat{\theta}_{ijk}\begin{bmatrix} \left(\cos\hat{\omega}_P\cos\hat{\kappa}_P - \sin\hat{\omega}_P\sin\hat{\kappa}_P\sin\hat{\phi}_P\right)c_1 \\ +\left(\sin\hat{\omega}_P\cos\hat{\kappa}_P + \cos\hat{\omega}_P\sin\hat{\kappa}_P\sin\hat{\phi}_P\right)c_2 \end{bmatrix} - \sin\hat{\theta}_{ijk}\begin{bmatrix} \left(\cos\hat{\omega}_P\sin\hat{\kappa}_P + \cos\hat{\kappa}_P\sin\hat{\phi}_P\sin\hat{\omega}_P\right)c_1 \\ -\left(\sin\hat{\omega}_P\sin\hat{\kappa}_P + \cos\hat{\omega}_P\cos\hat{\kappa}_P\sin\hat{\phi}_P\right)c_2 \end{bmatrix},$$

$$a_{12}^{ang} = -\cos\hat{\theta}_{ijk}\begin{bmatrix}\left(\sin\hat{\hat{\omega}}_P\cos\hat{\hat{\kappa}}_P+\cos\hat{\hat{\omega}}_P\sin\hat{\hat{\kappa}}_P\sin\hat{\hat{\phi}}_P\right)c_4\\+\left(\cos\hat{\hat{\omega}}_P\cos\hat{\hat{\kappa}}_P+\sin\hat{\hat{\omega}}_P\sin\hat{\hat{\kappa}}_P\sin\hat{\hat{\phi}}_P\right)c_3\\-\left(\sin\hat{\hat{\kappa}}_P\cos\hat{\hat{\phi}}_P\right)c_5\end{bmatrix}+\sin\hat{\theta}_{ijk}\begin{bmatrix}\left(\cos\hat{\hat{\omega}}_P\sin\hat{\hat{\kappa}}_P+\sin\hat{\hat{\omega}}_P\cos\hat{\hat{\kappa}}_P\sin\hat{\hat{\phi}}_P\right)c_3\\+\left(\sin\hat{\hat{\omega}}_P\sin\hat{\hat{\kappa}}_P-\cos\hat{\hat{\omega}}_P\cos\hat{\hat{\kappa}}_P\sin\hat{\hat{\phi}}_P\right)c_4\\-\left(\cos\hat{\hat{\kappa}}_P\cos\hat{\hat{\phi}}_P\right)c_5\end{bmatrix},$$

$$a_{13}^{ang} = \cos\hat{\theta}_{ijk}\begin{bmatrix}\left(\sin\hat{\hat{\omega}}_P\cos\hat{\hat{\kappa}}_P+\cos\hat{\hat{\omega}}_P\sin\hat{\hat{\kappa}}_P\sin\hat{\hat{\phi}}_P\right)c_6\\-\left(\cos\hat{\hat{\omega}}_P\cos\hat{\hat{\kappa}}_P-\sin\hat{\hat{\omega}}_P\sin\hat{\hat{\kappa}}_P\sin\hat{\hat{\phi}}_P\right)c_7\\+\left(\sin\hat{\hat{\kappa}}_P\cos\hat{\hat{\phi}}_P\right)c_8\end{bmatrix}+\sin\hat{\theta}_{ijk}\begin{bmatrix}\left(\cos\hat{\hat{\omega}}_P\sin\hat{\hat{\kappa}}_P+\sin\hat{\hat{\omega}}_P\cos\hat{\hat{\kappa}}_P\sin\hat{\hat{\phi}}_P\right)c_7\\-\left(\sin\hat{\hat{\omega}}_P\sin\hat{\hat{\kappa}}_P-\cos\hat{\hat{\omega}}_P\cos\hat{\hat{\kappa}}_P\sin\hat{\hat{\phi}}_P\right)c_6\\+\left(\cos\hat{\hat{\kappa}}_P\cos\hat{\hat{\phi}}_P\right)c_8\end{bmatrix},$$

$$a_{14}^{ang} = \cos\hat{\theta}_{ijk}\left[\sin\hat{\hat{\kappa}}_P\cos\hat{\hat{\phi}}_P\right]+\sin\hat{\theta}_{ijk}\left[\cos\hat{\hat{\kappa}}_P\cos\hat{\hat{\phi}}_P\right],$$

$$a_{15}^{ang} = -\cos\hat{\theta}_{ijk}\left[\cos\hat{\hat{\omega}}_P\cos\hat{\hat{\kappa}}_P-\sin\hat{\hat{\omega}}_P\sin\hat{\hat{\kappa}}_P\sin\hat{\hat{\phi}}_P\right]+\sin\hat{\theta}_{ijk}\left[\cos\hat{\hat{\omega}}_P\sin\hat{\hat{\kappa}}_P+\sin\hat{\hat{\omega}}_P\cos\hat{\hat{\kappa}}_P\sin\hat{\hat{\phi}}_P\right],$$

$$a_{16}^{ang} = -\cos\hat{\theta}_{ijk}\left[\sin\hat{\hat{\omega}}_P\cos\hat{\hat{\kappa}}_P+\cos\hat{\hat{\omega}}_P\sin\hat{\hat{\kappa}}_P\sin\hat{\hat{\phi}}_P\right]+\sin\hat{\theta}_{ijk}\left[\sin\hat{\hat{\omega}}_P\sin\hat{\hat{\kappa}}_P-\cos\hat{\hat{\omega}}_P\cos\hat{\hat{\kappa}}_P\sin\hat{\hat{\phi}}_P\right],$$

$$a_{21}^{ang} = -\sin\hat{\varphi}_{ijk}\begin{bmatrix}\left(\cos\hat{\hat{\omega}}_P\sin\hat{\hat{\kappa}}_P+\sin\hat{\hat{\omega}}_P\cos\hat{\hat{\kappa}}_P\sin\hat{\hat{\phi}}_P\right)c_1\\-\left(\sin\hat{\hat{\omega}}_P\sin\hat{\hat{\kappa}}_P-\cos\hat{\hat{\omega}}_P\cos\hat{\hat{\kappa}}_P\sin\hat{\hat{\phi}}_P\right)c_2\end{bmatrix}-\cos\hat{\hat{\phi}}_{ijk}\cos\hat{\theta}_{ijk}\left[\left(\cos\hat{\hat{\phi}}_P\sin\hat{\hat{\omega}}_P\right)c_1+\left(\cos\hat{\hat{\omega}}_P\cos\hat{\hat{\phi}}_P\right)c_2\right],$$

$$a_{22}^{ang} = \sin\hat{\varphi}_{ijk}\begin{bmatrix}\left(\cos\hat{\hat{\omega}}_P\sin\hat{\hat{\kappa}}_P+\sin\hat{\hat{\omega}}_P\cos\hat{\hat{\kappa}}_P\sin\hat{\hat{\phi}}_P\right)c_3\\+\left(\sin\hat{\hat{\omega}}_P\sin\hat{\hat{\kappa}}_P-\cos\hat{\hat{\omega}}_P\cos\hat{\hat{\kappa}}_P\sin\hat{\hat{\phi}}_P\right)c_4\\-\left(\cos\hat{\hat{\kappa}}_P\cos\hat{\hat{\phi}}_P\right)c_5\end{bmatrix}+\cos\hat{\varphi}_{ijk}\cos\hat{\theta}_{ijk}\left[\left(\sin\hat{\hat{\phi}}_P\right)c_5-\left(\cos\hat{\hat{\omega}}_P\cos\hat{\hat{\phi}}_P\right)c_4+\left(\sin\hat{\hat{\omega}}_P\cos\hat{\hat{\phi}}_P\right)c_3\right],$$

$$a_{23}^{ang} = \sin\hat{\varphi}_{ijk}\begin{bmatrix}\left(\cos\hat{\hat{\omega}}_P\sin\hat{\hat{\kappa}}_P+\sin\hat{\hat{\omega}}_P\cos\hat{\hat{\kappa}}_P\sin\hat{\hat{\phi}}_P\right)c_7\\-\left(\sin\hat{\hat{\omega}}_P\sin\hat{\hat{\kappa}}_P-\cos\hat{\hat{\omega}}_P\cos\hat{\hat{\kappa}}_P\sin\hat{\hat{\phi}}_P\right)c_6\\+\left(\cos\hat{\hat{\kappa}}_P\cos\hat{\hat{\phi}}_P\right)c_8\end{bmatrix}+\cos\hat{\varphi}_{ijk}\cos\hat{\theta}_{ijk}\left[\left(-\sin\hat{\hat{\phi}}_P\right)c_8+\left(\cos\hat{\hat{\omega}}_P\cos\hat{\hat{\phi}}_P\right)c_6+\left(\sin\hat{\hat{\omega}}_P\cos\hat{\hat{\phi}}_P\right)c_7\right],$$

$$a_{24}^{ang} = \sin\hat{\varphi}_{ijk}\cos\hat{\hat{\kappa}}_P\cos\hat{\hat{\phi}}_P-\cos\hat{\varphi}_{ijk}\cos\hat{\theta}_{ijk}\sin\hat{\hat{\phi}}_P,$$

$$a_{25}^{ang} = \sin\hat{\varphi}_{ijk}\left(\cos\hat{\hat{\omega}}_P\sin\hat{\hat{\kappa}}_P-\sin\hat{\hat{\omega}}_P\cos\hat{\hat{\kappa}}_P\sin\hat{\hat{\phi}}_P\right)+\cos\hat{\varphi}_{ijk}\cos\hat{\theta}_{ijk}\left(\cos\hat{\hat{\phi}}_P\sin\hat{\hat{\omega}}_P\right),$$

$$a_{26}^{ang} = \sin\hat{\varphi}_{ijk}\left(\sin\hat{\hat{\omega}}_P\sin\hat{\hat{\kappa}}_P-\cos\hat{\hat{\omega}}_P\cos\hat{\hat{\kappa}}_P\sin\hat{\hat{\phi}}_P\right)-\cos\hat{\varphi}_{ijk}\cos\hat{\theta}_{ijk}\left(\cos\hat{\hat{\phi}}_P\cos\hat{\hat{\omega}}_P\right),$$

in which the parameters c_1 to c_8 are respectively:

$$c_1 = x_k\left(\sin\hat{\hat{\omega}}_P\sin\hat{\hat{\kappa}}_P-\cos\hat{\hat{\kappa}}_P\cos\hat{\hat{\omega}}_P\sin\hat{\hat{\phi}}_P\right)+y_k\left(\sin\hat{\hat{\omega}}_P\cos\hat{\hat{\kappa}}_P+\sin\hat{\hat{\kappa}}_P\cos\hat{\hat{\omega}}_P\sin\hat{\hat{\phi}}_P\right)+z_k\left(\cos\hat{\hat{\omega}}_P\cos\hat{\hat{\phi}}_P\right),$$

$$c_2 = x_k\left(\cos\hat{\hat{\omega}}_P\sin\hat{\hat{\kappa}}_P+\cos\hat{\hat{\kappa}}_P\sin\hat{\hat{\omega}}_P\sin\hat{\hat{\phi}}_P\right)+y_k\left(\cos\hat{\hat{\omega}}_P\cos\hat{\hat{\kappa}}_P-\sin\hat{\hat{\kappa}}_P\sin\hat{\hat{\omega}}_P\sin\hat{\hat{\phi}}_P\right)-z_k\left(\sin\hat{\hat{\omega}}_P\cos\hat{\hat{\phi}}_P\right),$$

$$c_3 = x_k\left(\cos\hat{\hat{\omega}}_P\cos\hat{\hat{\kappa}}_P-\sin\hat{\hat{\kappa}}_P\sin\hat{\hat{\omega}}_P\sin\hat{\hat{\phi}}_P\right)-y_k\left(\cos\hat{\hat{\omega}}_P\sin\hat{\hat{\kappa}}_P+\cos\hat{\hat{\kappa}}_P\sin\hat{\hat{\omega}}_P\sin\hat{\hat{\phi}}_P\right),$$

$$c_4 = x_k\left(\sin\hat{\hat{\omega}}_P\cos\hat{\hat{\kappa}}_P+\sin\hat{\hat{\kappa}}_P\cos\hat{\hat{\omega}}_P\sin\hat{\hat{\phi}}_P\right)-y_k\left(\cos\hat{\hat{\omega}}_P\sin\hat{\hat{\kappa}}_P+\cos\hat{\hat{\kappa}}_P\sin\hat{\hat{\omega}}_P\sin\hat{\hat{\phi}}_P\right),$$

$$c_5 = x_k\left(\sin\hat{\hat{\kappa}}_P\cos\hat{\hat{\phi}}_P\right)+y_k\left(\cos\hat{\hat{\kappa}}_P\cos\hat{\hat{\phi}}_P\right),\ c_6 = x_k\left(\cos\hat{\hat{\omega}}_P\cos\hat{\hat{\kappa}}_P\cos\hat{\hat{\phi}}_P\right)-y_k\left(\cos\hat{\hat{\omega}}_P\sin\hat{\hat{\kappa}}_P\cos\hat{\hat{\phi}}_P\right)+z_k\left(\cos\hat{\hat{\omega}}_P\sin\hat{\hat{\phi}}_P\right),$$

$$c_7 = x_k\left(\sin\hat{\hat{\omega}}_P\cos\hat{\hat{\kappa}}_P\cos\hat{\hat{\phi}}_P\right)-y_k\left(\sin\hat{\hat{\omega}}_P\sin\hat{\hat{\kappa}}_P\cos\hat{\hat{\phi}}_P\right)+z_k\left(\sin\hat{\hat{\omega}}_P\sin\hat{\hat{\phi}}_P\right),$$

$$c_8 = -x_k\left(\cos\hat{\hat{\kappa}}_P\sin\hat{\hat{\phi}}_P\right)+y_k\left(\sin\hat{\hat{\kappa}}_P\sin\hat{\hat{\phi}}_P\right)+z_k\left(\cos\hat{\hat{\phi}}_P\right),\ c_9 = x_k\left(\cos\hat{\hat{\kappa}}_P\cos\hat{\hat{\phi}}_P\right)-y_k\left(\sin\hat{\hat{\kappa}}_P\cos\hat{\hat{\phi}}_P\right)+z_k\sin\hat{\hat{\phi}}_P,$$

and $\boldsymbol{B}_{ij}^{ang} = \boldsymbol{A}_{ij}^{ang} * \hat{\hat{\boldsymbol{X}}} + \begin{bmatrix} b_1^{ang} \\ b_2^{ang} \end{bmatrix}$, with

$$b_1^{ang} = \cos\hat{\theta}_{ijk}\left[\begin{array}{l}\left(\sin\hat{\hat{\omega}}_P\cos\hat{\hat{\kappa}}_P+\cos\hat{\hat{\omega}}_P\sin\hat{\hat{\kappa}}_P\sin\hat{\hat{\phi}}_P\right)\left(\begin{array}{l}\hat{\hat{Z}}_P - Z_{0_{ij}} + \\ +x_k\left(\sin\hat{\hat{\omega}}_P\sin\hat{\hat{\kappa}}_P-\cos\hat{\hat{\kappa}}_P\cos\hat{\hat{\omega}}_P\sin\hat{\hat{\phi}}_P\right)+ \\ +y_k\left(\sin\hat{\hat{\omega}}_P\cos\hat{\hat{\kappa}}_P+\sin\hat{\hat{\kappa}}_P\cos\hat{\hat{\omega}}_P\sin\hat{\hat{\phi}}_P\right)+ \\ +z_k\left(\cos\hat{\hat{\omega}}_P\cos\hat{\hat{\phi}}_P\right)\end{array}\right)+ \\ +\left(\cos\hat{\hat{\omega}}_P\cos\hat{\hat{\kappa}}_P-\sin\hat{\hat{\omega}}_P\sin\hat{\hat{\kappa}}_P\sin\hat{\hat{\phi}}_P\right)\left(\begin{array}{l}\hat{\hat{Y}}_P - Y_{0_{ij}} + \\ +x_k\left(\cos\hat{\hat{\omega}}_P\sin\hat{\hat{\kappa}}_P+\cos\hat{\hat{\kappa}}_P\sin\hat{\hat{\omega}}_P\sin\hat{\hat{\phi}}_P\right)+ \\ +y_k\left(\cos\hat{\hat{\omega}}_P\cos\hat{\hat{\kappa}}_P-\sin\hat{\hat{\kappa}}_P\sin\hat{\hat{\omega}}_P\sin\hat{\hat{\phi}}_P\right)+ \\ -z_k\left(\sin\hat{\hat{\omega}}_P\cos\hat{\hat{\phi}}_P\right)\end{array}\right)+ \\ -\left(\sin\hat{\hat{\kappa}}_P\cos\hat{\hat{\phi}}_P\right)\left(\hat{\hat{X}}_P - X_{0_{ij}} + x_k\cos\hat{\hat{\kappa}}_P\cos\hat{\hat{\phi}}_P - y_k\sin\hat{\hat{\kappa}}_P\cos\hat{\hat{\phi}}_P + z_k\sin\hat{\hat{\phi}}_P\right)\end{array}\right]+$$

$$
\begin{aligned}
-\sin\hat{\theta}_{ijk}\Bigg[& \left(\sin\hat{\hat{\omega}}_P\cos\hat{\hat{\kappa}}_P-\cos\hat{\hat{\omega}}_P\cos\hat{\hat{\kappa}}_P\sin\hat{\hat{\phi}}_P\right)\begin{pmatrix}\hat{\hat{Z}}_P-Z_{0_{ij}}+\\ +x_k\left(\sin\hat{\hat{\omega}}_P\sin\hat{\hat{\kappa}}_P-\cos\hat{\hat{\kappa}}_P\cos\hat{\hat{\omega}}_P\sin\hat{\hat{\phi}}_P\right)+\\ +y_k\left(\sin\hat{\hat{\omega}}_P\cos\hat{\hat{\kappa}}_P+\sin\hat{\hat{\kappa}}_P\cos\hat{\hat{\omega}}_P\sin\hat{\hat{\phi}}_P\right)+\\ +z_k\left(\cos\hat{\hat{\omega}}_P\cos\hat{\hat{\phi}}_P\right)\end{pmatrix}+\\
& +\left(\cos\hat{\hat{\omega}}_P\sin\hat{\hat{\kappa}}_P+\sin\hat{\hat{\omega}}_P\cos\hat{\hat{\kappa}}_P\sin\hat{\hat{\phi}}_P\right)\begin{pmatrix}\hat{\hat{Y}}_P-Y_{0_{ij}}+\\ +x_k\left(\cos\hat{\hat{\omega}}_P\sin\hat{\hat{\kappa}}_P+\cos\hat{\hat{\kappa}}_P\sin\hat{\hat{\omega}}_P\sin\hat{\hat{\phi}}_P\right)+\\ +y_k\left(\cos\hat{\hat{\omega}}_P\cos\hat{\hat{\kappa}}_P-\sin\hat{\hat{\kappa}}_P\sin\hat{\hat{\omega}}_P\sin\hat{\hat{\phi}}_P\right)+\\ -z_k\left(\sin\hat{\hat{\omega}}_P\cos\hat{\hat{\phi}}_P\right)\end{pmatrix}+\\
& -\left(\cos\hat{\hat{\kappa}}_P\cos\hat{\hat{\phi}}_P\right)\left(\hat{\hat{X}}_P-X_{0_{ij}}+x_k\cos\hat{\hat{\kappa}}_P\cos\hat{\hat{\phi}}_P-y_k\sin\hat{\hat{\kappa}}_P\cos\hat{\hat{\phi}}_P+z_k\sin\hat{\hat{\phi}}_P\right)\Bigg]
\end{aligned}
$$

and

$$
\begin{aligned}
b_2^{ang}=\cos\hat{\varphi}_{ijk}\cos\hat{\theta}_{ijk}\Bigg[& \left(\cos\hat{\hat{\omega}}_P\cos\hat{\hat{\phi}}_P\right)\begin{pmatrix}\hat{\hat{Z}}_P-Z_{0_{ij}}+\\ +x_k\left(\sin\hat{\hat{\omega}}_P\sin\hat{\hat{\kappa}}_P-\cos\hat{\hat{\kappa}}_P\cos\hat{\hat{\omega}}_P\sin\hat{\hat{\phi}}_P\right)+\\ +y_k\left(\sin\hat{\hat{\omega}}_P\cos\hat{\hat{\kappa}}_P+\sin\hat{\hat{\kappa}}_P\cos\hat{\hat{\omega}}_P\sin\hat{\hat{\phi}}_P\right)+\\ +z_k\left(\cos\hat{\hat{\omega}}_P\cos\hat{\hat{\phi}}_P\right)\end{pmatrix}+\\
& -\left(\sin\hat{\hat{\omega}}_P\cos\hat{\hat{\phi}}_P\right)\begin{pmatrix}\hat{\hat{Y}}_P-Y_{0_{ij}}+\\ +x_k\left(\cos\hat{\hat{\omega}}_P\sin\hat{\hat{\kappa}}_P+\cos\hat{\hat{\kappa}}_P\sin\hat{\hat{\omega}}_P\sin\hat{\hat{\phi}}_P\right)+\\ +y_k\left(\cos\hat{\hat{\omega}}_P\cos\hat{\hat{\kappa}}_P-\sin\hat{\hat{\kappa}}_P\sin\hat{\hat{\omega}}_P\sin\hat{\hat{\phi}}_P\right)+\\ -z_k\left(\sin\hat{\hat{\omega}}_P\cos\hat{\hat{\phi}}_P\right)\end{pmatrix}+\\
& -\left(\sin\hat{\hat{\phi}}_P\right)\left(\hat{\hat{X}}_P-X_{0_{ij}}+x_k\cos\hat{\hat{\kappa}}_P\cos\hat{\hat{\phi}}_P-y_k\sin\hat{\hat{\kappa}}_P\cos\hat{\hat{\phi}}_P+z_k\sin\hat{\hat{\phi}}_P\right)\Bigg]
\end{aligned}
$$

$$
\begin{bmatrix}
\left(\sin\hat{\hat{\omega}}_P \sin\hat{\hat{\kappa}}_P - \cos\hat{\hat{\omega}}_P \cos\hat{\hat{\kappa}}_P \sin\hat{\hat{\phi}}_P\right)\begin{pmatrix}\hat{\hat{Z}}_P - Z_{0_{ij}} + \\ + x_k\left(\sin\hat{\hat{\omega}}_P \sin\hat{\hat{\kappa}}_P - \cos\hat{\hat{\kappa}}_P \cos\hat{\hat{\omega}}_P \sin\hat{\hat{\phi}}_P\right) + \\ + y_k\left(\sin\hat{\hat{\omega}}_P \cos\hat{\hat{\kappa}}_P + \sin\hat{\hat{\kappa}}_P \cos\hat{\hat{\omega}}_P \sin\hat{\hat{\phi}}_P\right) + \\ + z_k\left(\cos\hat{\hat{\omega}}_P \cos\hat{\hat{\phi}}_P\right)\end{pmatrix} + \\
-\sin\hat{\varphi}_{ijk}\left(+\left(\cos\hat{\hat{\omega}}_P \sin\hat{\hat{\kappa}}_P + \sin\hat{\hat{\omega}}_P \cos\hat{\hat{\kappa}}_P \sin\hat{\hat{\phi}}_P\right)\begin{pmatrix}\hat{\hat{Y}}_P - Y_{0_{ij}} + \\ + x_k\left(\cos\hat{\hat{\omega}}_P \sin\hat{\hat{\kappa}}_P + \cos\hat{\hat{\kappa}}_P \sin\hat{\hat{\omega}}_P \sin\hat{\hat{\phi}}_P\right) + \\ + y_k\left(\cos\hat{\hat{\omega}}_P \cos\hat{\hat{\kappa}}_P - \sin\hat{\hat{\kappa}}_P \sin\hat{\hat{\omega}}_P \sin\hat{\hat{\phi}}_P\right) + \\ - z_k\left(\sin\hat{\hat{\omega}}_P \cos\hat{\hat{\phi}}_P\right)\end{pmatrix} + \right. \\
\left. -\left(\cos\hat{\hat{\kappa}}_P \cos\hat{\hat{\phi}}_P\right)\left(\hat{\hat{X}}_P - X_{0_{ij}} + x_k \cos\hat{\hat{\kappa}}_P \cos\hat{\hat{\phi}}_P - y_k \sin\hat{\hat{\kappa}}_P \cos\hat{\hat{\phi}}_P + z_k \sin\hat{\hat{\phi}}_P\right)\right)
\end{bmatrix}.
$$

It can be noticed that the matrix expression in Eq. A12 is similar to the one related to distance sensors (in Eq. A6). However, the latter encapsulates a single equation while the former encapsulates two equations.

A.3 Integrated sensors

The (inertial) integrated probe sensors (i.e., two-axis inclinometer and compass) may contribute to estimate the three orientation angles of the probe (i.e., ω_P, ϕ_P and κ_P), although not directly. Precisely, these integrated sensors perform angular measurements referring to a ground-referenced coordinate system ($O_IX_IY_IZ_I$), with arbitrary origin (O_I), Z_I axis coinciding with the vertical to the ground plane, and X_I axis pointing toward the magnetic north.

The two reference systems $O_IX_IY_IZ_I$ and $OXYZ$ are fixed in the 3D space and linked by a rototranslation; $\boldsymbol{R_{off}}$ is the relevant rotation matrix, whose elements are functions of the three rotation angles ω_{off}, ϕ_{off} and κ_{off}, representing the rotation of $O_IX_IY_IZ_I$ with respect to $OXYZ$ (see the schematic representation in Fig. A.4).

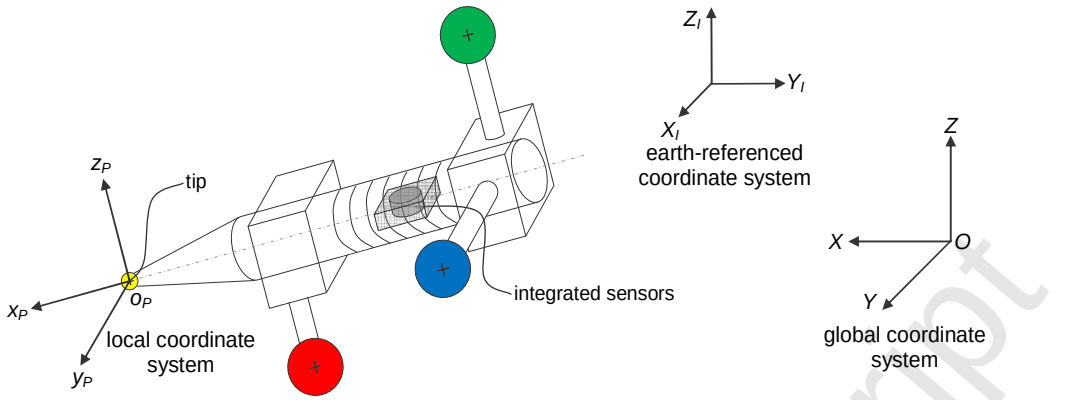

Fig. A.4. Schematic representation of the (local) coordinate system, integral the multi-target probe ($o_Px_Py_Pz_P$), and of two other (fixed) coordinate systems: the earth-referenced related to the integrated sensors ($o_Ix_Iy_Iz_I$) and the global coordinate system ($OXYZ$).

Assuming that the compass estimates the probe rotations (κ_I) around the vertical axis (Z_I) and the two-axis inclinometer estimates the probe rotations (ω_I and ϕ_I) with respect to the horizontal plan X_IY_I, $\boldsymbol{R_P}$ can be expressed as:

$$\boldsymbol{R}_P = \boldsymbol{R}_{off} \cdot \boldsymbol{R}_I \,, \tag{A13}$$

where $\boldsymbol{R_I}$ is another rotation matrix, whose elements are functions of the three rotation parameters ω_I, ϕ_I and κ_I , measured by the probe's integrated sensors (see the scheme in Fig. A.5).

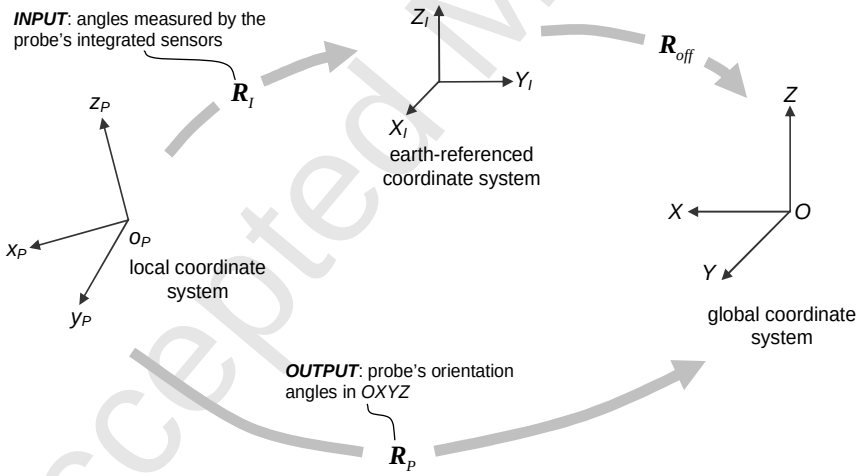

Fig. A.5. Schematic representation of the relationship in Eq. A13.

Since Eq. A13 is a 3x3 matrix function, it can be reformulated as a vector, function of the three angles ω_P, ϕ_P, κ_P:

$$\begin{bmatrix} \boldsymbol{R}_P - \boldsymbol{R}_{off}\boldsymbol{R}_I & \begin{bmatrix}0&0&0\\0&0&0\\0&0&0\end{bmatrix} & \begin{bmatrix}0&0&0\\0&0&0\\0&0&0\end{bmatrix} \\ \begin{bmatrix}0&0&0\\0&0&0\\0&0&0\end{bmatrix} & \boldsymbol{R}_P - \boldsymbol{R}_{off}\boldsymbol{R}_I & \begin{bmatrix}0&0&0\\0&0&0\\0&0&0\end{bmatrix} \\ \begin{bmatrix}0&0&0\\0&0&0\\0&0&0\end{bmatrix} & \begin{bmatrix}0&0&0\\0&0&0\\0&0&0\end{bmatrix} & \boldsymbol{R}_P - \boldsymbol{R}_{off}\boldsymbol{R}_I \end{bmatrix} \begin{bmatrix}\begin{bmatrix}1\\0\\0\end{bmatrix}\\ \begin{bmatrix}0\\1\\0\end{bmatrix}\\ \begin{bmatrix}0\\0\\1\end{bmatrix}\end{bmatrix} = \begin{bmatrix}\begin{bmatrix}0\\0\\0\end{bmatrix}\\ \begin{bmatrix}0\\0\\0\end{bmatrix}\\ \begin{bmatrix}0\\0\\0\end{bmatrix}\end{bmatrix}. \tag{A14}$$

The nine relationships in Eq. A14 can be linearized (e.g., by a first order Taylor expansion, using the Matlab's symbolic-calculation function "functionalDerivative".) with respect to the six parameters in $\boldsymbol{X}$ and expressed in matrix form, according to the following linearized model:

$$\boldsymbol{A}_{ij}^{\text{int}} \cdot \boldsymbol{X} - \boldsymbol{B}_{ij}^{\text{int}} = \boldsymbol{0}\,, \tag{A15}$$

being

$$\boldsymbol{A}_{ij}^{int} = \begin{bmatrix} a_{11}^{int} & a_{12}^{int} & a_{13}^{int} & a_{14}^{int} & a_{15}^{int} & a_{16}^{int} & a_{17}^{int} & a_{18}^{int} & a_{19}^{int} \\ a_{21}^{int} & a_{22}^{int} & a_{23}^{int} & a_{24}^{int} & a_{25}^{int} & a_{26}^{int} & a_{27}^{int} & a_{28}^{int} & a_{29}^{int} \\ a_{31}^{int} & a_{32}^{int} & a_{33}^{int} & a_{34}^{int} & a_{35}^{int} & a_{36}^{int} & a_{37}^{int} & a_{38}^{int} & a_{39}^{int} \\ a_{41}^{int} & a_{42}^{int} & a_{43}^{int} & a_{44}^{int} & a_{45}^{int} & a_{46}^{int} & a_{47}^{int} & a_{48}^{int} & a_{49}^{int} \\ a_{51}^{int} & a_{52}^{int} & a_{53}^{int} & a_{54}^{int} & a_{55}^{int} & a_{56}^{int} & a_{57}^{int} & a_{58}^{int} & a_{59}^{int} \\ a_{61}^{int} & a_{62}^{int} & a_{63}^{int} & a_{64}^{int} & a_{65}^{int} & a_{66}^{int} & a_{67}^{int} & a_{68}^{int} & a_{69}^{int} \end{bmatrix}, \tag{A16}$$

where

$a_{11}^{int} = 0,$

$a_{12}^{int} = -\cos\hat{\phi}_P \sin\hat{\kappa}_P,$

$a_{13}^{int} = -\sin\hat{\phi}_P \cos\hat{\kappa}_P,$

$a_{14}^{int} = 0,$

$a_{15}^{int} = 0,$

$a_{16}^{int} = 0,$

$a_{21}^{int} = \cos\hat{\kappa}_P \cos\hat{\omega}_P \sin\hat{\phi}_P - \sin\hat{\kappa}_P \sin\hat{\omega}_P,$

$a_{22}^{int} = \cos\hat{\kappa}_P \cos\hat{\omega}_P - \sin\hat{\phi}_P \sin\hat{\kappa}_P \sin\hat{\omega}_P,$

$a_{23}^{int} = \cos\hat{\kappa}_P \cos\hat{\phi}_P \sin\hat{\omega}_P,$

$a_{24}^{int} = 0,$

$a_{25}^{int} = 0,$

$a_{26}^{int} = 0,$

$a_{31}^{int} = \sin\hat{\kappa}_P \cos\hat{\omega}_P + \sin\hat{\phi}_P \cos\hat{\kappa}_P \sin\hat{\omega}_P,$

$a_{32}^{int} = \cos\hat{\kappa}_P \sin\hat{\omega}_P + \sin\hat{\phi}_P \sin\hat{\kappa}_P \cos\hat{\omega}_P,$

$a_{33}^{int} = -\cos\hat{\kappa}_P \cos\hat{\omega}_P \cos\hat{\phi}_P,$

$a_{34}^{int} = 0,$

$a_{35}^{int} = 0,$

$a_{36}^{int} = 0,$

$a_{41}^{int} = 0,$

$a_{42}^{int} = -\cos\hat{\kappa}_P \cos\hat{\phi}_P,$

$a_{43}^{int} = \sin\hat{\kappa}_P \sin\hat{\phi}_P,$

$a_{44}^{int} = 0,$

$a_{45}^{int} = 0,$

$a_{46}^{int} = 0,$

$a_{51}^{int} = -\cos\hat{\kappa}_P \sin\hat{\omega}_P - \sin\hat{\phi}_P \sin\hat{\kappa}_P \cos\hat{\omega}_P,$

$a_{52}^{int} = -\sin\hat{\kappa}_P \cos\hat{\omega}_P - \sin\hat{\phi}_P \cos\hat{\kappa}_P \sin\hat{\omega}_P,$

$a_{53}^{int} = -\cos\hat{\phi}_P \sin\hat{\kappa}_P \sin\hat{\omega}_P,$

$a_{54}^{int} = 0,$

$a_{55}^{int} = 0,$

$a_{56}^{int} = 0,$

$a_{61}^{int} = \cos\hat{\kappa}_P \cos\hat{\omega}_P - \sin\hat{\phi}_P \sin\hat{\kappa}_P \sin\hat{\omega}_P,$

$a_{62}^{int} = \cos\hat{\kappa}_P \cos\hat{\omega}_P \sin\hat{\phi}_P - \sin\hat{\kappa}_P \sin\hat{\omega}_P,$

$a_{63}^{int} = \sin\hat{\kappa}_P \cos\hat{\omega}_P \cos\hat{\phi}_P,$

$a_{64}^{int} = 0,$

$a_{65}^{int} = 0,$

$a_{66}^{int} = 0,$

$a_{71}^{int} = 0,$

$a_{72}^{int} = -\sin\hat{\kappa}_P \cos\hat{\phi}_P,$

$a_{73}^{int} = -\cos\hat{\kappa}_P \sin\hat{\phi}_P,$

$a_{74}^{int} = 0,$

$a_{75}^{int} = 0,$

$a_{76}^{int} = 0,$

$a_{81}^{int} = \cos\hat{\kappa}_P \cos\hat{\omega}_P \sin\hat{\phi}_P - \sin\hat{\kappa}_P \sin\hat{\omega}_P,$

$a_{82}^{int} = \cos\hat{\hat{\kappa}}_P \cos\hat{\hat{\omega}}_P - \sin\hat{\hat{\phi}}_P \sin\hat{\hat{\kappa}}_P \sin\hat{\hat{\omega}}_P$,
$a_{83}^{int} = \cos\hat{\hat{\kappa}}_P \cos\hat{\hat{\phi}}_P \sin\hat{\hat{\omega}}_P$,
$a_{84}^{int} = 0$,
$a_{85}^{int} = 0$,
$a_{86}^{int} = 0$,
$a_{91}^{int} = \sin\hat{\hat{\kappa}}_P \cos\hat{\hat{\omega}}_P + \sin\hat{\hat{\phi}}_P \cos\hat{\hat{\kappa}}_P \sin\hat{\hat{\omega}}_P$,
$a_{92}^{int} = \cos\hat{\hat{\kappa}}_P \sin\hat{\hat{\omega}}_P + \sin\hat{\hat{\phi}}_P \sin\hat{\hat{\kappa}}_P \cos\hat{\hat{\omega}}_P$,
$a_{93}^{int} = -\cos\hat{\hat{\kappa}}_P \cos\hat{\hat{\phi}}_P \cos\hat{\hat{\omega}}_P$,
$a_{94}^{int} = 0$,
$a_{95}^{int} = 0$,
$a_{96}^{int} = 0$,

and $\boldsymbol{B}_{ij}^{int} = \boldsymbol{A}_{ij}^{int} * \hat{\hat{\boldsymbol{X}}} + \left[b_1^{int}\ b_2^{int}\ b_3^{int}\ b_4^{int}\ b_5^{int}\ b_6^{int}\ b_7^{int}\ b_8^{int}\ b_9^{int}\right]^T$, where

$b_1^{int} = \sin\hat{\phi}_{off} d_8 - \cos\hat{\hat{\kappa}}_P \cos\hat{\hat{\phi}}_P - \cos\hat{\phi}_{off} \sin\hat{\kappa}_{off} d_1 + \cos\hat{\kappa}_I \cos\hat{\kappa}_{off} \cos\hat{\phi}_I \cos\hat{\phi}_{off}$,
$b_2^{int} = d_1 d_3 - \cos\hat{\hat{\omega}}_P \sin\hat{\hat{\kappa}}_P - \cos\hat{\phi}_{off} \sin\hat{\omega}_{off} d_8 + \cos\hat{\kappa}_I \cos\hat{\phi}_I d_5 - \cos\hat{\hat{\kappa}}_P \sin\hat{\hat{\omega}}_P \sin\hat{\hat{\phi}}_P$,
$b_3^{int} = d_1 d_4 - \sin\hat{\hat{\omega}}_P \sin\hat{\hat{\kappa}}_P + \cos\hat{\phi}_{off} \cos\hat{\omega}_{off} d_8 + \cos\hat{\kappa}_I \cos\hat{\phi}_I d_6 + \cos\hat{\hat{\kappa}}_P \cos\hat{\hat{\omega}}_P \sin\hat{\hat{\phi}}_P$,
$b_4^{int} = \sin\hat{\phi}_{off} d_7 + \sin\hat{\hat{\kappa}}_P \cos\hat{\hat{\phi}}_P - \cos\hat{\phi}_{off} \sin\hat{\kappa}_{off} d_2 - \sin\hat{\kappa}_I \cos\hat{\kappa}_{off} \cos\hat{\phi}_I \cos\hat{\phi}_{off}$,
$b_5^{int} = d_2 d_3 - \cos\hat{\hat{\omega}}_P \cos\hat{\hat{\kappa}}_P - \cos\hat{\phi}_{off} \sin\hat{\omega}_{off} d_7 - \sin\hat{\kappa}_I \cos\hat{\phi}_I d_5 + \sin\hat{\hat{\omega}}_P \sin\hat{\hat{\kappa}}_P \sin\hat{\hat{\phi}}_P$,
$b_6^{int} = d_2 d_4 - \sin\hat{\hat{\omega}}_P \cos\hat{\hat{\kappa}}_P + \cos\hat{\phi}_{off} \cos\hat{\omega}_{off} d_7 - \sin\hat{\kappa}_I \cos\hat{\phi}_I d_6 - \cos\hat{\hat{\omega}}_P \sin\hat{\hat{\kappa}}_P \sin\hat{\hat{\phi}}_P$,
$b_7^{int} = \sin\hat{\phi}_{off} d_8 - \cos\hat{\hat{\kappa}}_P \cos\hat{\hat{\phi}}_P - \cos\hat{\phi}_{off} \sin\hat{\kappa}_{off} d_1 + \cos\hat{\kappa}_I \cos\hat{\kappa}_{off} \cos\hat{\phi}_I \cos\hat{\phi}_{off}$,
$b_8^{int} = d_1 d_3 - \cos\hat{\hat{\omega}}_P \sin\hat{\hat{\kappa}}_P - \cos\hat{\phi}_{off} \sin\hat{\omega}_{off} d_8 + \cos\hat{\kappa}_I \cos\hat{\phi}_I d_5 - \sin\hat{\hat{\omega}}_P \cos\hat{\hat{\kappa}}_P \sin\hat{\hat{\phi}}_P$,
$b_9^{int} = d_1 d_4 - \sin\hat{\hat{\omega}}_P \sin\hat{\hat{\kappa}}_P + \cos\hat{\phi}_{off} \cos\hat{\omega}_{off} d_8 + \cos\hat{\kappa}_I \cos\hat{\phi}_I d_6 + \cos\hat{\hat{\omega}}_P \cos\hat{\hat{\kappa}}_P \sin\hat{\hat{\phi}}_P$,

and

$d_1 = \left(\sin\hat{\kappa}_I \cos\hat{\omega}_I + \cos\hat{\kappa}_I \sin\hat{\omega}_I \sin\hat{\phi}_I\right)$, $d_2 = \left(\cos\hat{\kappa}_I \cos\hat{\omega}_I - \sin\hat{\kappa}_I \sin\hat{\omega}_I \sin\hat{\phi}_I\right)$, $d_3 = \left(\cos\hat{\kappa}_{off} \cos\hat{\omega}_{off} - \sin\hat{\kappa}_{off} \sin\hat{\omega}_{off} \sin\hat{\phi}_{off}\right)$,
$d_4 = \left(\cos\hat{\kappa}_{off} \sin\hat{\omega}_{off} + \sin\hat{\kappa}_{off} \cos\hat{\omega}_{off} \sin\hat{\phi}_{off}\right)$, $d_5 = \left(\sin\hat{\kappa}_{off} \cos\hat{\omega}_{off} + \cos\hat{\kappa}_{off} \sin\hat{\omega}_{off} \sin\hat{\phi}_{off}\right)$,
$d_6 = \left(\sin\hat{\kappa}_{off} \sin\hat{\omega}_{off} - \cos\hat{\kappa}_{off} \cos\hat{\omega}_{off} \sin\hat{\phi}_{off}\right)$, $d_7 = \left(\cos\hat{\kappa}_I \sin\hat{\omega}_I + \sin\hat{\kappa}_I \cos\hat{\omega}_I \sin\hat{\phi}_I\right)$, $d_8 = \left(\sin\hat{\kappa}_I \sin\hat{\omega}_I - \cos\hat{\kappa}_I \cos\hat{\omega}_I \sin\hat{\phi}_I\right)$,

$\hat{\omega}_I, \hat{\phi}_I, \hat{\kappa}_I$ and $\hat{\omega}_{off}, \hat{\phi}_{off}, \hat{\kappa}_{off}$ being respectively the estimates of the angles $\omega_I, \phi_I, \kappa_I$ and $\omega_{off}, \phi_{off}, \kappa_{off}$.

A.4 Weighting and solution

Considering a generic combination of LVM systems equipped with distance and/or angular sensors, and a probe with multiple targets and integrated sensors (inclinometer and compass), the resulting linearized target-localization model is:

$$\boldsymbol{A} \cdot \boldsymbol{X} - \boldsymbol{B} = \begin{bmatrix} \boldsymbol{A}^{dist} \\ \boldsymbol{A}^{ang} \\ \boldsymbol{A}^{int} \end{bmatrix} \cdot \boldsymbol{X} - \begin{bmatrix} \boldsymbol{B}^{dist} \\ \boldsymbol{B}^{ang} \\ \boldsymbol{B}^{int} \end{bmatrix} = \boldsymbol{0}, \tag{A17}$$

where blocks $\boldsymbol{A}^{dist}$, $\boldsymbol{A}^{ang}$, $\boldsymbol{B}^{dist}$ and $\boldsymbol{B}^{ang}$ are defined as:

$$\boldsymbol{A}^{dist} = \begin{bmatrix} \vdots \\ \boldsymbol{A}_{ijk}^{dist} \\ \vdots \end{bmatrix}_{ijk \in I^{dist}}, \quad \boldsymbol{A}^{ang} = \begin{bmatrix} \vdots \\ \boldsymbol{A}_{ijk}^{ang} \\ \vdots \end{bmatrix}_{ijk \in I^{ang}}, \quad \boldsymbol{B}^{dist} = \begin{bmatrix} \vdots \\ \boldsymbol{B}_{ijk}^{dist} \\ \vdots \end{bmatrix}_{ijk \in I^{dist}}, \quad \boldsymbol{B}^{ang} = \begin{bmatrix} \vdots \\ \boldsymbol{B}_{ijk}^{ang} \\ \vdots \end{bmatrix}_{ijk \in I^{ang}},$$

where I^{dist} and I^{ang} are the sets of index-pair values (*ijk*) relating to the *ij*-th distance/angular sensors seeing the *k*-th target.

All the equations of the system in Eq. A17 are referenced to the global Cartesian coordinate system, *OXYZ*. As seen before, these equations include the roto-translation transformations to switch from other reference systems – e.g., the local reference system related to each distributed sensor ($o_{ij}x_{ij}y_{ij}z_{ij}$), that one related to the probe ($o_Px_Py_Pz_P$), or the ground-referenced system related to the integrated probe sensors – to *OXYZ*. In summary, the variables that appear in the system in Eq. A17 can be grouped into two families, i.e., *known* and *unknown*, as shown in Fig. A.6.

Known variables

- Spatial position $X_{0_{ij}}, Y_{0_{ij}}, Z_{0_{ij}}$ and orientation ω_{ij}, ϕ_{ij}, κ_{ij} of the *ij*-th distributed sensor; these data may result from initial calibration/alignment processes;
- Relative position x_k, y_k, z_k of the *k*-th probe target with respect to the tip; these data may result form an initial probe-calibration process.
- Rotations ω_{off}, ϕ_{off}, κ_{off} of the earth-referenced system – related to the inertial sensors integrated into the probe – with respect to *OXYZ*; these data may result from an initial calibration process;
- Distance d_{ijk} and/or angular φ_{ijk}, θ_{ijk} measurements between the *ij*-th sensor and the *k*-th probe target; these data are captured in each probe localization.
- Local angular measurements ω_I, ϕ_I, κ_I of the inertial sensors integrated into the probe; these data are captured in each probe localization.

Unknown variables

- Spatial position X_P, Y_P, Z_P and orientation ω_P, ϕ_P, κ_P of the probe, which represent the output of the probe-localization problem.

Fig. A.6. Summary of (known and unknown) variables in a generic probe-localization problem.

The system in Eq. 17 can be solved when at least six (independent) equations are available (e.g., one target is seen by at least two distance sensors, while two other targets are seen by at least one angular sensor). Since this system is generally overdefined (more equations than unknown parameters), there are several possible solution approaches, ranging from those based on the iterative minimization of a suitable error function (Franceschini et al., 2014) to those based on the *Least Squares* method (Wolberg, 2005).

It is worth remarking that the equations of the system may differently contribute to the uncertainty in the localization of the probe. Specifically, the main factors affecting this uncertainty are:

- *Uncertainty in the position/orientation of the distributed sensors* ($\hat{X}_{0_{ij}}, \hat{Y}_{0_{ij}}, \hat{Z}_{0_{ij}}$, $\hat{\omega}_{ij}$, $\hat{\phi}_{ij}$, $\hat{\kappa}_{ij}$) and *uncertainty in the mutual orientation of* $O_IX_IY_IZ_I$ and *OXYZ* (i.e., $\hat{\omega}_{off}$, $\hat{\phi}_{off}$, $\hat{\kappa}_{off}$), resulting from initial calibration process(es);
- *Uncertainty in the local measurements* ($\hat{d}_{ijk}$, $\hat{\theta}_{ijk}$ and $\hat{\varphi}_{ijk}$) *by the distributed sensors*, which generally depends on their metrological characteristics;
- *Relative position* between each probe target (T_k) and each *ij*-th distributed sensor; e.g., assuming that the uncertainty in angular measurements is fixed, the uncertainty in the

localization of P will tend to increase proportionally to the *distance* between T_k and the angular sensors (Maisano and Mastrogiacomo, 2016).

- *Uncertainty in the measurements* ($\hat{\omega}_I$, $\hat{\phi}_I$ and $\hat{\kappa}_I$) *by the probe's integrated sensors*, which depends on their metrological characteristics.
- *Uncertainty in the relative position of the probe targets* ($\hat{x}_k$, $\hat{y}_k$ and $\hat{z}_k$), *with respect to the probe tip* (P).

For the above reasons, the sensors that mostly contribute to uncertainty in the localization of P are the less accurate and/or the more distant from P.

Returning to the system in Eq. A17, it would be appropriate to solve it, giving greater weight to the contributions from equations that produce less uncertainty and *vice versa*. To this purpose, an elegant and practical method is that of the *Generalized Least Squares* (GLS) (Kariya and Kurata, 2004), in which a weight matrix ($\boldsymbol{W}$), which takes into account the uncertainty produced by the equations of the system, is defined. One of the more practical ways to define $\boldsymbol{W}$ is applying the *Multivariate Law of Propagation of Uncertainty* (MLPU) to the system in Eq. A17, referring to the parameters affected by uncertainty (Hall, 2004), which are collected in a vector $\boldsymbol{\xi}$:

$$\boldsymbol{\xi} = \begin{bmatrix} \boldsymbol{\xi}_{dist} \\ \boldsymbol{\xi}_{ang} \\ \boldsymbol{\xi}_{int} \end{bmatrix} = \begin{bmatrix} \begin{bmatrix} \boldsymbol{\xi}_{dist}^{calibr} \\ \boldsymbol{\xi}_{dist}^{meas} \end{bmatrix} \\ \begin{bmatrix} \boldsymbol{\xi}_{ang}^{calibr} \\ \boldsymbol{\xi}_{ang}^{meas} \end{bmatrix} \\ \begin{bmatrix} \boldsymbol{\xi}_{int}^{calibr} \\ \boldsymbol{\xi}_{int}^{meas} \end{bmatrix} \end{bmatrix}. \tag{A18}$$

Precisely, the calibration parameters of the distributed sensors (involved in the measurement) are contained into the sub-vectors $\boldsymbol{\xi}_{dist}^{calibr}$ and $\boldsymbol{\xi}_{ang}^{calibr}$, referring to distance and angular measurements respectively, while those of the integrated sensors are contained into $\boldsymbol{\xi}_{int}^{calibr}$. On the other hand, the local measurements by distributed sensors are contained in the sub-vectors $\boldsymbol{\xi}_{dist}^{meas}$ and $\boldsymbol{\xi}_{ang}^{meas}$ (for distance and angular sensors respectively); similarly, the measurements by integrated sensors are included in the sub-vector $\boldsymbol{\xi}_{int}^{meas}$. More in detail:

$$\boldsymbol{\xi}_{dist} = \begin{bmatrix} \vdots \\ \begin{bmatrix} \xi_{dist}^{calibr} \\ \xi_{dist}^{meas} \end{bmatrix}_{ijk \in I^{dist}} \\ \vdots \end{bmatrix} = \begin{bmatrix} \vdots \\ \begin{bmatrix} \begin{bmatrix} X_{0_{ij}} \\ Y_{0_{ij}} \\ Z_{0_{ij}} \\ \phi_{ij} \\ \kappa_{ij} \\ \omega_{ij} \end{bmatrix} \\ \begin{bmatrix} x_k \\ y_k \\ z_k \end{bmatrix} \\ d_{ijk} \end{bmatrix}_{ijk \in I^{dist}} \\ \vdots \end{bmatrix}, \quad \boldsymbol{\xi}_{ang} = \begin{bmatrix} \vdots \\ \begin{bmatrix} \xi_{ang}^{calibr} \\ \xi_{ang}^{meas} \end{bmatrix}_{ijk \in I^{ang}} \\ \vdots \end{bmatrix} = \begin{bmatrix} \vdots \\ \begin{bmatrix} \begin{bmatrix} X_{0_{ij}} \\ Y_{0_{ij}} \\ Z_{0_{ij}} \\ \phi_{ij} \\ \kappa_{ij} \\ \omega_{ij} \end{bmatrix} \\ \begin{bmatrix} x_k \\ y_k \\ z_k \end{bmatrix} \\ \begin{bmatrix} \theta_{ijk} \\ \varphi_{ijk} \end{bmatrix} \end{bmatrix}_{ijk \in I^{ang}} \\ \vdots \end{bmatrix} \text{ and}$$

$$\boldsymbol{\xi}_{int} = \begin{bmatrix} \xi_{int}^{calibr} \\ \xi_{int}^{meas} \end{bmatrix} = \begin{bmatrix} \begin{bmatrix} \hat{\phi}_{off} \\ \hat{\kappa}_{off} \\ \hat{\omega}_{off} \end{bmatrix} \\ \begin{bmatrix} \hat{\phi}_I \\ \hat{\kappa}_I \\ \hat{\omega}_I \end{bmatrix} \end{bmatrix}.$$

$\boldsymbol{W}$ can be determined propagating the uncertainty of the equations in Eq. A17 with respect to the elements in $\boldsymbol{\xi}$:

$$\boldsymbol{W} = \left[\boldsymbol{J}^T \cdot \Sigma_{\xi} \cdot \boldsymbol{J}\right]^{-1}. \tag{A19}$$

This operation can be (at least partly) automated, using the Matlab's symbolic-calculation function "functionalDerivative".

Focusing the attention on the elements in the second member of Eq. A19, $\boldsymbol{J}$ is the Jacobian (block-diagonal) matrix containing the partial derivatives of the elements of the equations in the first member of Eq. A17 with respect to the elements in $\boldsymbol{\xi}$:

$$\boldsymbol{J} = \begin{bmatrix} \boldsymbol{J}^{dist} & \boldsymbol{0} & \boldsymbol{0} \\ \boldsymbol{0} & \boldsymbol{J}^{ang} & \boldsymbol{0} \\ \boldsymbol{0} & \boldsymbol{0} & \boldsymbol{J}^{int} \end{bmatrix}, \tag{A20}$$

where, $\boldsymbol{J}^{dist} = \begin{bmatrix} \ddots & & \boldsymbol{0} \\ & \boldsymbol{J}_{ijk}^{dist} & \\ \boldsymbol{0} & & \ddots \end{bmatrix}_{ijk \in I^{dist}}$, $\boldsymbol{J}^{ang} = \begin{bmatrix} \ddots & & \boldsymbol{0} \\ & \boldsymbol{J}_{ijk}^{ang} & \\ \boldsymbol{0} & & \ddots \end{bmatrix}_{ijk \in I^{ang}}$.

$\boldsymbol{J}_{ijk}^{dist}$ is defined as the Jacobian matrix containing the partial derivatives of the elements of the equations in the first member of Eq. A17 with respect to the elements in $\boldsymbol{\xi}_{dist}$:

$$\boldsymbol{J}_{ijk}^{dist} = \begin{bmatrix} j_1^{dist} & j_2^{dist} & j_3^{dist} & j_4^{dist} & j_5^{dist} & j_6^{dist} & j_7^{dist} & j_8^{dist} & j_9^{dist} & j_{10}^{dist} \end{bmatrix}, \tag{A21}$$

where

$$j_1^{dist} = \left[-2\left(\hat{\hat{X}}_P - X_{0_{ij}} + x_k \cos\hat{\hat{\kappa}}_P \cos\hat{\hat{\phi}}_P - y_k \sin\hat{\hat{\kappa}}_P \cos\hat{\hat{\phi}}_P + z_k \sin\hat{\hat{\phi}}_P \right) \right],$$

$$j_2^{dist} = \left[-2\left(\hat{\hat{Y}}_P - Y_{0_{ij}} + x_k\left(\cos\hat{\hat{\omega}}_P \sin\hat{\hat{\kappa}}_P + \cos\hat{\hat{\kappa}}_P \sin\hat{\hat{\omega}}_P \sin\hat{\hat{\phi}}_P \right) + y_k\left(\cos\hat{\hat{\omega}}_P \cos\hat{\hat{\kappa}}_P - \sin\hat{\hat{\kappa}}_P \sin\hat{\hat{\omega}}_P \sin\hat{\hat{\phi}}_P \right) - z_k\left(\sin\hat{\hat{\omega}}_P \cos\hat{\hat{\phi}}_P \right) \right) \right],$$

$$j_3^{dist} = \left[-2\left(\hat{\hat{Z}}_P - Z_{0_{ij}} + x_k\left(\sin\hat{\hat{\omega}}_P \sin\hat{\hat{\kappa}}_P - \cos\hat{\hat{\kappa}}_P \cos\hat{\hat{\omega}}_P \sin\hat{\hat{\phi}}_P \right) + y_k\left(\sin\hat{\hat{\omega}}_P \cos\hat{\hat{\kappa}}_P + \sin\hat{\hat{\kappa}}_P \cos\hat{\hat{\omega}}_P \sin\hat{\hat{\phi}}_P \right) + z_k\left(\cos\hat{\hat{\omega}}_P \cos\hat{\hat{\phi}}_P \right) \right) \right],$$

$$j_4^{dist} = 0,\ j_5^{dist} = 0,\ j_6^{dist} = 0,$$

$$j_7^{dist} = 2\left(\sin\hat{\hat{\kappa}}_P \sin\hat{\hat{\omega}}_P - \cos\hat{\hat{\kappa}}_P \cos\hat{\hat{\omega}}_P \sin\hat{\hat{\phi}}_P \right)\left(\hat{\hat{Z}}_P - Z_{0_{ij}} + x_k\left(\sin\hat{\hat{\omega}}_P \sin\hat{\hat{\kappa}}_P - \cos\hat{\hat{\kappa}}_P \cos\hat{\hat{\omega}}_P \sin\hat{\hat{\phi}}_P \right) + y_k\left(\sin\hat{\hat{\omega}}_P \cos\hat{\hat{\kappa}}_P + \sin\hat{\hat{\kappa}}_P \cos\hat{\hat{\omega}}_P \sin\hat{\hat{\phi}}_P \right) + z_k\left(\cos\hat{\hat{\omega}}_P \cos\hat{\hat{\phi}}_P \right) \right) +$$
$$+ 2\left(\sin\hat{\hat{\kappa}}_P \cos\hat{\hat{\omega}}_P + \cos\hat{\hat{\kappa}}_P \sin\hat{\hat{\omega}}_P \sin\hat{\hat{\phi}}_P \right)\left(\hat{\hat{Y}}_P - Y_{0_{ij}} + x_k\left(\cos\hat{\hat{\omega}}_P \sin\hat{\hat{\kappa}}_P + \cos\hat{\hat{\kappa}}_P \sin\hat{\hat{\omega}}_P \sin\hat{\hat{\phi}}_P \right) + y_k\left(\cos\hat{\hat{\omega}}_P \cos\hat{\hat{\kappa}}_P - \sin\hat{\hat{\kappa}}_P \sin\hat{\hat{\omega}}_P \sin\hat{\hat{\phi}}_P \right) - z_k\left(\sin\hat{\hat{\omega}}_P \cos\hat{\hat{\phi}}_P \right) \right) +$$
$$+ 2\left(\cos\hat{\hat{\kappa}}_P \cos\hat{\hat{\phi}}_P \right)\left(\hat{\hat{X}}_P - X_{0_{ij}} + x_k \cos\hat{\hat{\kappa}}_P \cos\hat{\hat{\phi}}_P - y_k \sin\hat{\hat{\kappa}}_P \cos\hat{\hat{\phi}}_P + z_k \sin\hat{\hat{\phi}}_P \right),$$

$$j_8^{dist} = 2\left(\cos\hat{\hat{\kappa}}_P \sin\hat{\hat{\omega}}_P + \sin\hat{\hat{\kappa}}_P \cos\hat{\hat{\omega}}_P \sin\hat{\hat{\phi}}_P \right)\left(\hat{\hat{Z}}_P - Z_{0_{ij}} + x_k\left(\sin\hat{\hat{\omega}}_P \sin\hat{\hat{\kappa}}_P - \cos\hat{\hat{\kappa}}_P \cos\hat{\hat{\omega}}_P \sin\hat{\hat{\phi}}_P \right) + y_k\left(\sin\hat{\hat{\omega}}_P \cos\hat{\hat{\kappa}}_P + \sin\hat{\hat{\kappa}}_P \cos\hat{\hat{\omega}}_P \sin\hat{\hat{\phi}}_P \right) + z_k\left(\cos\hat{\hat{\omega}}_P \cos\hat{\hat{\phi}}_P \right) \right) +$$
$$+ 2\left(\cos\hat{\hat{\kappa}}_P \cos\hat{\hat{\omega}}_P - \sin\hat{\hat{\kappa}}_P \sin\hat{\hat{\omega}}_P \sin\hat{\hat{\phi}}_P \right)\left(\hat{\hat{Y}}_P - Y_{0_{ij}} + x_k\left(\cos\hat{\hat{\omega}}_P \sin\hat{\hat{\kappa}}_P + \cos\hat{\hat{\kappa}}_P \sin\hat{\hat{\omega}}_P \sin\hat{\hat{\phi}}_P \right) + y_k\left(\cos\hat{\hat{\omega}}_P \cos\hat{\hat{\kappa}}_P - \sin\hat{\hat{\kappa}}_P \sin\hat{\hat{\omega}}_P \sin\hat{\hat{\phi}}_P \right) - z_k\left(\sin\hat{\hat{\omega}}_P \cos\hat{\hat{\phi}}_P \right) \right) +$$
$$+ 2\left(\sin\hat{\hat{\kappa}}_P \cos\hat{\hat{\phi}}_P \right)\left(\hat{\hat{X}}_P - X_{0_{ij}} + x_k \cos\hat{\hat{\kappa}}_P \cos\hat{\hat{\phi}}_P - y_k \sin\hat{\hat{\kappa}}_P \cos\hat{\hat{\phi}}_P + z_k \sin\hat{\hat{\phi}}_P \right),$$

$$j_9^{dist} = 2\left(\cos\hat{\hat{\omega}}_P \cos\hat{\hat{\phi}}_P \right)\left(\hat{\hat{Z}}_P - Z_{0_{ij}} + x_k\left(\sin\hat{\hat{\omega}}_P \sin\hat{\hat{\kappa}}_P - \cos\hat{\hat{\kappa}}_P \cos\hat{\hat{\omega}}_P \sin\hat{\hat{\phi}}_P \right) + y_k\left(\sin\hat{\hat{\omega}}_P \cos\hat{\hat{\kappa}}_P + \sin\hat{\hat{\kappa}}_P \cos\hat{\hat{\omega}}_P \sin\hat{\hat{\phi}}_P \right) + z_k\left(\cos\hat{\hat{\omega}}_P \cos\hat{\hat{\phi}}_P \right) \right) +$$
$$- 2\left(\sin\hat{\hat{\omega}}_P \cos\hat{\hat{\phi}}_P \right)\left(\hat{\hat{Y}}_P - Y_{0_{ij}} + x_k\left(\cos\hat{\hat{\omega}}_P \sin\hat{\hat{\kappa}}_P + \cos\hat{\hat{\kappa}}_P \sin\hat{\hat{\omega}}_P \sin\hat{\hat{\phi}}_P \right) + y_k\left(\cos\hat{\hat{\omega}}_P \cos\hat{\hat{\kappa}}_P - \sin\hat{\hat{\kappa}}_P \sin\hat{\hat{\omega}}_P \sin\hat{\hat{\phi}}_P \right) - z_k\left(\sin\hat{\hat{\omega}}_P \cos\hat{\hat{\phi}}_P \right) \right) +$$
$$+ 2\left(\sin\hat{\hat{\phi}}_P \right)\left(\hat{\hat{X}}_P - X_{0_{ij}} + x_k \cos\hat{\hat{\kappa}}_P \cos\hat{\hat{\phi}}_P - y_k \sin\hat{\hat{\kappa}}_P \cos\hat{\hat{\phi}}_P + z_k \sin\hat{\hat{\phi}}_P \right),$$

$$j_{10}^{dist} = -2\hat{d}_{ijk}.$$

$\boldsymbol{J}_{ijk}^{ang}$ is defined as the Jacobian matrix containing the partial derivatives of the elements of the equations in the first member of Eq. A17 with respect to the elements in $\boldsymbol{\xi}_{ang}$:

$$\boldsymbol{J}_{ijk}^{ang} = \begin{bmatrix} j_{11}^{ang} & j_{12}^{ang} & j_{13}^{ang} & j_{14}^{ang} & j_{15}^{ang} & j_{16}^{ang} & j_{17}^{ang} & j_{18}^{ang} & j_{19}^{ang} & j_{110}^{ang} & j_{111}^{ang} \\ j_{21}^{ang} & j_{22}^{ang} & j_{23}^{ang} & j_{24}^{ang} & j_{25}^{ang} & j_{26}^{ang} & j_{27}^{ang} & j_{28}^{ang} & j_{29}^{ang} & j_{210}^{ang} & j_{211}^{ang} \end{bmatrix},$$

where

$$j_{11}^{ang} = -\cos(\hat{\kappa}_{ij})\cos(\hat{\phi}_{ij})\sin(\hat{\theta}_{ijk}) - \cos(\hat{\phi}_{ij})\sin(\hat{\kappa}_{ij})\cos(\hat{\theta}_{ijk}),$$

$$j_{12}^{ang} = \cos(\hat{\theta}_{ijk})\left(\cos\hat{\omega}_{ij}\cos\hat{\kappa}_{ij} - \sin\hat{\omega}_{ij}\sin\hat{\kappa}_{ij}\sin\hat{\phi}_{ij}\right) - \sin(\hat{\theta}_{ijk})\left(\cos\hat{\omega}_{ij}\sin\hat{\kappa}_{ij} + \sin\hat{\omega}_{ij}\cos\hat{\kappa}_{ij}\sin\hat{\phi}_{ij}\right),$$

$$j_{13}^{ang} = \cos(\hat{\theta}_{ijk})\left(\sin\hat{\omega}_{ij}\cos\hat{\kappa}_{ij} + \cos\hat{\omega}_{ij}\sin\hat{\kappa}_{ij}\sin\hat{\phi}_{ij}\right) - \sin(\hat{\theta}_{ijk})\left(\sin\hat{\omega}_{ij}\sin\hat{\kappa}_{ij} - \cos\hat{\omega}_{ij}\cos\hat{\kappa}_{ij}\sin\hat{\phi}_{ij}\right),$$

$$j_{14}^{ang} = -\sin(\hat{\theta}_{ijk})\left(\left(\cos\hat{\kappa}_{ij}\sin\hat{\phi}_{ij}\right)\left(\hat{\hat{X}}_P - X_{0_{ij}} + c_9 \right) + \left(\cos\hat{\kappa}_{ij}\cos\hat{\phi}_{ij}\cos\hat{\omega}_{ij}\right)\left(\hat{\hat{Z}}_P - Z_{0_{ij}} + c_1 \right) - \left(\cos\hat{\kappa}_{ij}\cos\hat{\phi}_{ij}\sin\hat{\omega}_{ij}\right)\left(\hat{\hat{Y}}_P - Y_{0_{ij}} + c_2 \right) \right) +$$
$$- \cos(\hat{\theta}_{ijk})\left(\left(\sin\hat{\kappa}_{ij}\sin\hat{\phi}_{ij}\right)\left(\hat{\hat{X}}_P - X_{0_{ij}} + c_9 \right) + \left(\sin\hat{\kappa}_{ij}\cos\hat{\phi}_{ij}\cos\hat{\omega}_{ij}\right)\left(\hat{\hat{Z}}_P - Z_{0_{ij}} + c_1 \right) - \left(\sin\hat{\kappa}_{ij}\cos\hat{\phi}_{ij}\sin\hat{\omega}_{ij}\right)\left(\hat{\hat{Y}}_P - Y_{0_{ij}} + c_2 \right) \right),$$

$$j_{15}^{ang} = \cos(\hat{\theta}_{ijk})\begin{pmatrix}(\sin\hat{\kappa}_{ij}\sin\hat{\omega}_{ij})-(\cos\hat{\kappa}_{ij}\sin\hat{\phi}_{ij}\cos\hat{\omega}_{ij})\left(\hat{\hat{Z}}_P - Z_{0_{ij}} + c_1\right)+(\sin\hat{\kappa}_{ij}\cos\hat{\omega}_{ij})+(\cos\hat{\kappa}_{ij}\sin\hat{\phi}_{ij}\sin\hat{\omega}_{ij})\left(\hat{\hat{Y}}_P - Y_{0_{ij}} + c_2\right)+\\ (\cos\hat{\kappa}_{ij}\cos\hat{\phi}_{ij})\left(\hat{\hat{X}}_P - X_{0_{ij}} + c_9\right)\end{pmatrix}+$$

$$+\sin(\hat{\theta}_{ijk})\begin{pmatrix}(\cos\hat{\kappa}_{ij}\sin\hat{\omega}_{ij})+(\sin\hat{\kappa}_{ij}\sin\hat{\phi}_{ij}\cos\hat{\omega}_{ij})\left(\hat{\hat{Z}}_P - Z_{0_{ij}} + c_1\right)+(\cos\hat{\kappa}_{ij}\cos\hat{\omega}_{ij})-(\sin\hat{\kappa}_{ij}\sin\hat{\phi}_{ij}\sin\hat{\omega}_{ij})\left(\hat{\hat{Y}}_P - Y_{0_{ij}} + c_2\right)+\\ -(\sin\hat{\kappa}_{ij}\cos\hat{\phi}_{ij})\left(\hat{\hat{X}}_P - X_{0_{ij}} + c_9\right)\end{pmatrix},$$

$$j_{16}^{ang} = \sin(\hat{\theta}_{ijk})\left((\sin\hat{\kappa}_{ij}\cos\hat{\omega}_{ij})+(\cos\hat{\kappa}_{ij}\sin\hat{\phi}_{ij}\sin\hat{\omega}_{ij})\left(\hat{\hat{Z}}_P - Z_{0_{ij}} + c_1\right)-(\sin\hat{\kappa}_{ij}\sin\hat{\omega}_{ij})-(\cos\hat{\kappa}_{ij}\sin\hat{\phi}_{ij}\cos\hat{\omega}_{ij})\left(\hat{\hat{Y}}_P - Y_{0_{ij}} + c_2\right)\right)+$$

$$-\cos(\hat{\theta}_{ijk})\left((\cos\hat{\kappa}_{ij}\cos\hat{\omega}_{ij})-(\sin\hat{\kappa}_{ij}\sin\hat{\phi}_{ij}\sin\hat{\omega}_{ij})\left(\hat{\hat{Z}}_P - Z_{0_{ij}} + c_1\right)-(\cos\hat{\kappa}_{ij}\sin\hat{\omega}_{ij})+(\sin\hat{\kappa}_{ij}\sin\hat{\phi}_{ij}\cos\hat{\omega}_{ij})\left(\hat{\hat{Y}}_P - Y_{0_{ij}} + c_2\right)\right),$$

$$j_{17}^{ang} = \sin(\hat{\theta}_{ijk})\begin{pmatrix}\left((\sin\hat{\hat{\kappa}}_P\cos\hat{\hat{\omega}}_P)+(\cos\hat{\hat{\kappa}}_P\sin\hat{\hat{\phi}}_P\sin\hat{\hat{\omega}}_P)\right)\left((\sin\hat{\kappa}_{ij}\cos\hat{\omega}_{ij})+(\cos\hat{\kappa}_{ij}\sin\hat{\phi}_{ij}\sin\hat{\omega}_{ij})\right)+\\ \left((\sin\hat{\hat{\kappa}}_P\sin\hat{\hat{\omega}}_P)-(\cos\hat{\hat{\kappa}}_P\sin\hat{\hat{\phi}}_P\cos\hat{\hat{\omega}}_P)\right)\left((\sin\hat{\kappa}_{ij}\sin\hat{\omega}_{ij})-(\cos\hat{\kappa}_{ij}\sin\hat{\phi}_{ij}\cos\hat{\omega}_{ij})\right)+\\ (\cos\hat{\kappa}_{ij}\cos\hat{\phi}_{ij}\cos\hat{\hat{\kappa}}_P\cos\hat{\hat{\phi}}_P)\end{pmatrix}$$

$$-\cos(\hat{\theta}_{ijk})\begin{pmatrix}\left((\sin\hat{\hat{\kappa}}_P\cos\hat{\hat{\omega}}_P)+(\cos\hat{\hat{\kappa}}_P\sin\hat{\hat{\phi}}_P\sin\hat{\hat{\omega}}_P)\right)\left((\cos\hat{\kappa}_{ij}\cos\hat{\omega}_{ij})-(\sin\hat{\kappa}_{ij}\sin\hat{\phi}_{ij}\sin\hat{\omega}_{ij})\right)+\\ \left((\sin\hat{\hat{\kappa}}_P\sin\hat{\hat{\omega}}_P)-(\cos\hat{\hat{\kappa}}_P\sin\hat{\hat{\phi}}_P\cos\hat{\hat{\omega}}_P)\right)\left((\cos\hat{\kappa}_{ij}\sin\hat{\omega}_{ij})+(\sin\hat{\kappa}_{ij}\sin\hat{\phi}_{ij}\cos\hat{\omega}_{ij})\right)-\\ (\sin\hat{\kappa}_{ij}\cos\hat{\phi}_{ij}\cos\hat{\hat{\kappa}}_P\cos\hat{\hat{\phi}}_P)\end{pmatrix},$$

$$j_{18}^{ang} = \sin(\hat{\theta}_{ijk})\begin{pmatrix}\left((\cos\hat{\hat{\kappa}}_P\sin\hat{\hat{\omega}}_P)+(\sin\hat{\hat{\kappa}}_P\sin\hat{\hat{\phi}}_P\cos\hat{\hat{\omega}}_P)\right)\left((\sin\hat{\kappa}_{ij}\sin\hat{\omega}_{ij})-(\cos\hat{\kappa}_{ij}\sin\hat{\phi}_{ij}\cos\hat{\omega}_{ij})\right)+\\ \left((\cos\hat{\hat{\kappa}}_P\cos\hat{\hat{\omega}}_P)-(\sin\hat{\hat{\kappa}}_P\sin\hat{\hat{\phi}}_P\sin\hat{\hat{\omega}}_P)\right)\left((\sin\hat{\kappa}_{ij}\cos\hat{\omega}_{ij})+(\cos\hat{\kappa}_{ij}\sin\hat{\phi}_{ij}\cos\hat{\omega}_{ij})\right)+\\ (\cos\hat{\kappa}_{ij}\cos\hat{\phi}_{ij}\sin\hat{\hat{\kappa}}_P\cos\hat{\hat{\phi}}_P)\end{pmatrix}+$$

$$-\cos(\hat{\theta}_{ijk})\begin{pmatrix}\left((\cos\hat{\hat{\kappa}}_P\sin\hat{\hat{\omega}}_P)+(\sin\hat{\hat{\kappa}}_P\sin\hat{\hat{\phi}}_P\cos\hat{\hat{\omega}}_P)\right)\left((\cos\hat{\kappa}_{ij}\sin\hat{\omega}_{ij})+(\sin\hat{\kappa}_{ij}\sin\hat{\phi}_{ij}\cos\hat{\omega}_{ij})\right)+\\ \left((\cos\hat{\hat{\kappa}}_P\cos\hat{\hat{\omega}}_P)-(\sin\hat{\hat{\kappa}}_P\sin\hat{\hat{\phi}}_P\sin\hat{\hat{\omega}}_P)\right)\left((\cos\hat{\kappa}_{ij}\cos\hat{\omega}_{ij})-(\sin\hat{\kappa}_{ij}\sin\hat{\phi}_{ij}\sin\hat{\omega}_{ij})\right)+\\ (\sin\hat{\kappa}_{ij}\cos\hat{\phi}_{ij}\sin\hat{\hat{\kappa}}_P\cos\hat{\hat{\phi}}_P)\end{pmatrix},$$

$$j_{19}^{ang} = \cos(\hat{\theta}_{ijk})\begin{pmatrix}\left(\cos\hat{\hat{\phi}}_P\sin\hat{\hat{\omega}}_P\right)\left((\cos\hat{\kappa}_{ij}\cos\hat{\omega}_{ij})-(\sin\hat{\kappa}_{ij}\sin\hat{\phi}_{ij}\sin\hat{\omega}_{ij})\right)-\\ \cos\hat{\hat{\omega}}_P\cos\hat{\hat{\phi}}_P\left(\cos\hat{\kappa}_{ij}\sin\hat{\omega}_{ij}+\sin\hat{\kappa}_{ij}\sin\hat{\phi}_{ij}\cos\hat{\omega}_{ij}\right)+\\ \cos\hat{\phi}_{ij}\sin\hat{\kappa}_{ij}\sin\hat{\hat{\phi}}_P\end{pmatrix}+\sin(\hat{\theta}_{ijk})\begin{pmatrix}\left(\cos\hat{\hat{\phi}}_P\cos\hat{\hat{\omega}}_P\right)\left((\sin\hat{\kappa}_{ij}\sin\hat{\omega}_{ij})-(\cos\hat{\kappa}_{ij}\sin\hat{\phi}_{ij}\cos\hat{\omega}_{ij})\right)-\\ \sin\hat{\hat{\omega}}_P\cos\hat{\hat{\phi}}_P\left(\sin\hat{\kappa}_{ij}\cos\hat{\omega}_{ij}+\cos\hat{\kappa}_{ij}\sin\hat{\phi}_{ij}\sin\hat{\omega}_{ij}\right)+\\ \cos\hat{\phi}_{ij}\cos\hat{\kappa}_{ij}\sin\hat{\hat{\phi}}_P\end{pmatrix},$$

$$j_{110}^{ang} = \cos(\hat{\theta}_{ijk})\begin{pmatrix}(\sin\hat{\kappa}_{ij}\sin\hat{\omega}_{ij})-(\cos\hat{\kappa}_{ij}\sin\hat{\phi}_{ij}\cos\hat{\omega}_{ij})\left(\hat{\hat{Z}}_P - Z_{0_{ij}} + c_1\right)+(\sin\hat{\kappa}_{ij}\cos\hat{\omega}_{ij})+(\cos\hat{\kappa}_{ij}\sin\hat{\phi}_{ij}\sin\hat{\omega}_{ij})\left(\hat{\hat{Y}}_P - Y_{0_{ij}} + c_2\right)+\\ (\cos\hat{\kappa}_{ij}\cos\hat{\phi}_{ij})\left(\hat{\hat{X}}_P - X_{0_{ij}} + c_9\right)\end{pmatrix}+$$

$$+\sin(\hat{\theta}_{ijk})\begin{pmatrix}(\cos\hat{\kappa}_{ij}\sin\hat{\omega}_{ij})+(\sin\hat{\kappa}_{ij}\sin\hat{\phi}_{ij}\cos\hat{\omega}_{ij})\left(\hat{\hat{Z}}_P - Z_{0_{ij}} + c_1\right)+(\cos\hat{\kappa}_{ij}\cos\hat{\omega}_{ij})-(\sin\hat{\kappa}_{ij}\sin\hat{\phi}_{ij}\sin\hat{\omega}_{ij})\left(\hat{\hat{Y}}_P - Y_{0_{ij}} + c_2\right)+\\ -(\sin\hat{\kappa}_{ij}\cos\hat{\phi}_{ij})\left(\hat{\hat{X}}_P - X_{0_{ij}} + c_9\right)\end{pmatrix},$$

$$J_{111}^{ang} = 0,$$

$$J_{21}^{ang} = \sin\hat{\phi}_{ij}\cos\hat{\theta}_{ijk}\cos\hat{\varphi}_{ijk} - \cos\hat{\kappa}_{ij}\cos\hat{\phi}_{ij}\sin\hat{\varphi}_{ijk},$$

$$J_{22}^{ang} = -\sin\hat{\varphi}_{ijk}\left(\cos\hat{\omega}_{ij}\sin\hat{\kappa}_{ij} + \cos\hat{\kappa}_{ij}\sin\hat{\phi}_{ij}\sin\hat{\omega}_{ij}\right) - \cos\hat{\phi}_{ij}\sin\hat{\omega}_{ij}\cos\hat{\varphi}_{ijk}\cos\hat{\theta}_{ijk},$$

$$J_{23}^{ang} = \cos\hat{\varphi}_{ijk}\cos\hat{\theta}_{ijk}\cos\hat{\phi}_{ij}\cos\hat{\omega}_{ij} - \sin\hat{\varphi}_{ijk}\left(\sin\hat{\omega}_{ij}\sin\hat{\kappa}_{ij} - \cos\hat{\kappa}_{ij}\sin\hat{\phi}_{ij}\cos\hat{\omega}_{ij}\right),$$

$$J_{24}^{ang} = -\sin\hat{\varphi}_{ijk}\begin{pmatrix}\left(\cos\hat{\kappa}_{ij}\sin\hat{\phi}_{ij} - \cos\hat{\kappa}_{ij}\cos\hat{\omega}_{ij}\right)\left(\hat{\hat{X}}_P - X_{0_{ij}} + c_9\right) + \\ + \left(\cos\hat{\kappa}_{ij}\cos\hat{\phi}_{ij}\cos\hat{\omega}_{ij}\right)\left(\hat{\hat{Z}}_P - Z_{0_{ij}} + c_1\right) + \\ - \left(\cos\hat{\kappa}_{ij}\cos\hat{\phi}_{ij}\sin\hat{\omega}_{ij}\right)\left(\hat{\hat{Y}}_P - Y_{0_{ij}} + c_2\right)\end{pmatrix} - \cos\hat{\varphi}_{ijk}\cos\hat{\theta}_{ijk}\begin{pmatrix}\left(\cos\hat{\phi}_{ij}\right)\left(\hat{\hat{X}}_P - X_{0_{ij}} + c_9\right) + \\ - \left(\sin\hat{\phi}_{ij}\cos\hat{\omega}_{ij}\right)\left(\hat{\hat{Z}}_P - Z_{0_{ij}} + c_1\right) + \\ + \left(\sin\hat{\phi}_{ij}\sin\hat{\omega}_{ij}\right)\left(\hat{\hat{Y}}_P - Y_{0_{ij}} + c_2\right)\end{pmatrix},$$

$$J_{25}^{ang} = \sin\hat{\varphi}_{ijk}\begin{pmatrix}\left(\cos\hat{\kappa}_{ij}\sin\hat{\omega}_{ij} + \cos\hat{\omega}_{ij}\sin\hat{\kappa}_{ij}\sin\hat{\phi}_{ij}\right)\left(\hat{\hat{Z}}_P - Z_{0_{ij}} + c_1\right) + \\ + \left(\cos\hat{\kappa}_{ij}\cos\hat{\omega}_{ij} - \sin\hat{\kappa}_{ij}\sin\hat{\omega}_{ij}\sin\hat{\phi}_{ij}\right)\left(\hat{\hat{Y}}_P - Y_{0_{ij}} + c_2\right) + \\ - \left(\cos\hat{\phi}_{ij}\sin\hat{\kappa}_{ij}\right)\left(\hat{\hat{X}}_P - X_{0_{ij}} + c_9\right)\end{pmatrix},$$

$$J_{26}^{ang} = \sin\hat{\varphi}_{ijk}\begin{pmatrix}\left(\sin\hat{\kappa}_{ij}\cos\hat{\omega}_{ij} + \sin\hat{\omega}_{ij}\cos\hat{\kappa}_{ij}\sin\hat{\phi}_{ij}\right)\left(\hat{\hat{Z}}_P - Z_{0_{ij}} + c_1\right) + \\ - \left(\sin\hat{\kappa}_{ij}\sin\hat{\omega}_{ij} - \cos\hat{\kappa}_{ij}\cos\hat{\omega}_{ij}\sin\hat{\phi}_{ij}\right)\left(\hat{\hat{Y}}_P - Y_{0_{ij}} + c_2\right)\end{pmatrix} + \cos\hat{\varphi}_{ijk}\cos\hat{\theta}_{ijk}\begin{pmatrix}\left(\cos\hat{\phi}_{ij}\cos\hat{\omega}_{ij}\right)\left(\hat{\hat{Y}}_P - Y_{0_{ij}} + c_2\right) + \\ - \left(\cos\hat{\phi}_{ij}\sin\hat{\omega}_{ij}\right)\left(\hat{\hat{Z}}_P - Z_{0_{ij}} + c_1\right)\end{pmatrix},$$

$$J_{27}^{ang} = \sin\hat{\varphi}_{ijk}\begin{pmatrix}\left(\cos\hat{\omega}_P\sin\hat{\kappa}_P + \cos\hat{\kappa}_P\sin\hat{\omega}_P\sin\hat{\phi}_P\right)\left(\sin\hat{\kappa}_{ij}\cos\hat{\omega}_{ij} + \sin\hat{\omega}_{ij}\cos\hat{\kappa}_{ij}\sin\hat{\phi}_{ij}\right) + \\ + \left(\sin\hat{\omega}_P\sin\hat{\kappa}_P - \cos\hat{\kappa}_P\cos\hat{\omega}_P\sin\hat{\phi}_P\right)\left(\sin\hat{\kappa}_{ij}\sin\hat{\omega}_{ij} - \cos\hat{\omega}_{ij}\cos\hat{\kappa}_{ij}\sin\hat{\phi}_{ij}\right) + \\ + \cos\hat{\kappa}_P\cos\hat{\phi}_P\cos\hat{\kappa}_P\cos\hat{\phi}_P\end{pmatrix} - \cos\hat{\varphi}_{ijk}\cos\hat{\theta}_{ijk}\begin{pmatrix}\left(\cos\hat{\phi}_{ij}\cos\hat{\omega}_{ij}\right)\left(\sin\hat{\kappa}_P\sin\hat{\omega}_P - \cos\hat{\kappa}_P\cos\hat{\omega}_P\sin\hat{\phi}_P\right) + \\ + \left(\sin\hat{\phi}_{ij}\right)\left(\cos\hat{\kappa}_P\cos\hat{\phi}_P\right) + \\ - \left(\cos\hat{\phi}_{ij}\sin\hat{\omega}_{ij}\right)\left(\sin\hat{\kappa}_P\cos\hat{\omega}_P + \cos\hat{\kappa}_P\sin\hat{\omega}_P\sin\hat{\phi}_P\right)\end{pmatrix},$$

$$J_{28}^{ang} = \sin\hat{\varphi}_{ijk}\begin{pmatrix}\left(\sin\hat{\omega}_P\cos\hat{\kappa}_P + \sin\hat{\kappa}_P\cos\hat{\omega}_P\sin\hat{\phi}_P\right)\left(\sin\hat{\kappa}_{ij}\sin\hat{\omega}_{ij} - \cos\hat{\omega}_{ij}\cos\hat{\kappa}_{ij}\sin\hat{\phi}_{ij}\right) + \\ + \left(\cos\hat{\omega}_P\cos\hat{\kappa}_P - \sin\hat{\kappa}_P\sin\hat{\omega}_P\sin\hat{\phi}_P\right)\left(\sin\hat{\kappa}_{ij}\cos\hat{\omega}_{ij} + \sin\hat{\omega}_{ij}\cos\hat{\kappa}_{ij}\sin\hat{\phi}_{ij}\right) + \\ - \cos\hat{\kappa}_{ij}\cos\hat{\phi}_{ij}\sin\hat{\kappa}_P\cos\hat{\phi}_P\end{pmatrix} - \cos\hat{\varphi}_{ijk}\cos\hat{\theta}_{ijk}\begin{pmatrix}\left(\cos\hat{\phi}_{ij}\sin\hat{\omega}_{ij}\right)\left(\cos\hat{\kappa}_P\cos\hat{\omega}_P - \sin\hat{\kappa}_P\sin\hat{\omega}_P\sin\hat{\phi}_P\right) + \\ + \left(\sin\hat{\phi}_{ij}\right)\left(\sin\hat{\kappa}_P\cos\hat{\phi}_P\right) + \\ - \left(\cos\hat{\phi}_{ij}\cos\hat{\omega}_{ij}\right)\left(\cos\hat{\kappa}_P\sin\hat{\omega}_P + \sin\hat{\kappa}_P\cos\hat{\omega}_P\sin\hat{\phi}_P\right)\end{pmatrix},$$

$$J_{29}^{ang} = \sin\hat{\varphi}_{ijk}\begin{pmatrix}\cos\hat{\omega}_P\cos\hat{\phi}_P\left(\sin\hat{\kappa}_{ij}\sin\hat{\omega}_{ij} - \cos\hat{\kappa}_{ij}\cos\hat{\omega}_{ij}\sin\hat{\phi}_{ij}\right) + \\ - \cos\hat{\phi}_P\sin\hat{\omega}_P\left(\cos\hat{\omega}_{ij}\sin\hat{\kappa}_{ij} + \cos\hat{\kappa}_{ij}\sin\hat{\phi}_{ij}\sin\hat{\omega}_{ij}\right) + \\ + \cos\hat{\kappa}_{ij}\cos\hat{\phi}_{ij}\sin\hat{\phi}_P\end{pmatrix} - \cos\hat{\varphi}_{ijk}\cos\hat{\theta}_{ijk}\begin{pmatrix}\sin\hat{\omega}_P\cos\hat{\phi}_P\left(\cos\hat{\omega}_{ij}\cos\hat{\phi}_{ij}\right) + \\ + \cos\hat{\phi}_P\cos\hat{\omega}_P\left(\cos\hat{\omega}_{ij}\cos\hat{\phi}_{ij}\right) + \\ + \sin\hat{\phi}_{ij}\sin\hat{\phi}_P\end{pmatrix},$$

$$J_{210}^{ang} = \cos\hat{\varphi}_{ijk}\sin\hat{\theta}_{ijk}\begin{pmatrix}\left(\sin\hat{\phi}_{ij}\right)\left(\hat{\hat{X}}_P - X_{0_{ij}} + c_2\right) + \\ + \left(\cos\hat{\phi}_{ij}\cos\hat{\omega}_{ij}\right)\left(\hat{\hat{Z}}_P - Z_{0_{ij}} + c_1\right) + \\ - \left(\cos\hat{\phi}_{ij}\sin\hat{\omega}_{ij}\right)\left(\hat{\hat{Y}}_P - Y_{0_{ij}} + c_2\right)\end{pmatrix},$$

$$J_{211}^{ang} = \cos\hat{\varphi}_{ijk}\begin{pmatrix}\left(\sin\hat{\kappa}_{ij}\sin\hat{\omega}_{ij}\right) + \\ - \left(\sin\hat{\phi}_{ij}\cos\hat{\kappa}_{ij}\cos\hat{\omega}_{ij}\right)\left(\hat{\hat{Z}}_P - Z_{0_{ij}} + c_1\right) + \\ + \left(\cos\hat{\omega}_{ij}\sin\hat{\kappa}_{ij} + \cos\hat{\kappa}_{ij}\sin\hat{\phi}_{ij}\sin\hat{\omega}_{ij}\right)\left(\hat{\hat{Y}}_P - Y_{0_{ij}} + c_2\right) + \\ + \left(\cos\hat{\kappa}_{ij}\cos\hat{\phi}_{ij}\right)\left(\hat{\hat{X}}_P - X_{0_{ij}} + c_2\right)\end{pmatrix} + \sin\hat{\varphi}_{ijk}\cos\hat{\theta}_{ijk}\begin{pmatrix}\left(\sin\hat{\phi}_{ij}\right)\left(\hat{\hat{X}}_P - X_{0_{ij}} + c_2\right) + \\ + \left(\cos\hat{\phi}_{ij}\cos\hat{\omega}_{ij}\right)\left(\hat{\hat{Z}}_P - Z_{0_{ij}} + c_1\right) + \\ - \left(\cos\hat{\phi}_{ij}\sin\hat{\omega}_{ij}\right)\left(\hat{\hat{Y}}_P - Y_{0_{ij}} + c_2\right)\end{pmatrix}.$$

$\boldsymbol{J}^{int}$ is defined as the Jacobian matrix containing the partial derivatives of the elements of the equations in the first member of Eq. A17 with respect to the elements in $\boldsymbol{\xi}_{int}$:

$$\boldsymbol{J}_{ijk}^{int} = \begin{bmatrix} j_{11}^{int} & j_{12}^{int} & \cdots & j_{16}^{int} \\ j_{21}^{int} & \ddots & & \\ \vdots & & & \\ j_{91}^{int} & & & j_{96}^{int} \end{bmatrix},$$

where

$$j_{11}^{int} = \cos\hat{\kappa}_I \cos\hat{\kappa}_{off} \cos\hat{\phi}_I \sin\hat{\phi}_{off} - \sin\hat{\kappa}_{off} \sin\hat{\phi}_{off} d_1 - \cos\hat{\phi}_{off} d_8,$$
$$j_{12}^{int} = \cos\hat{\kappa}_{off} \cos\hat{\phi}_{off} d_1 + \cos\hat{\kappa}_I \cos\hat{\phi}_I \cos\hat{\phi}_{off} \sin\hat{\kappa}_{off},$$
$$j_{13}^{int} = 0,$$
$$j_{14}^{int} = \cos\hat{\kappa}_I \cos\hat{\kappa}_{off} \cos\hat{\phi}_{off} \sin\hat{\phi}_I + \cos\hat{\kappa}_I \cos\hat{\omega}_I \cos\hat{\phi}_I \sin\hat{\phi}_{off} + \cos\hat{\kappa}_I \cos\hat{\phi}_I \cos\hat{\phi}_{off} \sin\hat{\kappa}_{off} \sin\hat{\omega}_I,$$
$$j_{15}^{int} = \cos\hat{\phi}_{off} \sin\hat{\kappa}_{off} d_2 - \sin\hat{\phi}_{off} d_7 + \cos\hat{\kappa}_{off} \cos\hat{\phi}_I \cos\hat{\phi}_{off} \sin\hat{\kappa}_I,$$
$$j_{16}^{int} = -\sin\hat{\phi}_{off} d_1 - \cos\hat{\phi}_{off} \sin\hat{\kappa}_{off} d_8,$$

$$j_{21}^{int} = \cos\hat{\phi}_{off} \sin\hat{\kappa}_{off} \sin\hat{\omega}_{off} d_1 - \sin\hat{\omega}_{off} \sin\hat{\phi}_{off} d_8 - \cos\hat{\kappa}_{off} \cos\hat{\kappa}_I \cos\hat{\phi}_I \cos\hat{\phi}_{off} \sin\hat{\omega}_{off},$$
$$j_{22}^{int} = d_1 d_5 - \cos\hat{\kappa}_I \cos\hat{\phi}_I d_3,$$
$$j_{23}^{int} = d_1 d_4 + \cos\hat{\kappa}_I \cos\hat{\phi}_I d_6 + \cos\hat{\omega}_{off} \cos\hat{\phi}_{off} d_8,$$
$$j_{24}^{int} = \cos\hat{\kappa}_I \sin\hat{\phi}_I d_5 - \cos\hat{\kappa}_I \sin\hat{\phi}_I \sin\hat{\omega}_I d_3 - \cos\hat{\kappa}_I \cos\hat{\omega}_I \cos\hat{\phi}_I \cos\hat{\phi}_{off} \sin\hat{\omega}_{off},$$
$$j_{25}^{int} = \cos\hat{\phi}_I \sin\hat{\kappa}_I d_5 - d_2 d_3 + \cos\hat{\phi}_{off} \sin\hat{\omega}_{off} d_7,$$
$$j_{26}^{int} = d_8 d_3 + \cos\hat{\phi}_{off} \sin\hat{\omega}_{off} d_1,$$

$$j_{31}^{int} = \cos\hat{\omega}_{off} \sin\hat{\phi}_{off} d_8 - \cos\hat{\omega}_{off} \cos\hat{\phi}_{off} \sin\hat{\kappa}_{off} d_1 + \cos\hat{\kappa}_I \cos\hat{\kappa}_{off} \cos\hat{\omega}_{off} \cos\hat{\phi}_I \cos\hat{\phi}_{off},$$
$$j_{32}^{int} = d_1 d_6 - \cos\hat{\kappa}_I \cos\hat{\phi}_I d_4,$$
$$j_{33}^{int} = \cos\hat{\phi}_{off} \sin\hat{\omega}_{off} d_8 - \cos\hat{\kappa}_I \cos\hat{\phi}_I d_5 - d_1 d_3$$
$$j_{34}^{int} = \cos\hat{\kappa}_I \sin\hat{\phi}_I d_6 - \cos\hat{\kappa}_I \cos\hat{\phi}_I \sin\hat{\omega}_I d_4 + \cos\hat{\kappa}_I \cos\hat{\omega}_I \cos\hat{\omega}_{off} \cos\hat{\phi}_I \cos\hat{\phi}_{off}$$
$$j_{35}^{int} = \cos\hat{\phi}_I \sin\hat{\kappa}_I d_6 - \cos\hat{\omega}_{off} \cos\hat{\phi}_{off} d_7 - d_2 d_4,$$
$$j_{36}^{int} = d_8 d_4 - \cos\hat{\omega}_{off} \cos\hat{\phi}_{off} d_1,$$

$$j_{41}^{int} = -\cos\hat{\phi}_{off} d_7 - \sin\hat{\kappa}_{off} \sin\hat{\phi}_{off} d_2 - \cos\hat{\kappa}_{off} \cos\hat{\phi}_I \sin\hat{\kappa}_I \sin\hat{\phi}_{off}$$
$$j_{42}^{int} = \cos\hat{\kappa}_{off} \cos\hat{\phi}_{off} d_2 - \cos\hat{\phi}_I \cos\hat{\phi}_{off} \sin\hat{\kappa}_I \sin\hat{\kappa}_{off},$$
$$j_{43}^{int} = 0,$$
$$j_{44}^{int} = -\cos\hat{\kappa}_{off} \cos\hat{\phi}_{off} \sin\hat{\kappa}_I \sin\hat{\phi}_I - \cos\hat{\omega}_I \cos\hat{\phi}_I \sin\hat{\kappa}_I \sin\hat{\phi}_{off} - \cos\hat{\phi}_I \cos\hat{\phi}_{off} \sin\hat{\kappa}_I \sin\hat{\kappa}_{off} \sin\hat{\omega}_I,$$
$$j_{45}^{int} = \sin\hat{\phi}_{off} d_8 - \cos\hat{\phi}_{off} \sin\hat{\kappa}_{off} d_1 + \cos\hat{\kappa}_I \cos\hat{\kappa}_{off} \cos\hat{\phi}_I \cos\hat{\phi}_{off},$$
$$j_{46}^{int} = -\sin\hat{\phi}_{off} d_2 - \cos\hat{\phi}_{off} \sin\hat{\kappa}_{off} d_7,$$

$$j_{51}^{int} = \cos\hat{\phi}_{off} \sin\hat{\kappa}_{off} \sin\hat{\omega}_{off} d_2 - \sin\hat{\omega}_{off} \sin\hat{\phi}_{off} d_7 + \cos\hat{\kappa}_{off} \cos\hat{\phi}_I \cos\hat{\phi}_{off} \sin\hat{\kappa}_I \sin\hat{\omega}_{off},$$
$$j_{52}^{int} = d_2 d_5 + \cos\hat{\phi}_I \sin\hat{\kappa}_I d_3,$$
$$j_{53}^{int} = d_2 d_4 + \cos\hat{\omega}_{off} \cos\hat{\phi}_{off} d_7 - \cos\hat{\phi}_I \sin\hat{\kappa}_I d_6,$$
$$j_{54}^{int} = \cos\hat{\phi}_I \sin\hat{\kappa}_I \sin\hat{\omega}_I d_3 - \sin\hat{\kappa}_I \sin\hat{\phi}_I d_5 + \cos\hat{\omega}_I \cos\hat{\phi}_I \cos\hat{\phi}_{off} \sin\hat{\kappa}_I \sin\hat{\omega}_{off},$$
$$j_{55}^{int} = d_1 d_3 + \cos\hat{\kappa}_I \cos\hat{\phi}_I d_5 - \cos\hat{\phi}_{off} \sin\hat{\omega}_{off} d_8,$$
$$j_{56}^{int} = d_3 d_7 + \cos\hat{\phi}_{off} \sin\hat{\omega}_{off} d_2,$$

$$j_{61}^{int} = \cos\hat{\omega}_{off} \sin\hat{\phi}_{off} d_7 - \cos\hat{\omega}_{off} \cos\hat{\phi}_{off} \sin\hat{\kappa}_{off} d_2 - \cos\hat{\kappa}_{off} \cos\hat{\omega}_{off} \cos\hat{\phi}_I \cos\hat{\phi}_{off} \sin\hat{\kappa}_I,$$
$$j_{62}^{int} = d_2 d_6 + \cos\hat{\phi}_I \sin\hat{\kappa}_I d_4,$$
$$j_{63}^{int} = \cos\hat{\phi}_I \sin\hat{\kappa}_I d_5 - d_2 d_3 + \cos\hat{\phi}_{off} \sin\hat{\omega}_{off} d_7,$$

$$j_{64}^{int} = \cos\hat{\phi}_I \sin\hat{\kappa}_I \sin\hat{\omega}_I d_4 - \sin\hat{\kappa}_I \sin\hat{\phi}_I d_6 - \cos\hat{\omega}_I \cos\hat{\omega}_{off} \cos\hat{\phi}_I \cos\hat{\phi}_{off} \sin\hat{\kappa}_I,$$
$$j_{65}^{int} = d_1 d_4 + \cos\hat{\phi}_I \cos\hat{\kappa}_I d_6 + \cos\hat{\omega}_{off} \cos\hat{\phi}_{off} d_8,$$
$$j_{66}^{int} = d_7 d_4 - \cos\hat{\omega}_{off} \cos\hat{\phi}_{off} d_2,$$

$$j_{71}^{int} = \cos\hat{\kappa}_I \cos\hat{\kappa}_{off} \cos\hat{\phi}_I \sin\hat{\phi}_{off} - \sin\hat{\kappa}_{off} \sin\hat{\phi}_{off} d_1 - \sin\hat{\phi}_{off} d_8,$$
$$j_{72}^{int} = \cos\hat{\kappa}_{off} \cos\hat{\phi}_{off} d_1 + \cos\hat{\kappa}_I \cos\hat{\phi}_I \cos\hat{\phi}_{off} \sin\hat{\kappa}_{off},$$
$$j_{73}^{int} = 0,$$
$$j_{74}^{int} = \cos\hat{\kappa}_I \cos\hat{\kappa}_{off} \sin\hat{\phi}_I \cos\hat{\phi}_{off} + \cos\hat{\kappa}_I \cos\hat{\omega}_I \cos\hat{\phi}_I \sin\hat{\phi}_{off} + \cos\hat{\kappa}_I \cos\hat{\phi}_I \cos\hat{\phi}_{off} \sin\hat{\kappa}_{off} \sin\hat{\omega}_I,$$
$$j_{75}^{int} = \cos\hat{\phi}_{off} \sin\hat{\kappa}_{off} d_2 - \sin\hat{\phi}_{off} d_7 + \cos\hat{\kappa}_{off} \cos\hat{\phi}_I \cos\hat{\phi}_{off} \sin\hat{\kappa}_I,$$
$$j_{76}^{int} = -\sin\hat{\phi}_{off} d_1 - \cos\hat{\phi}_{off} \sin\hat{\kappa}_{off} d_8,$$

$$j_{81}^{int} = \cos\hat{\phi}_{off} \sin\hat{\kappa}_{off} \sin\hat{\omega}_{off} d_1 - \sin\hat{\omega}_{off} \sin\hat{\phi}_{off} d_8 - \cos\hat{\kappa}_I \cos\hat{\kappa}_{off} \cos\hat{\phi}_I \cos\hat{\phi}_{off} \sin\hat{\omega}_{off},$$
$$j_{82}^{int} = d_1 d_5 - \cos\hat{\kappa}_I \cos\hat{\phi}_I d_3,$$
$$j_{83}^{int} = d_1 d_4 + \cos\hat{\kappa}_I \cos\hat{\phi}_I d_6 + \cos\hat{\omega}_{off} \cos\hat{\phi}_{off} d_8,$$
$$j_{84}^{int} = \cos\hat{\kappa}_I \sin\hat{\phi}_I d_5 - \cos\hat{\kappa}_I \cos\hat{\phi}_I \sin\hat{\omega}_I d_3 - \cos\hat{\kappa}_I \cos\hat{\omega}_I \cos\hat{\phi}_I \cos\hat{\phi}_{off} \sin\hat{\omega}_{off},$$
$$j_{85}^{int} = \cos\hat{\phi}_I \sin\hat{\kappa}_I d_5 - d_2 d_3 + \cos\hat{\phi}_{off} \sin\hat{\omega}_{off} d_7,$$
$$j_{86}^{int} = d_8 d_3 + \cos\hat{\phi}_{off} \sin\hat{\omega}_{off} d_1,$$

$$j_{91}^{int} = \cos\hat{\omega}_{off} \sin\hat{\phi}_{off} d_8 - \cos\hat{\omega}_{off} \cos\hat{\phi}_{off} \sin\hat{\kappa}_{off} d_1 + \cos\hat{\kappa}_I \cos\hat{\kappa}_{off} \cos\hat{\omega}_{off} \cos\hat{\phi}_I \cos\hat{\phi}_{off},$$
$$j_{92}^{int} = d_6 d_1 - \cos\hat{\kappa}_I \cos\hat{\phi}_I d_4,$$
$$j_{93}^{int} = \cos\hat{\phi}_{off} \sin\hat{\omega}_{off} d_8 - \cos\hat{\kappa}_I \cos\hat{\phi}_I d_5 - d_3 d_1,$$
$$j_{94}^{int} = \cos\hat{\kappa}_I \sin\hat{\phi}_I d_6 - \cos\hat{\kappa}_I \cos\hat{\phi}_I \sin\hat{\omega}_I d_4 + \cos\hat{\kappa}_I \cos\hat{\omega}_I \cos\hat{\omega}_{off} \cos\hat{\phi}_I \cos\hat{\phi}_{off},$$
$$j_{95}^{int} = \cos\hat{\phi}_I \cos\hat{\kappa}_I d_6 - \cos\hat{\omega}_{off} \cos\hat{\phi}_{off} d_7 - d_2 d_4,$$
$$j_{96}^{int} = d_8 d_4 - \cos\hat{\omega}_{off} \cos\hat{\phi}_{off} d_1.$$

Returning to the description of Eq. A19, $\boldsymbol{\Sigma}_{\xi}$ is the covariance matrix of $\boldsymbol{\xi}$, defined as:

$$\sum_{\xi} = \begin{bmatrix} \sum_{\xi_{dist}} & \boldsymbol{0} & \boldsymbol{0} \\ \boldsymbol{0} & \sum_{\xi_{ang}} & \boldsymbol{0} \\ \boldsymbol{0} & \boldsymbol{0} & \sum_{\xi_{\text{int}}} \end{bmatrix} = \begin{bmatrix} \begin{bmatrix} \ddots & & \boldsymbol{0} \\ & \left(\sum_{\xi}^{dist}\right)_{ijk} & \\ \boldsymbol{0} & & \ddots \end{bmatrix}_{ijk \in I^{dist}} & \boldsymbol{0} & \boldsymbol{0} \\ \boldsymbol{0} & \begin{bmatrix} \ddots & & \boldsymbol{0} \\ & \left(\sum_{\xi}^{ang}\right)_{ijk} & \\ \boldsymbol{0} & & \ddots \end{bmatrix}_{ijk \in I^{ang}} & \boldsymbol{0} \\ \boldsymbol{0} & \boldsymbol{0} & \sum_{\xi_{\text{int}}} \end{bmatrix}. \quad \text{(A22)}$$

where blocks $\left(\sum_{\xi}^{dist}\right)_{ijk}$ and $\left(\sum_{\xi}^{ang}\right)_{ijk}$ can in turn be split into other sub-blocks related to calibration and measurement parameters:

$$\left(\sum_{\xi}^{dist}\right)_{ijk} = \left[\begin{matrix} \sum_{\xi_{dist}^{calib}} & \boldsymbol{0} \\ \boldsymbol{0} & \sum_{\xi_{dist}^{meas}} \end{matrix}\right]_{ijk \in I^{dist}}$$
$$\left(\sum_{\xi}^{ang}\right)_{ijk} = \left[\begin{matrix} \sum_{\xi_{ang}^{calib}} & \boldsymbol{0} \\ \boldsymbol{0} & \sum_{\xi_{ang}^{meas}} \end{matrix}\right]_{ijk \in I^{ang}} \quad \text{(A23)}$$

$\boldsymbol{\Sigma}_{\xi}$ is therefore a block-diagonal matrix containing the (co)variances of the parameters in $\boldsymbol{\xi}$. While the data related to the positioning/orientation of the sensors in use can be obtained from initial calibration process(es), those related to their local (angular and distance) measurements can be determined in other ways: e.g., (i) from manuals or technical documents relating to the distributed/integrated sensors in use, or (ii) estimated through *ad hoc* experimental tests.

The off-diagonal entries in the blocks concerning local measurements are zeros, assuming no correlation between these parameters. This assumption is reasonable upon the hypothesis that sensors work independently from each other and there is no correlation between the local measurements related to different sensors.

By applying the GLS method to the system in Eq. A17, we obtain the final estimate of $\boldsymbol{X}$ as:

$$\hat{\boldsymbol{X}} = \left(\boldsymbol{A}^T \cdot \boldsymbol{W} \cdot \boldsymbol{A}\right)^{-1} \cdot \boldsymbol{A}^T \cdot \boldsymbol{W} \cdot \boldsymbol{B}\,. \quad \text{(A23)}$$

For further details on the GLS method, see (Kariya and Kurata, 2004).

We emphasize that an (at least rough) initial estimate of $\boldsymbol{X}$ is required to define some elements of the matrices $\boldsymbol{A}$, $\boldsymbol{B}$ and $\boldsymbol{W}$ (see Eqs. A6, A12, A19).

This problem can be overcome applying the formula in Eq. A23 recursively: (i) setting no-matter-what initial $\hat{\hat{\boldsymbol{X}}}$, in order to determine the elements of matrices $\boldsymbol{A}$, $\boldsymbol{B}$ and $\boldsymbol{W}$, (ii) obtaining a not very accurate localization of P, and (iii) iterating the localization using the result of the previous one as a new $\hat{\hat{\boldsymbol{X}}}$. We verified that the localization tends to converge to the correct solution after about four-five iterations.

Highlights

- A new modular probe for Large-Volume Metrology (LVM) applications is described.
- The probe enhances the measurement process when using combinations of LVM systems.
- The probe can be customized depending on the combination of LVM systems in use.
- A mathematical/statistical model for the real-time probe localization is presented.
- The description is supported by realistic application examples.